

2014-12-17

# Surface Chemistry and Spectroscopy of Human Insulin Langmuir Monolayer

Sheba Johnson

*University of Miami*, s.johnson29@umiami.edu

Follow this and additional works at: [https://scholarlyrepository.miami.edu/oa\\_dissertations](https://scholarlyrepository.miami.edu/oa_dissertations)

---

## Recommended Citation

Johnson, Sheba, "Surface Chemistry and Spectroscopy of Human Insulin Langmuir Monolayer" (2014). *Open Access Dissertations*. 1360.

[https://scholarlyrepository.miami.edu/oa\\_dissertations/1360](https://scholarlyrepository.miami.edu/oa_dissertations/1360)

This Open access is brought to you for free and open access by the Electronic Theses and Dissertations at Scholarly Repository. It has been accepted for inclusion in Open Access Dissertations by an authorized administrator of Scholarly Repository. For more information, please contact [repository.library@miami.edu](mailto:repository.library@miami.edu).

UNIVERSITY OF MIAMI

SURFACE CHEMISTRY AND SPECTROSCOPY OF HUMAN INSULIN  
LANGMUIR MONOLAYER

By

Sheba Johnson

A DISSERTATION

Submitted to the Faculty  
of the University of Miami  
in partial fulfillment of the requirements for  
the degree of Doctor of Philosophy

Coral Gables, Florida

December 2014

©2014  
Sheba Johnson  
All Rights Reserved

UNIVERSITY OF MIAMI

A dissertation submitted in partial fulfillment of  
the requirements for the degree of  
Doctor of Philosophy

SURFACE CHEMISTRY AND SPECTROSCOPY OF HUMAN INSULIN  
LANGMUIR MONOLAYER

Sheba Johnson

Approved:

\_\_\_\_\_  
Roger Leblanc, Ph.D.  
Professor of Chemistry

\_\_\_\_\_  
Carl Hoff, Ph.D.  
Professor of Chemistry

\_\_\_\_\_  
James Wilson, Ph.D.  
Professor of Chemistry

\_\_\_\_\_  
M. Brian Blake, Ph.D.  
Dean of the Graduate School

\_\_\_\_\_  
Kerim Gattas-Asfura, Ph.D.  
Post Doctoral Associate  
Diabetes Research Institute

JOHNSON, SHEBA  
Surface Chemistry and Spectroscopy of  
Human Insulin Langmuir Monolayer.

(Ph.D., Chemistry)  
(December 2014)

Abstract of a dissertation at the University of Miami.

Dissertation supervised by Professor Roger Leblanc.  
No. of pages in text. (130)

The focus of this thesis can be categorized as study of two molecules, namely human insulin and carbon dots at 1) air-water interface as a Langmuir monolayer and 2) in solution. Aggregation of proteins into amyloids has been related to several diseases like Alzheimer's, Parkinson's and Amyloidosis. Human insulin was chosen as a model protein to study fibrillation of the proteins. Effect of carbon dots on the rate of human insulin fibrillation was examined through spectroscopic techniques and imaging.

Both human insulin and carbon dots were examined at air-water interface as a Langmuir monolayer. The conformation of human insulin in presence of various salt concentration and  $ZnCl_2$  was examined at air-water interface. Based on the results of the surface pressure isotherms and spectroscopic studies of the protein at air-water interface, an scheme was proposed for the conformation of human insulin at air-water interface. Carbon dots at air-water interface were imaged by Atomic Force Microscopy using Langmuir-Blodgett films.

*Dedicated to:  
My mother Valsamma from whom I get my audacity for adventures, including this Ph.D;  
and  
My father Johnson Samual from whom I get my unrelenting persistence.*

*The Lord God is my strength;  
He will make my feet like the deer's feet,  
And He will make me walk on my high hills.  
-Habakkuk 3: 19*

## ACKNOWLEDGEMENTS

I consider it a privilege to have Dr. Leblanc as my mentor. I thank him for his encouragement throughout my five years of graduate school in my research and in my life. I admire his outlook on life and ability to see the positive in every circumstance. I am truly fortunate to be under his guidance for these years. I would like to thank my committee members Dr. Hoff, Dr. Wilson and Dr. Gattas Asfura for their questions, suggestions and advice in my research. I would like to thank all the professors in the Chemistry Department and the staff in the Departmental Office.

I would like to thank the past and current members of Dr. Leblanc's lab who I was privileged to work and collaborate with: Garima Thakur, Wei Liu, Andrew Garcia, Lisa Joseph, Blake Fortes, Ian Zhang, Jerome Mullor, Qun Huo, Micic Miodrag and Jhony Orbulescu. Special thanks to Nicholas Crawford and Shanghao Li who are the best labmates one could ask for; I am sure our paths will cross again! I would like to thank some of my good friends from the Chemistry Department for their friendship throughout my graduate school: Barnali Mondal, Anjaneyulu Koppaka, Tingting Zhang, Xiaoxia Zhu, Yanhua Qiu, Shampa Samanta, Mintu Sadhukhan, Subhojit Majumdar and Subramani Swaminathan.

I would like to thank all my teachers from kindergarten to graduate school. They have all played a role in molding me into who I am as a student. There are four teachers, who were a Godsend in my life. They are Emily Andrews, my Science and Physics teacher from grades 7 through 10 at Mater Dei Convent, New Delhi, India. Also, I thank Dr. Stacey Boyette and Dr. Carmen Gauthier, my Chemistry advisors at Florida Southern College, Lakeland, Florida. I would like to extend special thanks to Dr. James Worden,

who was my supervisor when I worked as a lab assistant during my undergraduate studies. I would like to thank the chaplain, Pastor Joseph Lortie for his sound advice and for “seeing” how God sees. I also thank all my friends at University Christian Fellowship (Chi Alpha) church at University of Miami for their sweet friendship. A special thanks to my roommates and good friends, Vy Vo, SaptarniBandyopashyay and Noeline Prins.

I am grateful to my family for their love and support of me. I would like to mention my sister Laura who did many things including editing my papers and this thesis, helping me move apartments, assembling and disassembling my furniture, coming to visit me several times to encourage me before presentations and this list is endless.....What would I do without you, Laura? I would like to thank my husband Daniel who is a source of strength to me. He waits for me on the other side of the country, we will be together soon! I thank my parents for their great love for me. I am thankful for my father for being a man of integrity and for being an example to me by working hard. I am thankful for a mother for who sees no limits or boundaries in what one can achieve. Their love and example prods me to move forward.

I end with a quote from Matthew 19:26: “With man this is impossible, but with God, all things are possible.” I thank God for being with me and making impossible things possible.



## TABLE OF CONTENTS

	Page
LIST OF FIGURES.....	xi
LIST OF TABLES.....	xix
LIST OF ABBREVIATIONS.....	xxi
CHAPTER 1 INTRODUCTION	
1.1 Background.....	1
1.2 Insulin: A model protein.....	2
1.3 Carbon dots: An overview.....	7
CHAPTER 2 MATERIALS AND INSTRUMENTATION	
2.1 Materials.....	10
2.2 Instrumentation.....	11
2.2.1 Surface pressure and surface potential-area isotherm.....	11
2.2.2 Langmuir monolayer: surface tension and surface pressure.....	12
2.2.3 Langmuir-Blodgett (LB) or Langmuir-Schaeffer (LS) film.....	17
2.2.4 Conditions for preparation of a Langmuir monolayer.....	18
2.2.5 Epifluorescence microscopy.....	19
2.2.6 Brewster angle microscopy.....	21
2.2.7 Circular dichroism.....	22
2.2.8 Infrared microscopy: Bio-ATR and IRRAS.....	22

2.2.9 Atomic Force Microscopy.....	24
2.3 Procedures.....	25
2.3.1 Insulin fiber formation.....	25
2.3.2 Preparation of congo red and thioflavin T.....	25
2.3.3 CdSe QD synthesis and capping QDs with DHLA.....	26
2.3.4 Synthesis of carbon dots.....	27
2.4 Summary.....	27

## CHAPTER 3 HUMAN INSULIN AND CARBON DOTS: SURFACE CHEMISTRY AND SPECTROSCOPY

3.1 History and background.....	28
3.2 Surface chemistry of human insulin.....	31
3.2.1 Surface pressure and surface potential area isotherms.....	31
3.2.2 Compression-decompression cycles and stability isotherms of human insulin Langmuir monolayer.....	32
3.2.3 UV-vis and fluorescence spectroscopy of human insulin in aqueous phase and Langmuir monolayer.....	34
3.2.4 Epifluorescence and Brewster angle microscopy of human insulin Langmuir monolayer.....	36
3.2.5 Secondary structure of human insulin at air-water interface.....	38

3.2.5.1 CD and FTIR examination of insulin in solution.....	38
3.2.5.2 IRRAS examination of insulin Langmuir monolayer.....	40
3.3 Carbon dots: background.....	47
3.4 Carbon dots: synthesis.....	47
3.5 Carbon dots Langmuir monolayer.....	49
3.6 Carbon dots Langmuir Blodgett film.....	52
3.7 Conclusion.....	55

CHAPTER 4 STUDY OF AGGREGATION OF HUMAN INSULIN LANGMUIR  
MONOLAYER

4.1 History and background.....	57
4.2 Sample preparation.....	58
4.3 Surface pressure-and potential-area isotherms: effect of zinc concentration in subphase.....	59
4.4 UV-vis and fluorescence spectroscopy of human insulin in aqueous phase and as Langmuir monolayer.....	62
4.5 FTIR and IRRAS of human insulin in aqueous phase and Langmuir monolayer.....	65
4.6 CD spectroscopy of human insulin aqueous solution.....	70
4.7 A proposed model for the human insulin Langmuir monolayer.....	72
4.8 Conclusion.....	74

CHAPTER 5 HUMAN INSULIN-FIBRIL ASSISTED SYNTHESIS OF  
FLUORESCENT GOLD NANOCCLUSERS

5.1 Background.....	75
5.2 Gold nanoparticles: An overview.....	75
5.3 Literature review and limitations of proposed mechanism for synthesis of gold nanoclusters by proteins.....	76
5.4 Synthesis of gold nanoclusters.....	77
5.5 Characterization of gold nanoclusters by AFM and TEM imaging.....	79
5.6 Fluorescence spectroscopy analysis of gold nanoclusters.....	81
5.7 Synthesis of CdS quantum dots.....	88
5.8 Characterization of CdS quantum dots.....	88
5.9 Conclusion.....	90

CHAPTER 6 WATER SOLUBLE CARBON DOTS ARE CATALYST FOR HUMAN  
INSULIN FIBRILLATION

6.1 History and background.....	92
6.2 Synthesis and methods.....	94
6.3 Characterization of the water soluble carbon dots.....	97
6.4 Spectroscopic characterization of fibrillation of human insulin with water soluble carbon dots.....	100
6.5 Secondary structure changes in fibrillation of insulin.....	105
6.6 Imaging and analysis.....	112
6.7 Conclusion.....	115

REFERENCES..... 118

## LIST OF FIGURES

### Chapter 1

- Figure 1.1** The amino acid sequence of bovine insulin..... 5
- Figure 1.2** Insulin is stored as a hexamers in the pancreas, held together by three zinc ions..... 6
- Figure 1.3** Timeline showing recent activity regarding carbon dots in the literature..... 8

### Chapter 2

- Figure 2.1** KSV Langmuir minitrough suitable for surface pressure-area isotherm, UV-vis and fluorescence at the air-water interface ..... 11
- Figure 2.2** Illustration of unequal forces at the interface responsible for surface tension.....13
- Figure 2.3** Illustration of Whilhemmy plate at air-water interface..... 13
- Figure 2.4** Compression of a Langmuir monolayer. (A) Scheme of a Langmuir trough as the movable barrier reduces the area available to the monolayer. (B) Idealized surface pressure-area isotherm indicating phase transitions of the Langmuir monolayer..... 15
- Figure 2.5** Langmuir-Schaefer and Langmuir-Blodgett film deposition of monolayers from the air-water interface to solid hydrophobic support..... 17
- Figure 2.6** Internal view of Olympus IX70 inverted microscope..... 20
- Figure 2.7** Diagram of the IElli-2000 imaging ellipsometer design (A) and diagram showing the Brewster angle for water (no reflection) and change in reflection when monolayer is present (reflection is present)..... 21

<b>Figure 2.8</b> CD spectra of proteins representative of 5 different secondary structure.....	22
<b>Figure 2.9</b> Diagram of atomic force microscope.....	24
 <b>Chapter 3</b>	
<b>Figure 3.1</b> The amino acid sequence of bovine insulin.....	28
<b>Figure 3.2</b> Insulin is stored as a hexamers in the pancreas, held together by three zinc ions.....	29
<b>Figure 3.3</b> Surface pressure–( $-\Delta-$ ) and surface potential–area ( $-o-$ ) isotherms of human insulin Langmuir monolayer at subphase pH 5.6.....	31
<b>Figure 3.4</b> Three compression-decompression cycles up to a surface pressure of 10 and 30 mN/m of human insulin Langmuir monolayer at subphase pH 5.6.....	33
<b>Figure 3.5</b> Stability measurements at surface pressure 10 (A) and 30 mN/m (B) held for 90 minutes for human insulin Langmuir monolayer at subphase pH 5.6.....	33
<b>Figure 3.6</b> UV-vis ( $5 \times 10^{-5}$ M) and fluorescence ( $5 \times 10^{-7}$ M; $\lambda_{\text{excitation}} = 270$ nm, slit width at the excitation and emission, 5 and 5 nm, respectively) spectra of aqueous solution of human insulin.....	35
<b>Figure 3.7</b> UV-vis spectra of human insulin Langmuir at subphase pH 5.6. Inset shows the variation of the absorbance at 224 and 276 nm in function of the surface pressure...	35
<b>Figure 3.8</b> Circular dichroism spectrum of aqueous insulin at pH 2 and temperature $20 \pm 1$ °C. The concentration of the insulin was 0.3 mg/ml.....	39
<b>Figure 3.9</b> FTIR spectrum of aqueous insulin at pH 2 and temperature $20 \pm 1$ °C. The concentration of the insulin was 0.3 and 2 mg ml <sup>-1</sup> , respectively.....	39

<b>Figure 3.10</b> p-Polarized IRRAS of human insulin Langmuir monolayer at subphase pH 5.6 using an incident angle of 60°, and varying the surface pressures.....	44
<b>Figure 3.11</b> p-Polarized IRRAS of human insulin Langmuir monolayer at subphase pH 5.6 and surface pressure 10 mN/m, and varying the incident angles.....	45
<b>Figure 3.12</b> s-Polarized IRRAS of human insulin Langmuir monolayer at subphase pH 5.6 and incident angle of 25°, and varying the surface pressures.....	46
<b>Figure 3.13</b> Absorption (dash line) and photoemission (solid line, $\lambda_{ex} = 340$ nm) for carbon dots in a aqueous solution of chloroform.....	48
<b>Figure 3.14</b> TEM Image of carbon dots.....	49
<b>Figure 3.15</b> Surface pressure–area isotherms of carbon dots Langmuir monolayer at subphase pH 5.6.....	50
<b>Figure 3.16</b> Stability measurements at surface pressure 30 mN/m held for 30 minutes for carbon dots Langmuir monolayer at subphase pH 5.6.....	51
<b>Figure 3.17</b> Three compression-decompression cycles up to a surface pressure of 30 mN/m of carbon dots Langmuir monolayer at subphase pH 5.6.....	51
<b>Figure 3.18</b> AFM image (10 $\mu\text{m} \times 10 \mu\text{m}$ ) of blank quartz slide and the B) topography of the imaged quartz slide.....	52
<b>Figure 3.19</b> AFM image (4 $\mu\text{m} \times 4 \mu\text{m}$ ) of A) blank quartz slide drop casted with carbon dots, B) topography of the imaged quartz slide and C) Fluorescence spectra of blank quartz slide (black line) and slide drop casted with carbon dots dissolved in chloroform	



(red line). ( $\lambda_{\text{excitation}} = 340 \text{ nm}$ , slit width at the excitation and emission, 5 and 5 nm, respectively)..... 53-54

## Chapter 4

**Figure 4.1** Insulin is stored as a hexamers in the pancreas, held together by three zinc ions..... 58

**Figure 4.2** Surface pressure- and surface potential-area isotherms of recombinant human insulin aqueous solution (pH 2) spread at the air-water interface in absence and presence of  $\text{ZnCl}_2$  in the subphase (A); compression-decompression isotherm cycles in absence and presence of  $\text{ZnCl}_2$  in the subphase (B)..... 60

**Figure 4.3** Surface pressure- and surface potential-area isotherms of recombinant human insulin aqueous solution (pH 9) spread at the air-water interface in absence and presence of  $\text{ZnCl}_2$  in the subphase (A); compression-decompression isotherm cycles in absence and presence of  $\text{ZnCl}_2$  in the subphase (B)..... 61

**Figure 4.4** UV-vis and fluorescence (excitation at 270 nm, Raman at 297 nm) spectra of  $10^{-4} \text{ M}$  human insulin aqueous solutions (A, B) and UV-vis spectra of human insulin Langmuir monolayer at pH 2 and pH 9 in absence and presence of  $\text{ZnCl}_2$  ( $10^{-3} \text{ M}$ ) in the subphase at 5 mN/m (C) and at 25 mN/m (D)..... 63

**Figure 4.5** FTIR spectra of human insulin aqueous solution and IRRAS spectra of insulin Langmuir monolayer: Bio-ATR cell spectra of insulin (1.5 mg/mL) in absence and presence of  $\text{ZnCl}_2$  at pH 2 and pH 9 (A); p-polarization IRRAS spectra of insulin Langmuir monolayer at a surface pressure of 10 mN/m and various angles of incidence at

pH 2 (B); p-polarization at 60° IRRAS spectra of insulin Langmuir monolayer at pH 2 and pH 9 in absence and presence of ZnCl<sub>2</sub> in the subphase at surface pressure 5 (C) and 25 mN/m (D)..... 66

**Figure 4.6** CD spectra of human insulin aqueous solutions at pH 2 and pH 9 in absence of ZnCl<sub>2</sub> and at pH 5.6 in presence of ZnCl<sub>2</sub>. (Concentration of solution 10<sup>-4</sup> M; optical path length: 1 mm).....70

**Figure 4.7** The proposed insulin hexamer orientation at the air-water interface with acidic (A) and basic human insulin samples (B)..... 73

## Chapter 5

**Figure 5.1** AFM image (6 μm × 6 μm scan) of (A) human insulin (256 μM) in aqueous solution pH 10.5 after 6 h of incubation at 37 °C. (B) The magnified section (3 μm × 3 μm scan) of (A) (green box) shows rod-like insulin aggregates (green arrows)..... 78

**Figure 5.2** TEM images of (A) the insulin fibrils Au NCs and its corresponding insulin reference (B) in aqueous solution, pH 10. The insulin reference emulates the current synthesis of insulin Au NCs shown in (B), replacing H<sub>2</sub>AuCl<sub>4</sub> for HCl, with an initial insulin incubation of 6 h and secondary incubation of 36 h at 37 °C. Final insulin concentrations in insulin Au NCs and in the insulin reference were both approximated to be around 128 μM in solution..... 80

**Figure 5.3** Method comparison fluorescence spectrum (λ<sub>excitation</sub> = 470 nm) of human insulin Au NCs, normalized at the water Raman peak at 559 nm (Au NCs emission at

620 nm). All samples had a 12 h Au NCs incubation time; the heated samples were heated at 37 °C for 6 h prior to the 12 h of Au NCs incubation..... 82

**Figure 5.4** UV–visible absorption spectrum of insulin fibrils (128 μM) Au NCs synthesized under optimized conditions. Initial insulin concentration: 256 μM in 5 mL alkaline solution..... 84

**Figure 5.5** Time evolution of the fluorescence spectrum ( $\lambda_{\text{excitation}} = 470 \text{ nm}$ ) of insulin fibrils Au NCs synthesized under optimized conditions: pre-incubated (6 h at 37 °C) human insulin addition to HAuCl<sub>4</sub> solution and subsequent incubation at 37 °C for the listed times: 12 h (black) and 36 h (blue). NCs emitted at 620 n..... 86

**Figure 5.6** Combined fluorescence spectra of insulin fibrils (128 μM) Au NCs at successive excitation wavelengths in 5 nm intervals: 460 nm (front) to 485 nm (back)..... 86

**Fig 5.7** UV–visible and fluorescence absorption spectrum of insulin CdS quantum dots..... 88

**Fig 5.8** AFM images (2 μm × 2 μm scan) at 30 minutes for (A) insulin quantum dots B) insulin and at 12 hours for C) insulin quantum dots and D) insulin reference..... 89

## Chapter 6

**Figure 6.1** Characterization of oil soluble carbon dots (OCD) dissolved in chloroform. A) fluorescence spectra when excited at 360 nm, slit width of 5 nm, 5 nm and cell length 1

cm. Visual confirmation presence of OCD by B) AFM image (11  $\mu\text{m}$  X 11  $\mu\text{m}$ ) of OCD;  
 C) Extracted profile of one WCD; D) TEM image of WCD..... 96

**Figure 6.2** Visual confirmation presence of WCD by B) AFM image (11  $\mu\text{m}$  X 11  $\mu\text{m}$ ) of  
 WCD; C) Extracted profile of one WCD; D) AFM topography image of WCD and E)  
 TEM image of WCD..... 98

**Figure 6.3** Time evolution of Thioflavin T fluorescence of Human Insulin and Human  
 Insulin-WCD at 37 C and pH 2, where (■, black) Human Insulin, (●, red circle) Human  
 Insulin: WCD (5000:1) and, (▲, blue triangle) Human Insulin: WCD (500:1). Slit width  
 at the excitation and emission, 5 and 5 nm, respectively..... 101

**Figure 6.4** A) Absorption spectra of Congo Red in Human Insulin and Human Insulin-  
 WCD solution at incubation time of A) 0.5 hours. Congo Red alone (black), Human  
 Insulin (red), Human Insulin: WCD (5000:1) (blue) and Human Insulin: WCD (500:1)  
 (green). Absorption spectra of Congo Red in Human Insulin and Human Insulin-WCD  
 solution at incubation time of B) 3.5 hours and C) 6 hours..... 102

**Figure 6.5** A) Circular dichroism spectra of human insulin before incubation at time 0  
 hours (black), human insulin (red), human insulin: WCD with ration 5000:1 (blue) and  
 human insulin: WCD with ratio of 500:1 (green) at incubation times of A) 0.5 hours,  
 human insulin:WCD with ratio of 500:1 (green) at incubation times of B) 3.5 hours and  
 C) 6 hours..... 105

**Figure 6.6** A) UV-vis ( $5 \times 10^{-5}$  M) and fluorescence ( $5 \times 10^{-7}$  M;  $\lambda_{\text{excitation}} = 270$  nm)  
 spectra of aqueous solution of human insulin, B) Insulin fibrillation detected by tyrosine  
 fluorescence when excited at 276 nm and emission measured at 305 nm : (■, black)

Human Insulin, (●, red circle) Human Insulin: WCD (5000:1) , (▲, blue triangle) Human Insulin: WCD ( 500:1). Slit width at the excitation and emission, 5 and 5 nm, respectively..... 110

**Figure 6.7:** AFM images (3 um X 3 um) of Insulin and Human Insulin: WCD at two different ratios..... 113

**Figure 6.8:** TEM images of Insulin and Human Insulin: WCD at two different ratios. 114

## LIST OF TABLES

### Chapter 1

<b>Table 1.1</b> Nobel Prizes for Insulin-related research.....	2
---	---

### Chapter 3

<b>Table 3.1</b> Four surface pressures of 10, 20, 30, and 40 mN/m were measured by A) Epifluorescence for a sample of HI-FITC Langmuir monolayer; B) BAM for insulin HI Langmuir monolayer; C) BAM for arachidic acid Langmuir monolayer. (Insulin concentration: 0.30 mg/ml).....	37
---	----

<b>Table 3.2</b> Major bands characteristic of $\alpha$ helix and $\beta$ sheet.....	41
--	----

<b>Table 3.3</b> Assignment of bands present in p-polarization IRRAS of human insulin Langmuir monolayer in Figure 3.10.....	41
--	----

<b>Table 3.4</b> Assignment of bands present in p-polarization IRRAS of human insulin Langmuir monolayer in Figure 3.11.....	42
--	----

### Chapter 4

<b>Table 4.1</b> Band assignment of the FTIR and IRRAS spectra related to the secondary structure of human insulin in aqueous solution and as Langmuir monolayer.....	68
---	----

<b>Table 4.2</b> Secondary structure estimation of the aqueous human insulin CD spectra using Softsec software.....	71
---	----

## Chapter 6

<b>Table 6. 1</b> Secondary structure estimation of Human Insulin fibrillation in the presence and absence of WCD using Dichroweb software.....	108
---	-----

## LIST OF ABBREVIATIONS

AFM	atomic force microscopy
BAM	Brewster angle microscopy
BSA	bovine serum albumin
CD	carbon dots
CR	congo red
DHLA	dihydrolipoic acid
FITC	fluorescein isothiocyanate
HI	human insulin
HSA	human serum albumin
IRRAS	infrared absorption-reflection spectroscopy
LB	Langmuir–Blodgett
NMR	nuclear magnetic resonance
PEG	polyethylene glycol
QD	quantum dots
IRRAS	infrared reflection-absorption spectroscopy
TEM	transmission electron microscopy
ThT	thioflavin T
Trp	tryptophan
Tyr	tyrosine
WCD	water soluble carbon dots



## Chapter 1

### Introduction

#### 1.1 Background

Protein misfolding resulting in formation of amyloid plaques has been indicated to play a role in several diseases like Alzheimer's disease, diabetes type 2 and Parkinson's disease.<sup>1,2</sup> In the human body, there are 18 known proteins which have been observed to misfold and play a causative role in diseases. Various nanoparticles have been used to prevent protein fibrillation such as CdSe quantum dots.<sup>1; 2</sup> This thesis will be examining human insulin (HI) as a model protein to study fibrillation of proteins and the role of nanoparticle carbon dots (CD) in HI fibrillation. The work in this thesis can be divided into two main parts, which are i) surface chemistry studies of molecules as Langmuir monolayer at air-water interface and ii) study in aqueous solution. Experiments with HI Langmuir monolayer under various conditions such as pH and ions were conducted to understand the conformational changes in the protein molecule. Stability of CD was observed at air-water interface and CD Langmuir Blodgett films were examined. The work in solution involves synthesis of nanoparticles like gold nanoclusters, CdS quantum dots and CD. Interaction between CD and HI in solution was found accelerate the HI fibril formation. This chapter will give a brief background on the research done on HI and CD.

## 1.2 Insulin: A model protein

Insulin serves as a model protein for studying structure and properties of proteins. Due to

Year	Category	Recipient	Contribution
1923	Medicine	F.G. Banting and J.J.R. Macleod	Discovery of insulin
1947	Medicine	C.F. Cori and G.T. Cori	Discovery of the course of the catalytic conversion of glycogen
1947	Medicine	B.A. Houssay	Discovery of the role of hormones released by the anterior pituitary lobe in the metabolism of sugar
1958	Chemistry	F. Sanger	Work on the structure of proteins, especially insulin
1971	Medicine	E.W. Sutherland	Discoveries concerning the mechanisms of action of hormones
1977	Medicine	R. Yalow	Development of radioimmunoassays for peptide hormones
1992	Medicine	E.H. Fischer and E.G. Krebs	Discoveries concerning reversible protein phosphorylation as a biologic regulatory mechanism

**Table 1.1 Nobel Prizes for Insulin-related research.** <sup>4</sup>

This, insulin holds the distinction for a lot of ‘firsts’ among the proteins and seven Nobel Prizes have been awarded for insulin related research (Table 1.1).<sup>3</sup> Insulin was the first protein to be generated by recombinant DNA.<sup>5</sup> Insulin was also the first protein to have its amino acid sequenced in 1955 (Figure 1.1) and to be detected by immunoassay.<sup>6</sup> Insulin is most known for its association with diabetes. Diabetes’s first recorded observation comes from ancient Egypt, where it was observed that a person lost weight and urinated excessively. Greek physician Aretaeus was responsible for coining the term ‘diabetes mellitus’ which meant that the urine had has sweet taste. <sup>4</sup>

The first person to quantitatively measure glucose content in urine was Matthew Dobson in 1776. He found the concentration of glucose in urine of people with diabetes to be elevated. <sup>7</sup> In 1869, Paul Langerhans studies pancreas under microscope and was able see what we know today as the islets of Langerhans. Islets of Langerhans are present in the

beta cell of pancreas, which is the site of insulin production and storage. The next major development in the study of diabetes was in 1889 when Minkowski and von Mering removed pancreas from a dog, which resulted in fatal diabetes for the dog. This established a direct link between glucose regulations and pancreas.<sup>8</sup> Once it was established that diabetes and insulin were related and, that insulin was produced in the pancreas, several attempts were made to extract insulin from pancreas over the years. These attempts were partially successful until Macleod and Banting were able to extract, purify and administer insulin to patients with successful results.<sup>3; 6; 9-15</sup>

The structure of bovine insulin was established in 1958, for which Fredrick Sagner was awarded the Nobel Prize. The pathway of insulin synthesis from proinsulin precursor in the beta cells of pancreas was studied by Steiner in 1967.<sup>16</sup> D. Hodgkin was able to solve the 3D structure of insulin using X-ray crystallography.<sup>17</sup> The protein is conserved in other animal species and has been used to treat diabetes in humans. Porcine and bovine insulin differs from human insulin in one and two amino acids, respectively. Human insulin (HI) is a peptide hormone, which is produced in islets of Langerhans, and its main function in the human body is to control blood glucose level. Since the discovery of insulin, diabetes has become treatable. Insulin is composed of 51 amino acids and has a mass of 5807 daltons. Insulin is produced by the Beta cells in the pancreases and is stored in the pancreases as a hexamers.<sup>18-21</sup> Insulin is made up of two polypeptide chains called the A chain with 21 residues and the B chain with 30 residues are joined to each other by disulfide bridges.

Besides the monomeric structure of HI, it is also found to exist as dimers, hexamers and amyloids. As a monomer, majority of the structure of HI is composed of an  $\alpha$ -helical structure and it dimerizes through the formation of  $\beta$  sheet. As a monomer, the majority of the structure of insulin is composed of  $\alpha$ -helical structure and it dimerizes through the formation of  $\beta$ -sheet. Insulin is often found having a dimer structure which is due to hydrogen bonding between the C terminus of B chains.<sup>22</sup> Insulin dimers come together to form hexamers in the presence of zinc ions (Figure 3.2). Monomers and dimers readily diffuse into blood, whereas hexamers diffuse poorly. Increase in glucose levels in the blood is one of the major triggers for release of stored insulin from the pancreas. Hence, absorption of insulin preparations containing a high proportion of hexamers is delayed and somewhat slow.<sup>23</sup> HI amyloid is characterized by  $\beta$  sheet. Tissue deposition of normally soluble proteins as insoluble amyloid fibrils is associated with serious diseases including the systemic amyloidoses, maturity onset diabetes and Alzheimer's disease. In vitro, HI is readily converted to an inactive fibrillar form by incubation at high HI concentrations, low pH and high temperatures. The first reported study of insulin Langmuir monolayer was in 1940 by I. Langmuir and D.F Waugh. The results of the study shows that there was no differences in surface pressure isotherms for native and denatured insulin.<sup>24</sup> B.S Harrap experiments of insulin Langmuir monolayer were based on insulin having 114 residues and an isoelectric point of 5.7, which was the information available then.<sup>25</sup> This study examined surface pressure and surface potential of insulin with change in subphase pH from 2.10 to 9.70. The experiments by B.S Harrap show that surface pressure of insulin decreases when the subphase pH ranges from 2.10 to 5.7 and then increases for pH ranges from 5.7 to 9.10.<sup>26</sup> The surface potential was observed to

decrease when the subphase pH was increased and shown to fluctuate wildly at pH 5.7. These results were found to complement with electrometric titration studies of insulin. Various studies were performed to determine the molecular weight of insulin in the

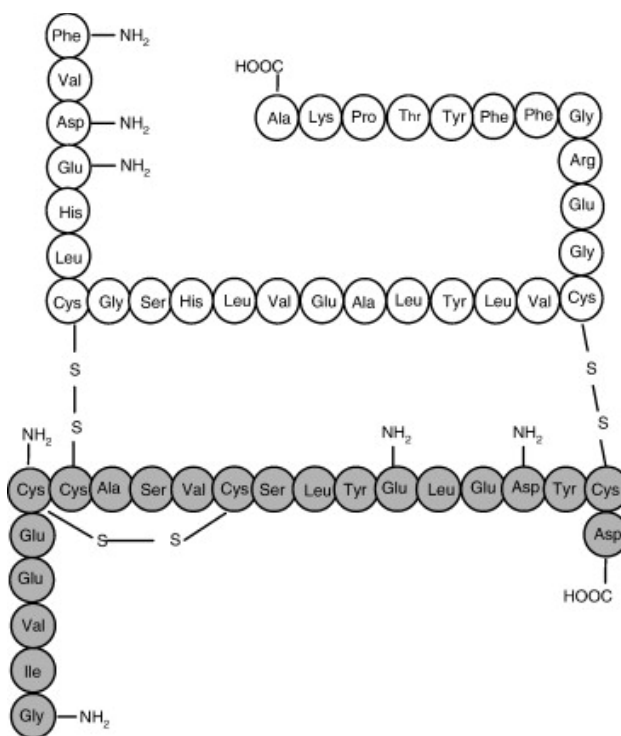


**Figure 1.1 The amino acid sequence of bovine insulin.**<sup>23</sup>

1950s. These studies gave the molecular mass of insulin to be between 6000-12,000 daltons.<sup>27; 28</sup> B.S. Harrap's paper in 1955 estimated the molecular mass around 6000 daltons by examining surface pressure-area isotherms of insulin with subphase having different ionic strengths.<sup>29</sup> In the 1960, Llopis and Rebollo's study examined insulin Langmuir monolayer on air-water, oil-water interface and with subphase of various pHs.<sup>30</sup> There were no more papers published on study of insulin Langmuir monolayer in that decade.

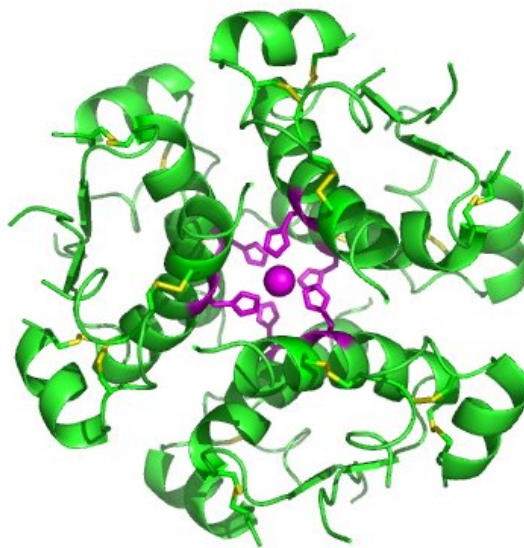


**Figure 1.2 Insulin is stored as a hexamers in the pancreas, held together by three zinc ions.**<sup>22</sup>

In 1976, K.S Birdi published his studies detailing interaction of insulin with lipid monolayers. This was the first Langmuir monolayer study of insulin since insulin's molecular mass had been determined to be 5807 daltons. Therefore, the surface area isotherm of insulin Langmuir monolayer in this study was reproduced and all future studies on insulin monolayer build on this study.<sup>31</sup> Insulin's interaction with lipids like spingomyelin and phosphatidycholine, salts, carbohydrates like glucose and enzymes like savinase has been studied by various groups since K.S Birdi's study.<sup>23; 32-40</sup> In this study on HI, chapters 2 and 3 examine HI Langmuir monolayer at air water interface in the presence of various concentrations of ions like  $ZnCl_2$  to propose a structure for the protein at air-water interface.

### 1.3 Carbon dots: An overview

For the past two decades, semiconductor quantum dots (QDs) like have increasingly emerged as an alternative to fluorescent dyes due to their high fluorescence and stability over a longer period of time.<sup>41-46</sup> However, applications of QDs in the area of drug delivery, bioconjugation and medicine have serious shortcomings due to the toxic nature of the composition of the quantum dots.<sup>47; 48</sup> QDs core is composed of semiconductor materials like Cadmium Selenium (CdSe) or Cadmium Tellurium (CdTe), these elements have been known to leach out with time and have been shown to be toxic to biological systems.<sup>49; 50</sup> Carbon dots are a new class of highly fluorescent nanoparticles, which are less than 10 nm in size. They have been touted as a replacement for toxic quantum dots due to their benign nature, which makes them an attractive tool for biological research. Carbon dots were first reported in 2004 as one of the three components of single walled carbon nanotubes (SWNT).<sup>52</sup> Scrivens' group was purifying SWNT by gel electrophoresis and found 3 bands, one of which was a fast moving band of highly fluorescent material. This material was characterized and found to make up 10% by mass of SWNT. The paper ends with the observation that the carbon dots, "promise to be interesting nanomaterials in their own right." Since then these nanoparticles called 'C-dots or carbon dots (CD) have been synthesized by various routes, surface modified and characterized by various groups to better understand their properties. Figure 1 is a timeline showing recent activity of carbon dots. Several studies using carbon dots in biological systems, including various embryos of various organisms have shown carbon dots to be non-toxic and a viable source for use in as a probe and for imaging.<sup>9-13</sup> However, effect of CD on protein fibrillation and aggregation in terms of their toxicity is

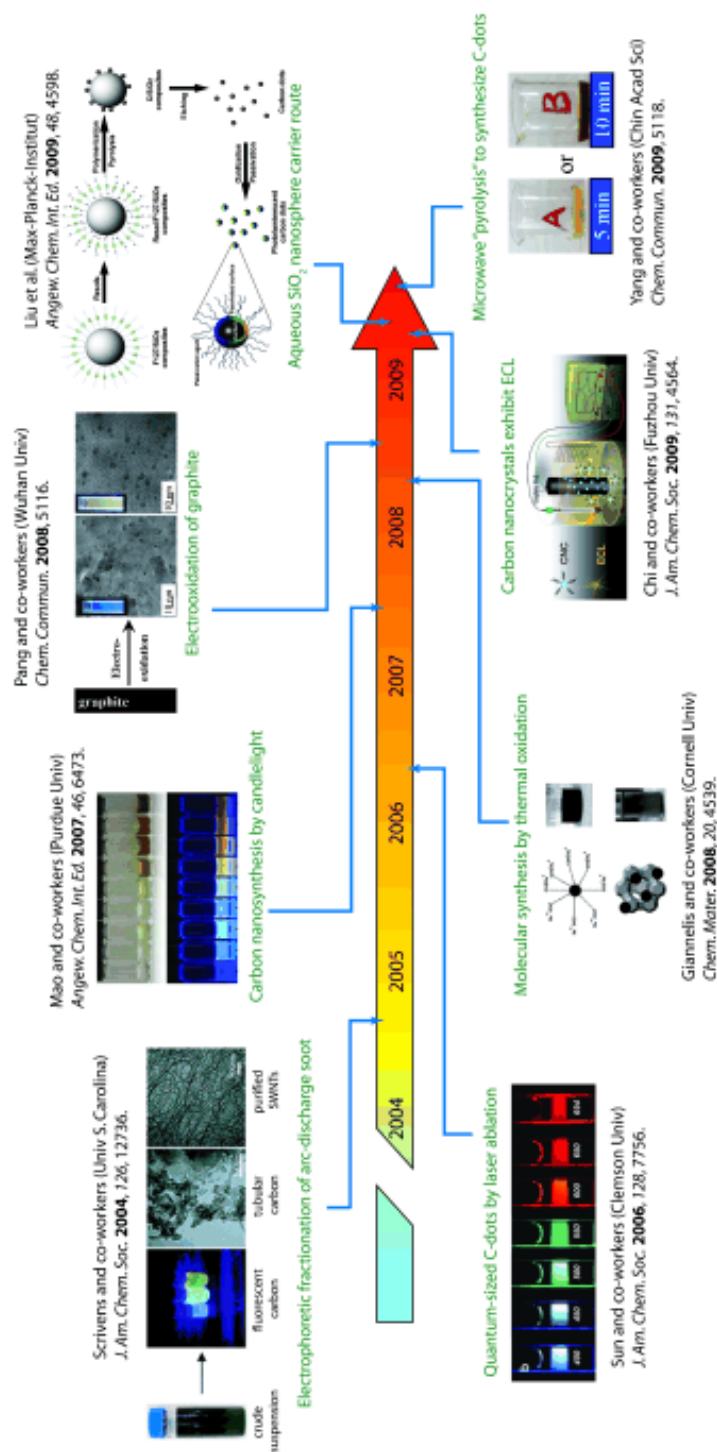


Figure 1.3 Timeline showing recent activity regarding carbon dots in the literature.<sup>51</sup>



an area which has not been investigated yet. Chapter 3 examines CD at air water interface as a Langmuir monolayer and chapter 6 investigates the effects of CD on HI fibrillation. Chapter one is the introduction chapter. It gives the overarching objective for this project.

Chapter two describes the instrumentation used for the experimentation. It discusses the Langmuir monolayer technique in detail. Synthesis of quantum dots and CD are also discussed in this section.

Chapter three describes in detail the surface chemistry of HI and spectroscopic techniques of the protein in solution and at air-water interface using Langmuir monolayer. Chapter three also looks at surface chemistry of CD at air-water interface focusing on stability of the carbon dots Langmuir monolayer and characterization of carbon dots Langmuir Blodgett film.

Chapter four describes influence of zinc ions on insulin aggregation at air-water interface using Langmuir monolayer. It examines the change in conformation of native insulin in different conditions and puts forward a model for the conformation of insulin molecules in aggregated and monomeric form at air-water interface.

Chapter five describes synthesis of gold Nanoclusters and CdS quantum dots with human insulin as the reducing agent. The effect of human insulin fibrillation on the synthesis of gold nanoclusters is examined. It explores the conditions where the most stable and high quality nanoparticles can be obtained.

Chapter six investigates the effect of CD on HI fibrillation through spectroscopy and imaging techniques.

## Chapter 2

### Materials and Instrumentation

#### 2.1 Materials

Recombinant human insulin (molecular weight 5807 Da) was produced in E.coli expression system and purified using affinity purification. Bovine serum albumin, human serum albumin, lysozyme, amyloid  $\beta$  (1-40) were the other proteins that were examined. DL- $\alpha$ -lipoic acid, cholesterol (Chol), acetone, methanol, chloroform, A $\beta$  (1-42), octadecane and dye thioflavin T were purchased from MP Biomedicals (Solon, OH)

Potassium chloride, zinc chloride, sodium sulfate, Trizma base, sodium hydroxide and hydrochloric acid were obtained from VWR Co. (Westchester, PA). NaOH (0.1 M) and HCl (1 M) were used for reaching different pH values. Cadmium oxide (CdO), selenium (Se), trioctylphosphine oxide (TOPO), trioctylphosphine (TOP), hexamethyldisilathiane [(TMS)<sub>2</sub>S] were purchased from Sigma-Aldrich (Milwaukee, WI). The tetradecylphosphonic acid (TDPA) was obtained from Alfa Aesar (Ward Hill, MA).

The diethylzinc (ZnEt<sub>2</sub>, 15 wt% solution in hexane) was obtained from Acros Organics (Morris Plains, New Jersey). Sphingomyelin (from bovine brain) (SM), monoganglioside (GM1), 1-palmitoyl-2-oleoyl-sn-glycero-3-phosphocholine (POPC) and 1,2-dipalmitoyl-sn-glycero-3-phospho-(1'-rac-glycerol) (sodium salt) (DPPG) were purchased from Sigma Aldrich (St. Louis, MO). All Chemicals were purchased commercially and used without further purification.

## 2.2 Instrumentation

### 2.2.1 Surface pressure and surface potential-area isotherm

A Kibron  $\mu$ -trough (Kibron Inc., Helsinki, Finland) with an area of  $5.9 \text{ cm} \times 21.1 \text{ cm}$  was utilized for the surface pressure–area ( $\pi$ – $A$ ) isotherm, compression–decompression cycles, and stability studies. Surface potential–area ( $\Delta V$ – $A$ ) isotherms were obtained on the Kibron trough using a Kelvin probe consisting of a capacitor-like system. The vibrating plate was set at approximately 1 mm above the surface of the Langmuir monolayer, and a gold-plated trough-base was used as a counter electrode.

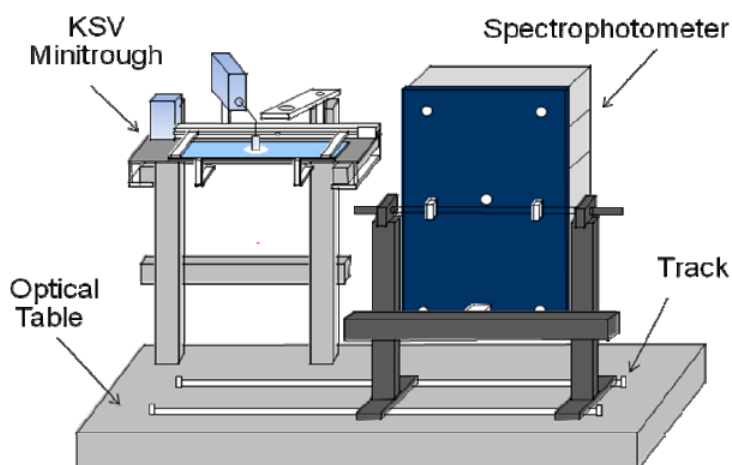


**Figure 2.1 KSV Langmuir minitrough suitable for surface pressure-area isotherm, UV-vis and fluorescence at the air-water interface.**<sup>53</sup>

Spectroscopic measurements at the air-water interface were obtained with an HP spectrophotometer model 8452 A for UV-vis and Fluorolog-3 spectrofluorimeter (Horiba Scientific, Edison, NJ) for fluorescence. Figure 2.1 shows the set up for spectroscopy at

air-water interface.<sup>53</sup> The fluorescence spectra of HI Langmuir monolayer at the air-water interface were measured using a bifurcated optical fiber with an area of 0.25 cm<sup>2</sup> and was placed 1 mm above the surface of the subphase. The excitation light was transmitted through the optical fiber from the light source to the Langmuir monolayer, and the emission light from the Langmuir monolayer was sent back to the detector through the optical fiber. UV-vis absorption and fluorescence spectra of aqueous solutions were recorded on a Perkin-Elmer Lambda 900 UV/vis/NIR spectrometer (Norwalk, CT) and Fluorolog-3 spectrofluorimeter (same as the one used for Langmuir monolayer) using a quartz cuvette of 1 cm optical path length, respectively.

### **2.2.2 Langmuir monolayer: surface tension and surface pressure**

Langmuir monolayer is one of the major model membrane systems when molecules forms film at air-water interface. It is named after Irvine Langmuir who introduced this technique.<sup>54; 55</sup> The basic and widely used technique to characterize a Langmuir monolayer is the surface pressure ( $\pi$ ) – area (A) isotherm, which is a plot of the change in surface pressure as a function of the area available to each molecule on the aqueous subphase surface.

Surface Tension is a sum of the cohesive energy present at the air-water interface. In solution, the molecules of a liquid are attracted to each other and therefore, are balanced by an equal attractive force in all directions. However, at air-water interface, molecules of a liquid experience an imbalance of forces as shown in Figure 2.2. At air-water interface, the molecules' energy is expressed as the ratio of energy to area and is defined as:

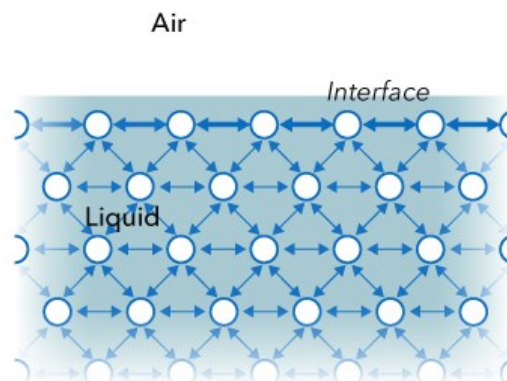


**Figure 2.2 Illustration of unequal forces at the interface responsible for surface tension.**<sup>56</sup>

$$\gamma = (\Delta G/S)_{T,P,n_i} \quad (2.1)$$

where  $\gamma$  is the surface tension that is defined by the smallest change in free energy ( $\Delta G$ ) per unit area ( $S$ ) under constant temperature ( $T$ ), pressure ( $P$ ) and number of moles of the components ( $n_i$ ). Surface pressure is measured by measuring the surface tension using the Whilhemmy plate method. In this method, the Whilhemmy plate is partially immersed in subphase and the force due to surface tension on the plate is measured.

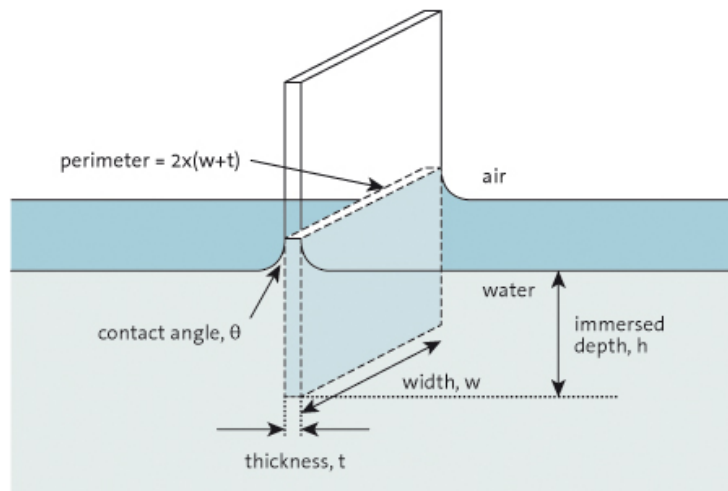


**Figure 2.3 Illustration of Whilhemmy plate at air-water interface**<sup>56</sup>

The plate is thin and usually made of platinum, but even plates made of glass, quartz, mica and filter paper can be used. In the experiments performed, the plates made of platinum and filter paper were used. There are two downward forces acting on the plate, namely surface tension and gravity. Buoyancy due to displaced water is the upward acting force. For a rectangular plate of dimensions  $l_p$ ,  $w_p$  and  $t_p$ , of material density  $\rho_p$ , immersed to a depth  $h_l$  in a liquid of density  $\rho_l$ , the net downward force is given by the following equation:

$$F = \rho_p g l_p w_p t_p + 2\gamma(t_p w_p)(\cos\theta) - \rho_l g t_l w_l h_l \quad (2.2)$$

where  $\gamma$  is the liquid surface tension,  $\theta$  is the contact angle of the liquid on the solid plate and  $g$  is the gravitational constant. The surface pressure is then determined by measuring the change in  $F$  for a stationary plate between a clean surface and the same surface with a monolayer present. If the plate is completely wetted by the liquid (i.e.  $\cos\theta = 1$ ) the surface pressure is then obtained from the following equation:

$$\Pi = -\Delta\gamma = -[\Delta F / 2(t_p + w_p)] = -\Delta F / 2w_p, \text{ if } w_p \gg t_p. \quad (2.3)$$

The sensitivity can thus be increased by using a very thin plate. The force is in this way determined by measuring the changes in the mass of the plate, which is directly coupled to a sensitive surface pressure sensor.<sup>57</sup> An idealized surface pressure-area isotherm is showed in Figure 2.3. As the pressure increases, the two-dimensional monolayer goes through different phases that have some analogy with the three-dimensional states, i. e.

gas, liquid, and solid. If the area per molecule is sufficiently large, then the floating film will be in a two-dimensional gas phase where the surfactant molecules are not interacting. Generally, the state of the monolayer on the water surface is monitored by measuring the surface pressure ( $\pi$ ), defined as the difference between the surface tension of the pure subphase ( $\gamma_0$ ) and the monolayer at the air-water interface ( $\gamma$ ):

$$\pi = \gamma_0 - \gamma \quad (2.4)$$

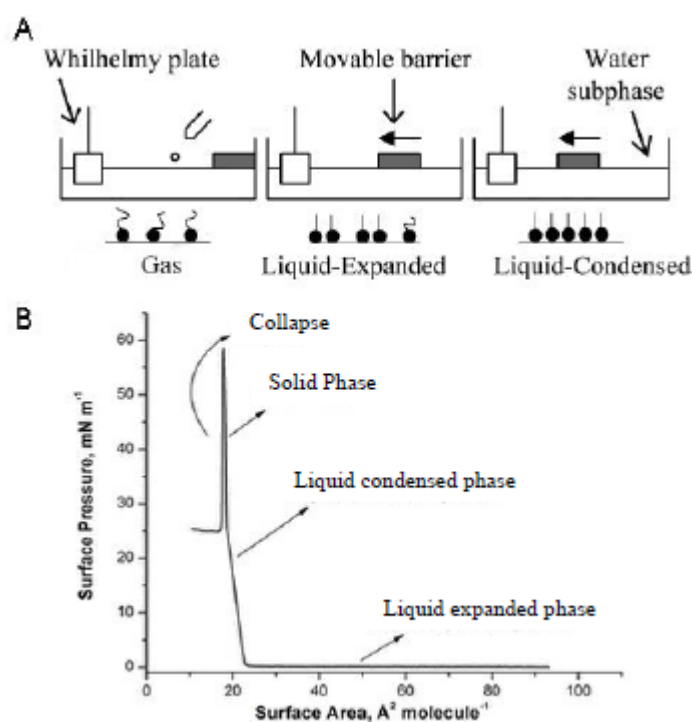


**Figure 2.4 Compression of a Langmuir monolayer. (A) Scheme of a Langmuir trough as the movable barrier reduces the area available to the monolayer. (B) Idealized surface pressure-area isotherm indicating phase transitions of the Langmuir monolayer.<sup>58</sup>**

The compound must be dissolved completely in a volatile inert solvent. The solution is then spread usually in microliter amounts using a syringe at the air-water interface between the two movable barriers. 10 to 15 minutes are required for the solution to

evaporate and the molecule to be at the air-water interface. The barriers are then compressed at a constant rate which results reorganization and reorientation of the molecule at the air-water interface. As the barriers continue compressing the monolayer of the molecule, the molecule undergoes phase transitions and finally collapse due to formation of multiple monolayers. Figure 2.4 shows the different states of the monolayer for the molecule of stearic acid dissolved in chloroform. As soon as stearic acid is spread at air-water interface, the stearic acid molecules are in a gaseous phase (G) as the molecules are floating on the air-water interface and are far apart from each other and are not interacting with each other. When the barriers are compressed at a constant rate, the area per unit molecule decreases and the surface pressure increases. This results in stearic acid molecules coming closer to each other. There is a change in phase from gaseous phase (G) to liquid- expanded (LE) which is comparable to three-dimensional liquid.

As the barriers continue compression, the stearic acid molecules phase transition from liquid-expanded (LE) to liquid- condensed (LC) occurs. In this phase, the molecules are in a close-packed vertically oriented chains. As the surface pressure is high,, the molecular area corresponds to true cross-sectional molecular area and the compressibility is low. When the barriers continue to compress beyond the LC phase, the monolayer reaches the solid phase and reaches the collapse surface pressure which is the least area where the molecule can form a stable monolayer. Beyond the collapse surface pressure, the monolayer collapses and there is a steep decrease in surface pressure. Extrapolating the solid phase monolayer to zero surface pressure gives the limiting molecular area (LMA) of stearic acid which corresponds to the most closely area occupied by one molecule of stearic acid.



### 2.2.3 Langmuir-Blodgett (LB) or Langmuir-Schaeffer (LS) film

Before the collapse of a monolayer, it can be deposited onto a solid support such as glass or quartz slide, silicon wafer, or other substrate. The deposited film is called Langmuir-Blodgett (LB) or Langmuir-Schaeffer (LS) film, depending on whether the deposition method is vertical dipping or horizontal lifting illustrated in Figure 2.5.<sup>59</sup>

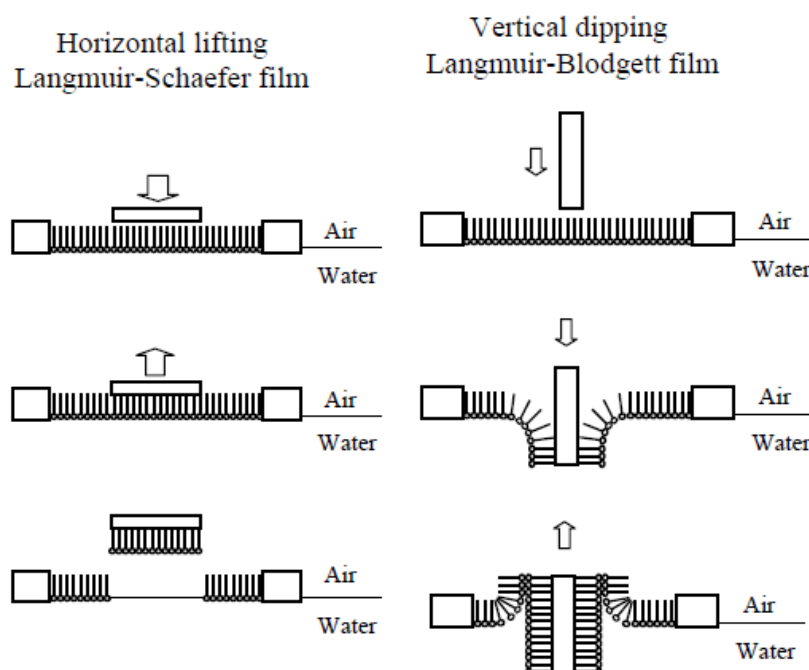


**Figure 2.5 Langmuir-Schaeffer and Langmuir-Blodgett film deposition of monolayers from the air-water interface to solid hydrophobic support.**<sup>58</sup>

The optimal condition for a successful deposition of LB film on a solid support is maintaining a constant surface pressure between 10 mN/m and the collapse surface pressure. The ratio between decrease in area of the monolayer and the area coated by the monolayer is expected to be closer to 1 in a successful LB film deposition. The substrate

is held mechanically by a clamp and dipped into the subphase. Once the needed surface pressure is obtained, the substrate is withdrawn from the subphase at a speed of 1 mm/min and left to air dry for 30 minutes. If the surface pressure remains constant, the substrate can be dipped again in the subphase for multiple layers of film. In contrast to LB film, LS film is quicker and prone to more experimental error. The substrate is held with a tweezer and held parallel to the subphase and manually lowered until it touched the subphase. This might take a few seconds. Usually multilayers of film are not deposited in LS technique.

As an example, the LB film of carbon dots was examined on a quartz slide. The slide has been dipped in the water subphase and the carbon dots spreading solution was deposited at air-water interface. After formation of Langmuir monolayer and the needed surface pressure, the slide was slowly pulled away from the trough. The quartz slide now has one layer of carbon dots on it and was left to dry for 1 hour. For multiple layers of carbon dots, this process can be repeated. The LB slide can be examined by UV-vis, fluorescence, circular dichroism and atomic force microscopy.

#### **2.2.4 Conditions for preparation of a Langmuir monolayer**

There are three main criteria while preparing a Langmuir monolayer namely 1) the environment of the experiment, 2) the subphase to be used, 3) and the spreading solvent. The Langmuir monolayer preparations should preferably take place in a clean room with constant temperature and humidity. Increase in either temperature or humidity can prevent monolayer from forming. As most molecules for Langmuir monolayer preparation are used in low concentrations (1-0.1 mg/ml), it essential that the solvents

and compounds used are not contaminated. The barriers, trough and Wilhemy plate must be cleaned before each experiment.

Human insulin solution used in the Langmuir monolayer experiments had a concentration of 0.30 mg/mL and was prepared by dissolving human insulin powder in aqueous HCl solution (pH 2). For all experiments performed as Langmuir monolayer, the subphase (pure water) was at pH of 5.6. The volume of the human insulin spreading solution was 80 and 40  $\mu\text{L}$  for Kibron and KSV troughs, respectively. The HI solution was spread at the air–water interface, using a 100  $\mu\text{L}$  syringe (Hamilton Co., Reno, Nevada) by small droplet deposition uniformly over the subphase surface, followed by a 15 min waiting time period for the Langmuir monolayer to reach equilibrium. The compression rate was set at 10  $\text{mm}\cdot\text{min}^{-1}$ . All the isotherms and in situ UV-vis, fluorescence and IRRAS spectroscopic measurements were conducted in a clean room (class 1000) where temperature ( $20.0 \pm 0.5$  °C) and humidity ( $50\% \pm 1\%$ ) were kept constant.

Proteins, protein fibers and carbon dots were analyzed using Langmuir monolayer methodology and will be discussed in details in the coming chapters.

### **2.2.5 Epifluorescence microscopy**

Epifluorescence microscopy was employed to visualize the formation of domains in a Langmuir monolayer, if any. Figure 2.6 shows the internal view of the microscope.<sup>53; 60</sup> The microscope requires a Langmuir trough to be placed on top of the sample stage. A quartz window allows the excitation light to penetrate the subphase so that one could excite the fluorophore at the air-water interface. The experimental setup used a Kibron  $\mu$ trough (Kibron Inc., Helsinki, Finland) combined with an epifluorescence microscope

(Olympus IX-FLA). The area available for the spreading solution was  $5.9 \text{ cm} \times 21.1 \text{ cm}$ . The epifluorescence image was captured by a thermoelectrically cooled Optronics Magnafire™ CCD camera.

Epifluorescence microscopy is used to visualize the presence of domains or aggregates in a Langmuir monolayer. The change in monolayer with phase transitions is another area that can be visualized using epifluorescence. Epifluorescence can be used only if the molecule has a

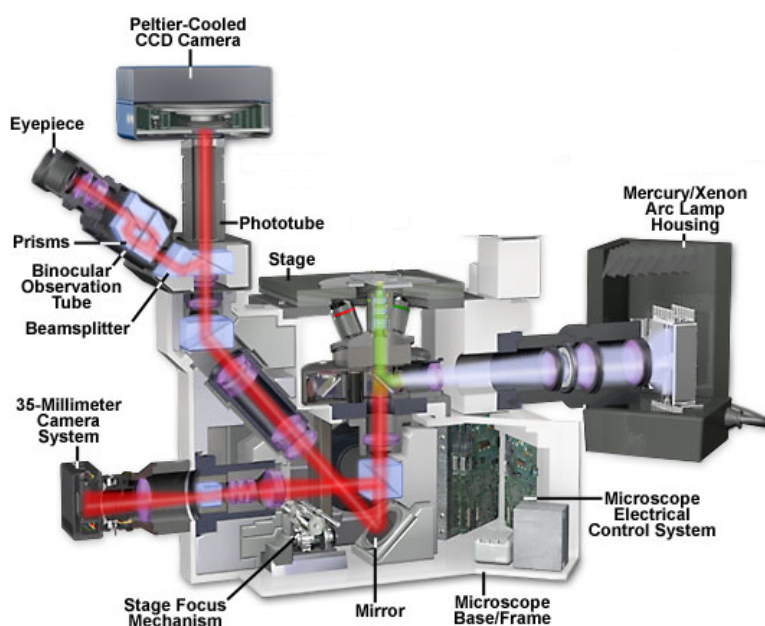


**Figure 2.6 Internal view of Olympus IX70 inverted microscope<sup>53: 60</sup>**

fluorophore like 5-octadecanoylamino fluorescein (ODFL). If a molecule does not have a built in fluorophore, a fluorophore can be attached to the molecule. In this study, insulin was examined by epifluorescence. Insulin on its own cannot be visualized by epifluorescence due to lack of a built in a fluorophore and therefore, fluorescein isothiocyanate (FITC) was attached to insulin to visualize it.

## 2.2.6 Brewster angle microscopy

Brewster Angle Microscopy (BAM) was used to visualize the topography of the Langmuir monolayer. The measurements were performed using the IELLI-2000 imaging ellipsometer with the compensator turned off and BAM2plus software. The standard laser of the IELLI2000 system is a frequency doubled Nd-YAG laser (50 mW output) using the 532 nm line.<sup>61</sup>

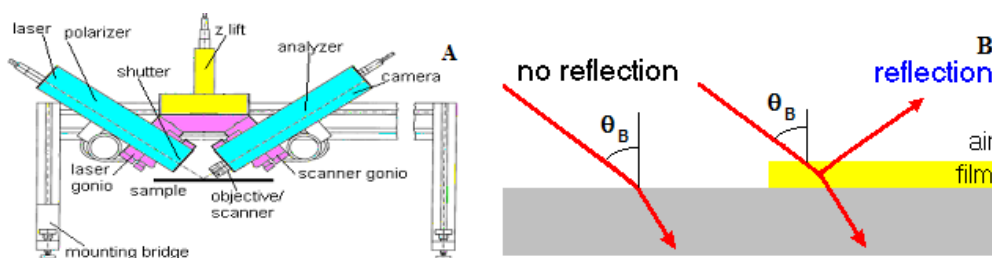


**Figure 2.7 Diagram of the IELLI-2000 imaging ellipsometer design (A) and diagram showing the Brewster angle for water (no reflection) and change in reflection when monolayer is present (reflection is present).<sup>61</sup>**

Figure 2.7 A shows the instrument components. BAM provides topographical information on the monolayer. It uses the different refractive index intrinsic to molecules as an important property for examination of a monolayer. When a light beam is applied at the air-water interface, the reflection light is monitored by the camera. The beam will not be reflected by the water and this will be observed as a dark field for the image. In the presence of a monolayer, a bright region will be seen by the camera as shown in Figure 2.7 B. The brightness of the monolayer is influenced by the refractive index of the molecules composed in the monolayer.

### 2.2.7 Circular dichroism

Circular dichroism (CD) spectra were obtained using a JASCO J-810 spectropolarimeter. The spectra were recorded between 195 and 250 nm at 25°C using a 2.0 mm optical path length quartz cell. Circular dichroism can give information about chirality of molecules and in case of proteins for this study, the secondary structure of protein.<sup>62</sup> Figure 2.8 shows the curves for 5 different secondary protein structures. Usually proteins are a mixture of a few different secondary structures.

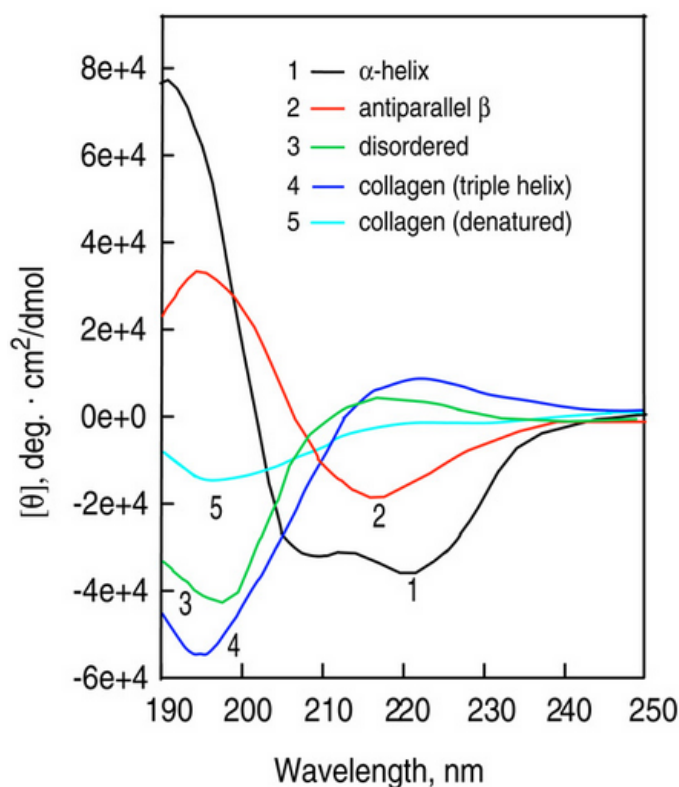


**Figure 2.8** CD spectra of proteins representative of 5 different secondary structure.<sup>63</sup>

### 2.2.8 Infrared microscopy: Bio-ATR and IRRAS

The infrared spectrum of an aqueous solution was obtained using attenuated total reflectance. With the Bio-ATR accessory, the aqueous sample was deposited on the ATR

crystal surface, and the IR spectrum was readily obtained. The static mode required only 15 – 20  $\mu\text{L}$  of aqueous solution however, the concentration of the aqueous solution should be larger than 0.5 mg/mL to assure a proper contact with the ATR crystal. A solid sample is placed on top of the ATR crystal for the spectra. A mercury-cadmium- telluride (MCT) detector (Kolmar Technologies) was used with a scanner velocity of 5 kHz. The background spectrum was pure water. The Bio-ATR cell II was placed in the cell compartment of a Bruker Optics Equinox55 FTIR.

Infrared reflection-absorption spectroscopy (IRRAS) measurements of the Langmuir monolayer were performed using an EQUINOX-55 Fourier transform infrared (FTIR) spectrometer (Bruker Optics, Billerica, MA) equipped with an XA-511 external reflection accessory suitable for the air–water interface experiments. The IR beam was focused at the air–water interface of the Kibron  $\mu$ -trough. The reflected IR beam went to a HgCdTe (MCT) detector cooled by liquid nitrogen. The spectra were acquired with a resolution of  $8\text{ cm}^{-1}$  by coaddition of 1200 scans for p-polarized and 800 scans for s-polarized IRRAS.

Infrared spectroscopy is usually used for identification of functional groups that are IR active.<sup>64</sup> In this study, protein structure and conformation was examined by following the amide I and amide II bonds present in the proteins.<sup>65</sup> IRRAS measurements were obtained as reflectance–absorbance (RA) vs wavenumber. RA is defined as  $-\log_{10}(R/R_F)$  where R is the reflectivity of the film covered surface and  $R_F$  is the reflectivity of the water.<sup>66</sup> When the vibrations are parallel to the air–water interface, for p-polarized radiation, which is parallel to the plane of incidence, the bands are initially negative and their intensities increase as the incident angle is increased until the Brewster angle ( $54.5^\circ$  for  $2920\text{ cm}^{-1}$  of IR radiation) is reached . By using IRRAS at different surface pressures,

we investigated the change of orientation and conformation of HI Langmuir monolayer . IRRAS was used to analyze structural features of the proteins, such as  $\alpha$ -helix and  $\beta$ -sheet interpreted through amide I and amide II bands in the region of 1700–1600 and 1600–1500  $\text{cm}^{-1}$ , respectively.<sup>67; 68</sup>

### 2.2.9 Atomic force microscopy

The Atomic Force Microscopy (AFM) experiments were performed on an Agilent 5420 AFM unit using AC (tapping) mode. Figure 2.9 shows the diagram of AFM. The tip had

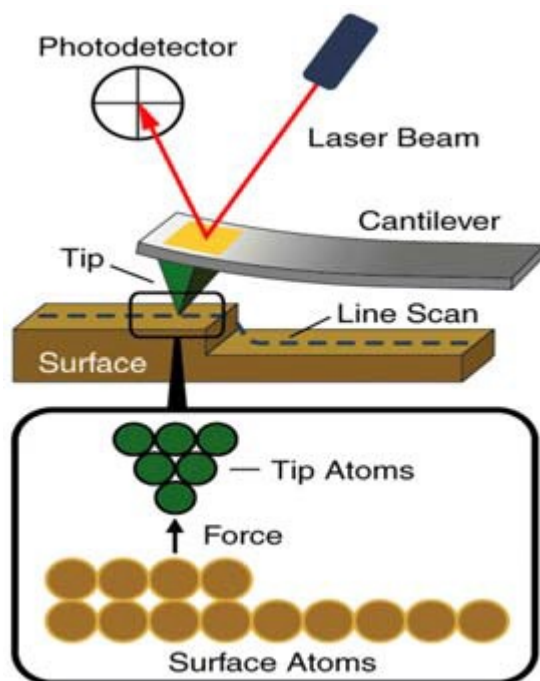


**Figure 2.9 Diagram of atomic force microscope**

a resonant frequency of 159.6 kHz, a tip radius of  $< 10$  nm, and a force constant of 27 N/m. All images were taken with a resolution of 512 x 512 points/line. Transmission Electron Microscopy (TEM) measurements were taken with a Philips CM-10 TEM



operated at 80 kV. Micrographs were taken with a Gatan digital camera.<sup>69</sup>The two main components of an AFM are the laser beam and the detector. Firstly, laser beam hits the tip of the cantilever. Secondly, the contact of the cantilever with the film on the substrate will change the reflected beam and thirdly, the reflected beam is captured by the photodetector. AFM was used in this study to examine LB films on a quartz slide.

## **2.3 Procedures**

### **2.3.1 Insulin fiber formation**

Insulin (1mg/ml) in a pH 2 buffer was stirred constantly at 37 C. Aliquots were taken at intervals and examined by ThT fluorescence, Congo Red UV-vis, TEM and AFM. Insulin mixed with carbon dots and insulin mixed with CdSe quantum dots were examined to compare the effect on fibrillation.

### **2.3.2 Preparation of congo red and thioflavin T**

Thioflavin T binding assays were conducted by first preparing a 1 mM Thioflavin T stock solution in 1× PBS buffer and stored at 4° C and protected from light until usage. Aliquots of protein solutions were diluted 50-fold into the Thioflavin T stock solution (the final Thioflavin T concentration was 20 μM). Fluorescence sample measurements used a quartz cuvette with a 10 mm optical path length. Wavelength measurements were taken from 460- 700 nm using an excitation wavelength of 450 nm. Emission and excitation slit widths were typically 5 nm. All fluorescence intensity measurements were background corrected with a 20 μM Thioflavin T solution that did not contain protein. The fluorescence emission spectra of the protein were

taken to analyze the conformational variation of the Trp residue of the insulin protein. Fluorescence sample measurements used a quartz cuvette with a 10 mm optical path length. Wavelength measurements were taken from 300- 500 nm using an excitation wavelength of 295 nm. Emission and excitation slit widths were typically 5 nm. Absorption spectra of the protein solution in the presence of the Congo red dye were compared with that of the Congo red buffer alone and the protein solutions in the absence of the Congo red dye.

### **2.3.3 CdSe QD synthesis and capping of QDs with DHLA**

CdSe/ZnS quantum dots (QDs) were synthesized using already given protocol.<sup>70</sup> Briefly, cadmium oxide was reacted with a selenium reagent in the presence of a phosphine oxide surfactant at high temperature under argon flow. After the formation of the CdSe core, the diethyl zinc and hexamethyldisilathane in TOP were added drop-wise at 130 °C. After the synthesis of TOPO-capped hydrophobic QDs modification to hydrophilic DHLA- and PEG-capped QDs was carried out.

Briefly, DL- $\alpha$ -lipoic acid (1g) was reduced using sodium borohydride (2 g) in methanol and water. After workup product was isolated in chloroform and characterized using <sup>1</sup>H NMR (400 MHz, CDCl<sub>3</sub>):  $\delta$  (ppm) 1.3 (d, 1H), 1.35 (t, 1H), 1.4- 1.8 (m, 6H), 1.9 (m, 2H), 2.4 (t, 2H), 2.6 2.8 (m, 2H), 2.9 (m, 1H), 11 (s, 1H). DHLA was used for ligand exchange with TOPO, excess of DHLA (0.5 g) was added in 5 ml of TOPO-capped QDs in methanol and heated at 60-70 °C for 4 hour. The QDs solution was basified using potassium tert-butoxide and centrifuged to get the precipitate. The precipitate was suspended in water to obtain the hydrophilic QDs. These water soluble quantum dots were filtered through 0.2  $\mu$ m filter to get the clear solution.

### **2.3.4 Synthesis of carbon dots**

Carbon dots were synthesized according to given protocol.<sup>71</sup> To synthesize hydrophobic carbon dots, 15 ml octadecane and 1.5 g 1-hexydecylamine (HAD) were heated until stabilized at 300 C under argon atmosphere and then 1 g citric acid was quickly injected into the mixture. The carbon dots was purified with acetone and characterized by UV-vis and fluorescence spectroscopy, AFM and TEM microscopy. To make hydrophilic carbon dots, PEG and glycerine were used in place of octadecane and HAD. The sample was purified by running down a sephadex column.

### **2.4 Summary**

Chapter 2 describes the methods and equipments used to perform experiments in the different chapters. The procedures for synthesis of QDs and carbon dots are mentioned in this chapter. The experimental procedure for preparation of the solutions for fibrillation and surface chemistry experiments are described in detail.

## Chapter 3

### Human Insulin and Carbon Dots: Surface Chemistry and Spectroscopy

#### 3.1 History and background

Human insulin (HI) is a peptide hormone which is produced in islets of Langerhans and its main function in the human body is to control blood glucose level. Since the discovery of insulin, diabetes has become treatable. HI is composed of two polypeptide chains, an A chain with 21 residues and a B chain with 30 residues, linked together by two disulfide bonds.<sup>72</sup> Figure 3.1 shows the amino acid structure of HI.

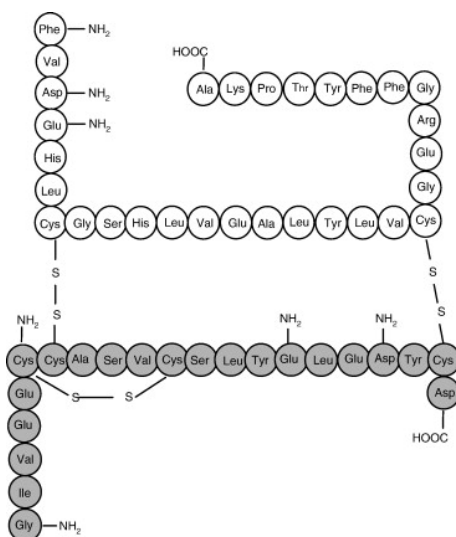


**Figure 3.1** The amino acid sequence of bovine insulin.<sup>23</sup>

Besides the monomeric structure of HI, it is also found to exist as dimers, hexamers and amyloids. As a monomer, majority of the structure of HI is composed of an  $\alpha$ -helical

structure and it dimerizes through the formation of  $\beta$  sheet.<sup>73</sup> HI is often found having a dimer structure which is due to hydrogen bonding between the C terminus of B chains. HI dimers come together to form hexamers in the presence of zinc ions.<sup>74</sup> Monomers and dimers readily diffuse into blood, whereas hexamers diffuse poorly. Hence, absorption of HI preparations containing a high proportion of hexamers is delayed and somewhat slow.<sup>75</sup> Figure 3.2 shows the proposed structure of a hexamers of insulin. HI amyloid is characterized by  $\beta$  sheet.<sup>76</sup> Tissue deposition of normally soluble proteins as insoluble amyloid fibrils is associated with serious diseases including the systemic amyloidoses, maturity onset diabetes and Alzheimer's disease.<sup>77</sup> In vitro, HI is readily converted to an inactive fibrillar form by incubation at high HI concentrations, low pH and high temperatures.<sup>76</sup>

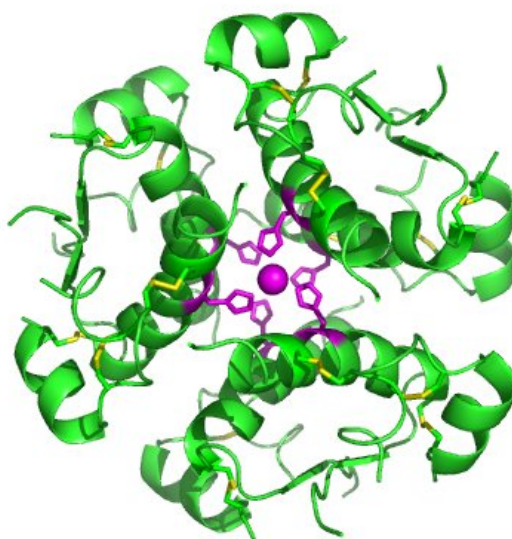


**Figure 3.2** Insulin is stored as a hexamers in the pancreas, held together by three zinc ions.<sup>22</sup>

Interactions of proteins like HI with human cellular membrane can be studied by using Langmuir monolayer methodology.<sup>6</sup> Langmuir monolayers are used as in vitro model of biological membranes.<sup>78</sup> This technique allows us to study intermolecular interactions between molecules spread at the interface which form the monolayer. In this method, HI dissolved in acidic solution is first spread onto a water surface to form the Langmuir or floating monolayer. Monolayer formation is usually monitored with the surface pressure ( $\pi$ )-area(A) isotherm.<sup>8-10</sup> Surface pressures ranging between 30 and 35 mN/m are commonly found in the natural biomembrane, and can be simulated on the Langmuir monolayer to mimic human cell membrane.<sup>7</sup> One of the earliest studies employing this technique was published in 1954 and it reported the change in insulin surface pressure with change in pH.<sup>79</sup> A series of studies on insulin Langmuir monolayer reported the effect of temperature, monolayer composition and nature of cations in the subphase.<sup>3,12-17</sup> Insulin Langmuir-Blodgett (LB) films on mica slides have been also studied by atomic force microscopy (AFM).<sup>18</sup>

The present study brings new data on the optical properties of the HI Langmuir monolayer. UV-vis at air-water interface correlates with the surface pressure-area isotherm curve. Domain formation in 2-D was not observed based on the Brewster Angle and epifluorescence microscopies of HI and FITC-labeled HI Langmuir monolayer, respectively. One has observed through IRRAS measurements that the protein conserves an  $\alpha$ -helix conformation in 2-D, knowing that, the IRRAS approach permits detection of the amide I and amide II bands, which correlates with the  $\alpha$ -helix and  $\beta$ -sheet in the protein sample.

## 3.2 Surface chemistry of human insulin

### 3.2.1 Surface pressure and surface potential area isotherms

The surface pressure and surface potential-area isotherms of the HI Langmuir monolayer are shown in Figure 3.3. The lift-off of the surface pressure and surface potential correspond to 750 and 900  $\text{\AA}^2 \text{ molecule}^{-1}$ , respectively. One would expect to observe a lift-off at a larger area for the surface potential compared with the surface pressure. This is due to the long range interaction of the surface dipoles compared to the van der Waals interaction, which is mainly measured by the surface pressure. With regard to the limiting molecular area, that is the extrapolation of the linear part of the surface pressure –area isotherm to zero surface pressure, a value of 620  $\text{\AA}^2 \text{ molecule}^{-1}$  is obtained. This area

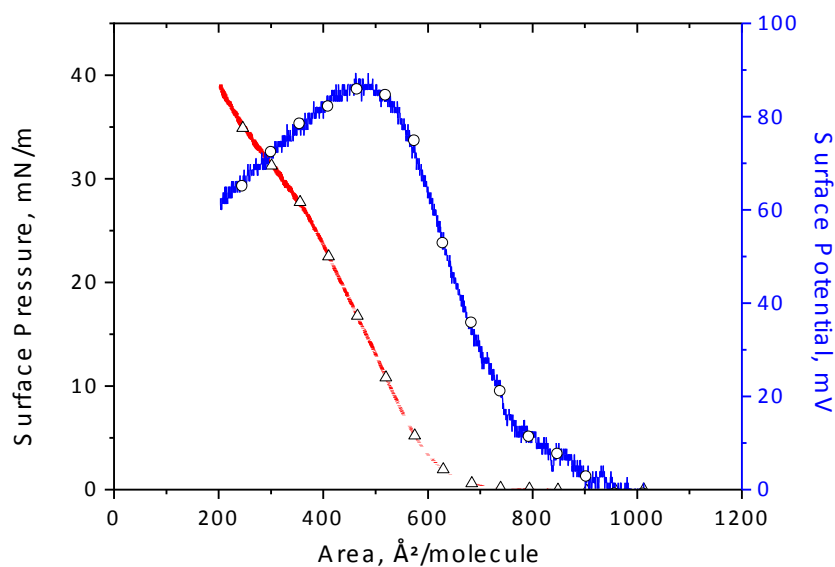


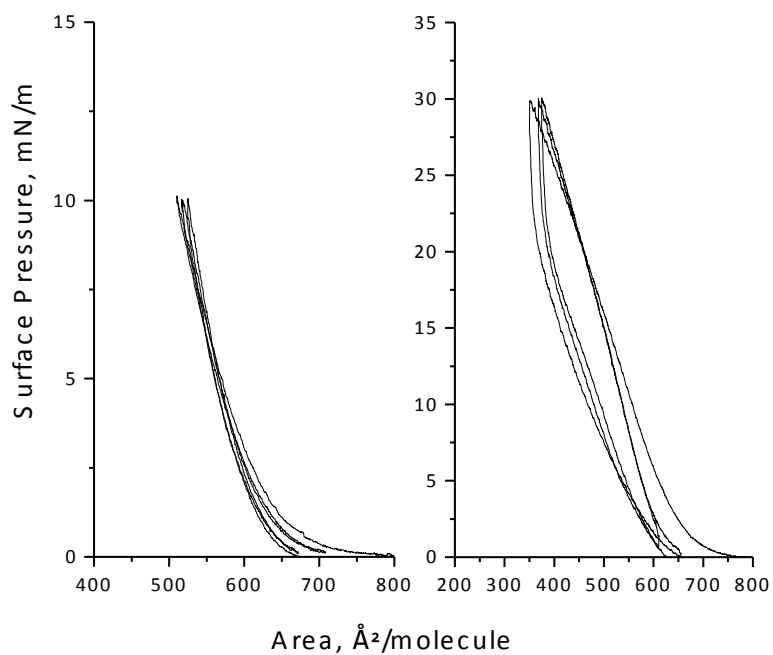
**Figure 3.3** Surface pressure–( $\Delta$ ) and surface potential–area (o) isotherms of human insulin Langmuir monolayer at subphase pH 5.6.

corresponds to the most compact state of the HI protein at the air-water interface, a value in line with previous published studies on bovine insulin Langmuir monolayer.<sup>23; 32; 33</sup> Decreasing the molecular area from 750, one observes a gaseous to liquid expanded phase transition in the surface pressure - area isotherm. Further decrease from 585 to 350 shows the liquid condensed phase of the Langmuir monolayer. One reaches the collapse surface pressure  $25.2 \text{ mN m}^{-1}$ . The surface pressure measurement till collapse shows a linear increase in the  $\pi$ -A isotherm.

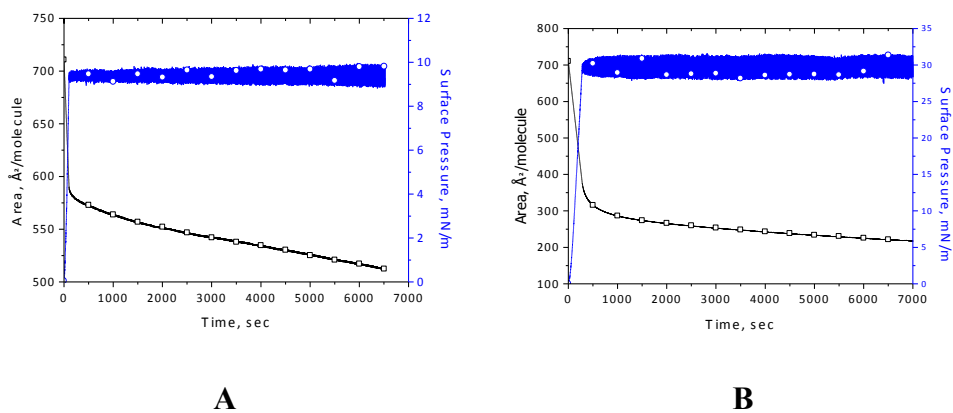
### **3.2.2 Compression-decompression cycles and stability isotherms of human insulin Langmuir monolayer**

Figure 3.4 presents the compression-decompression cycle isotherms measured at two target surface pressures, namely  $10$  and  $30 \text{ mN m}^{-1}$ . The rationale to choose these two surface pressures was to observe the stability of the film in a liquid condensed film before and after the collapse surface pressure. After the compression-decompression cycles from  $0$  up to  $10$  and  $30 \text{ mNm}^{-1}$ , one observes a variation of less than  $5$  and  $10\%$  between the initial compression and last decompression (third cycle), respectively. This result indicates that the HI protein remains at the interface. It has to be mentioned that the cycles up to  $10 \text{ mNm}^{-1}$  showed an overlap of the isotherms which supports the interpretation that the insulin protein might keep its conformation in the liquid expanded and condensed phases. Regarding the stability of the HI Langmuir monolayer (Figure 3.5), one has observed the decrease in area with time when the monolayer was kept constant at  $10$  and  $30 \text{ mN m}^{-1}$  during a  $6500 \text{ s}$  time period. A decrease of  $15$  and  $60\%$  was measured for the  $10$  and  $30 \text{ mN m}^{-1}$ , respectively. One would expect a large decrease at the collapse surface pressure. Possibility of aggregation of HI was studied by





**Figure 3.4** Three compression-decompression cycles up to a surface pressure of 10 and 30 mN/m of human insulin Langmuir monolayer at subphase pH 5.6.



**Figure 3.5** Stability measurements at surface pressure 10 (A) and 30 mN/m (B) held for 90 minutes for human insulin Langmuir monolayer at subphase pH 5.6.

BAM, and conjugating HI with FITC, and will be discussed later.

### **3.2.3 UV-vis and fluorescence spectroscopy of human insulin in aqueous phase and Langmuir monolayer**

The photophysical properties of the HI were investigated in aqueous solution (pH 2) and as a Langmuir monolayer as shown in Figures 6 and 7, respectively. There is a correlation between the UV-vis spectra of HI in aqueous phase and in Langmuir monolayer, i.e. two bands observed at 224 and 276 nm. These bands are due to the tyrosine absorption, which is characteristic of phenol. There are 4 tyrosine amino acids in HI, which are responsible for the characteristic absorption spectrum shown in Figures 3.6 and 3.7. Our results correspond to the ones already reported for the tyrosine maxima (at pH 6) at 222 nm ( $\epsilon = 9.0 \times 10^3 \text{ M}^{-1} \text{ cm}^{-1}$ ) and 275 nm ( $\epsilon = 1.4 \times 10^3 \text{ M}^{-1} \text{ cm}^{-1}$ )<sup>80</sup>

The emission peak of aqueous HI (pH 2) was observed at 307 nm compared with values obtained in other work at pH 7, i.e. 303-305 nm. Although the UV-vis absorption spectrum is identical for the aqueous phase and Langmuir monolayer, one did not detect any fluorescence of HI Langmuir monolayer. The result is explained by the fact that the number of tyrosine moieties in the HI are quite low and the extinction coefficient at 276 nm is a relatively small value.

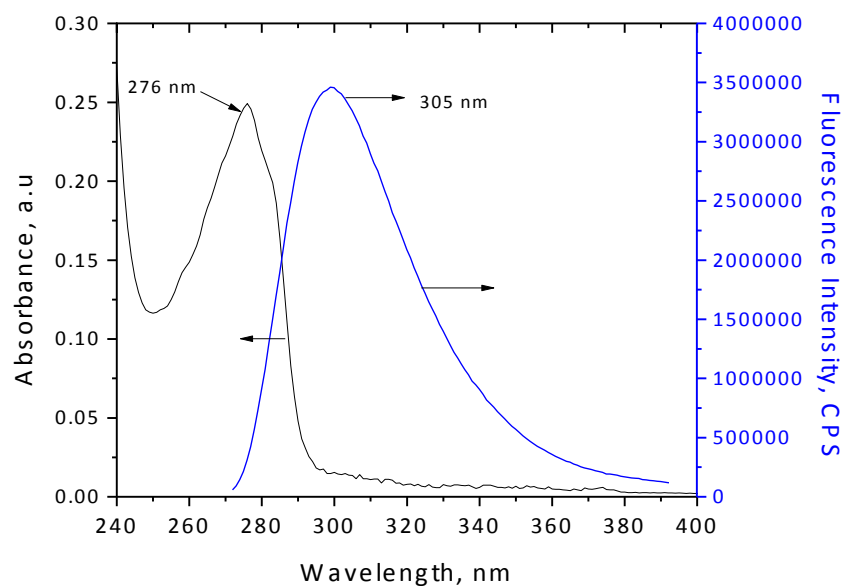


**Figure 3.6** UV-vis ( $5 \times 10^{-5}$  M) and fluorescence ( $5 \times 10^{-7}$  M;  $\lambda_{\text{excitation}} = 270$  nm, slit width at the excitation and emission, 5 and 5 nm, respectively) spectra of aqueous solution of human insulin.

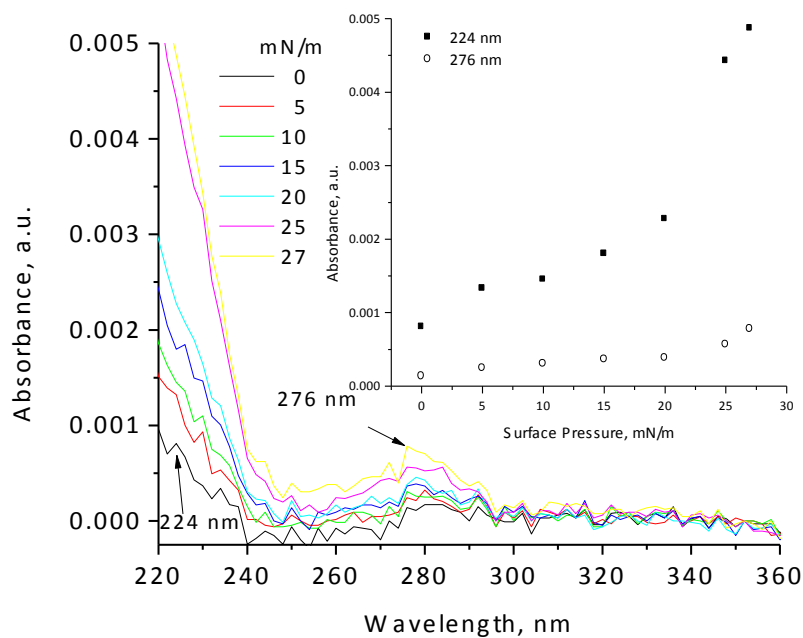


**Figure 3.7** UV-vis spectra of human insulin Langmuir at subphase pH 5.6. Inset shows the variation of the absorbance at 224 and 276 nm in function of the surface pressure.





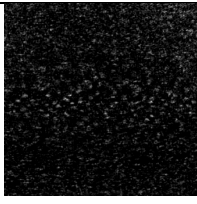
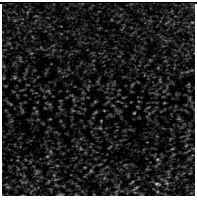
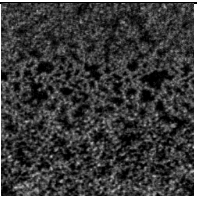
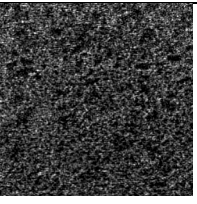
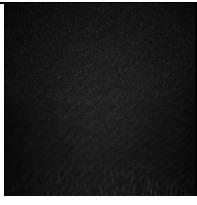
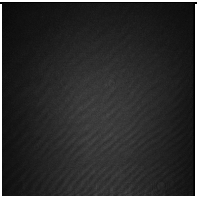
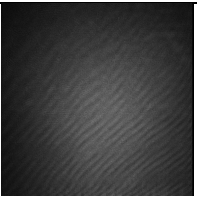
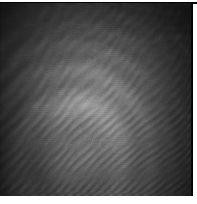
This interpretation could also be applied to the weak absorption at 276 nm for the HI Langmuir monolayer as shown in Figure 5. Increasing the surface pressure or the number of HI molecules per unit area does not show a larger absorbance at this wavelength. However, the inset of Figure 3.7 shows a steady increase in absorbance at 224 and 276 nm from 0 to 27 mN m<sup>-1</sup>, i.e. a region of surface pressure near the collapse surface pressure. Linearity in absorbance at air-water interface indicates stability of the HI monolayer till the collapse point.

The next section will look at the topography of the HI Langmuir monolayer in regards to the potential formation of domains in 2-D. Two methodologies were used for this observation, namely epifluorescence and Brewster angle microscopy.

### **3.2.4 Epifluorescence and brewster angle microscopy of human insulin Langmuir monolayer**

The topography of the human insulin Langmuir monolayer was examined using epifluorescence of the FITC-human insulin, whereas Brewster Angle was employed for pure human insulin in 2-D. Since insulin is weakly fluorescent as a Langmuir monolayer, one must attach a fluorophore to make use of the epifluorescence microscopy. The probe commonly used for proteins is fluorescein isothiocyanate (FITC).

Knowing the ratio of FITC-insulin (1:1), molecular weight was calculated to prepare the right concentration of aqueous solution to be spread at the air-water interface. Epifluorescence micrography was obtained at surface pressures of 5, 10, 20 and 30 mNm<sup>-1</sup> as shown in Table 3.1. A homogeneous HI Langmuir monolayer was observed at all surface pressures without any indication of the formation of domains in the  $\mu\text{m}$  range in

Measurements				
A) Epifluorescence: Insulin-FITC Langmuir monolayer Subphase: water (pH 5.6) (image size 895 x 713 $\mu\text{m}$ )				
	0 mN/m	10 mN/m	20 mN/m	25 mN/m
B) BAM Langmuir monolayer Arachidic acid (image size 200 x 200 $\mu\text{m}$ )				
	0	2	4	6
C) BAM: Insulin Langmuir monolayer Subphase: water (pH 5.6) (image size 200 x 200 $\mu\text{m}$ )				
	5	15	20	25

**Table 3.1** Four surface pressures of 10, 20, 30, and 40 mN/m were measured by A) Epifluorescence for a sample of HI-FITC Langmuir monolayer; B) BAM for insulin HI Langmuir monolayer; C) BAM for arachidic acid Langmuir monolayer. (Insulin concentration: 0.30 mg/ml).

the images. To verify this observation, Brewster angle microscopy (BAM) was employed to image the topography of the film at the same pressure as the epifluorescence ones. The BAM data confirms the epifluorescence measurements. To assure that the BAM system worked properly, the arachidic acid- Langmuir monolayer was examined. The topography observed corroborate the results already published. (Table 3.1)<sup>81</sup> To examine the nature of the interaction between insulin molecules in 2-D, the HI aqueous phase and Langmuir monolayer was examined by infrared spectroscopy. The FTIR and circular dichroism (CD) were studied for HI aqueous phase, whereas infrared reflection absorption spectroscopy (IRRAS) was used for the HI Langmuir monolayer.<sup>3.2.5. Examination of secondary-structure of insulin.</sup>

### **3.2.5 Secondary structure of human insulin at air-water interface**

#### **3.2.5.1 CD and FTIR examination of insulin in solution**

As shown in Figure 3.8, the CD spectrum contains a high proportion of  $\alpha$ -helix compared with  $\beta$ -sheet.<sup>82</sup> When analyzed by Softsec software, insulin was found to contain 75%  $\alpha$ -helix and 20%  $\beta$ -sheet. This indicates the presence of monomers and absence of aggregates in aqueous phase. Figure 3.9 shows the FTIR spectrum of aqueous HI with major peaks at 1650, 1542, 1440 and 1373  $\text{cm}^{-1}$ . Peaks at 1650 and 1542  $\text{cm}^{-1}$  correspond to amide I and amide II regions of  $\alpha$ -helix which are characteristic of  $\alpha$ -helix. <sup>66</sup>CD and FTIR spectra confirm that the aqueous HI exists as  $\alpha$ -helix, hence as a monomer in an aqueous phase.

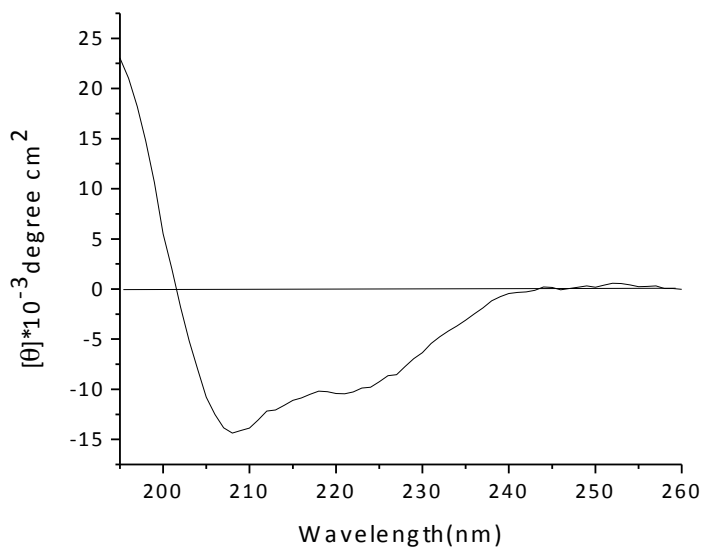


**Figure 3.8** Circular dichroism spectrum of aqueous insulin at pH 2 and temperature  $20 \pm 1$  °C. The concentration of the insulin was 0.3 mg/ml.

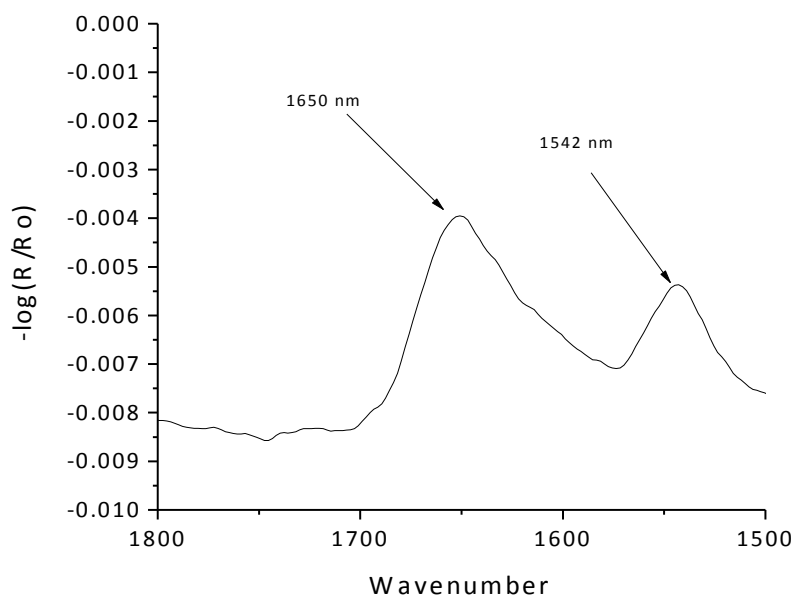


**Figure 3.9** FTIR spectrum of aqueous insulin at pH 2 and temperature  $20 \pm 1$  °C. The concentration of the insulin was 0.3 and 2 mg ml<sup>-1</sup>, respectively.

### 3.2.5.2 IRRAS examination of insulin Langmuir monolayer

IRRAS is an important technique to study the orientation and conformation changes of Langmuir monolayer at the air–water interface. IRRAS measurements were obtained as reflectance–absorbance (RA) vs wavenumber. RA is defined as  $-\log_{10} (R/R_F)$  where R is the reflectivity of the film covered surface and  $R_F$  is the reflectivity of the water. When the vibrations are parallel to the air–water interface, for p-polarized radiation, which is parallel to the plane of incidence, the bands are initially negative and their intensities increase as the incident angle is increased until the Brewster angle ( $54.5^\circ$  for  $2920\text{ cm}^{-1}$  of IR radiation) is reached. By using IRRAS at different surface pressures, we investigated the change of orientation and conformation of HI Langmuir monolayer (Figures 3.10, 3.11 and 3.12). IRRAS was used to analyze structural features of the proteins, such as  $\alpha$ -helix and  $\beta$ -sheet interpreted through amide I and amide II bands in the region of  $1700\text{--}1600$  and  $1600\text{--}1500\text{ cm}^{-1}$ , respectively.

Three IRRAS spectra are presented. Figure 3.10 shows p-polarization at 60 degrees at various surface pressures, Figure 3.11 shows a constant surface pressure of 10 mN/m and varying angles in a range from 30-70 degrees and Figure 3.11 shows s-polarization at a constant angle of 25 degrees with varying surface pressures. Table 3.2 gives the bands characteristic of  $\alpha$ -helix and  $\beta$ -sheet and Amide I and Amide II vibrations corresponding to  $\alpha$ -helix. The major bands in each spectrum will be discussed. Tables 3.2 and 3.3 show the assignment for common band positions for p-polarization and s-polarization, respectively for Figures 3.10 and 3.12.



	Protein Structure	Wavenumber (cm <sup>-1</sup> )	
1.	$\alpha$ Helical structure	Amide I Absorption: 1650 to 1657 Amide II Absorption: 1545 to 1551 1515	Amide I: 80% C=O stretching vibration, 20% in plane C-N stretching. Amide II: 40% C-N stretching, 60% N-H bending
2.	$\beta$ Sheet structure	1628 to 1635 1524 to 1525 1690	

**Table 3.2 Major bands characteristic of  $\alpha$  helix and  $\beta$  sheet.**

<b>p-polarized IRRAS at 60 degrees</b> band position (cm <sup>-1</sup> ), surface pressure	Band Assignment
1652, 1 mN/m	$\alpha$ -helix
1648, 30 mN/m	$\alpha$ -helix
1550, 30 mN/m	$\alpha$ -helix
1536, 30 mN/m	$\alpha$ -helix and to $\beta$ -sheet
1531, 1 mN/m	$\alpha$ -helix and to $\beta$ -sheet
1522, 30 mN/m	$\beta$ sheet
1517, 20 mN/m	$\alpha$ -helix
1448, 30 mN/m	C-H scissoring of CH <sub>2</sub> and CH <sub>3</sub>
1406, 10 mN/m	Aspartic and glutamic residues (COO-systematic stretch)

**Table 3.3 Assignment of bands present in p-polarization IRRAS of human insulin Langmuir monolayer in Figure 3.10.**

<b>s-polarized IRRAS at 60 degrees</b> band position (cm <sup>-1</sup> ), surface pressure	Band Assignment
1694 cm <sup>-1</sup> , 20 mN/m	$\beta$ -sheet
1666, 30 mN/m	$\beta$ -turn and $\alpha$ -helix
1650, 1 mN/m	$\alpha$ -helix
1588, 30 mN/m	aspartic acid (COO <sup>-</sup> antisymmetric and symmetric stretch)
1554, 30 mN/m	$\alpha$ -helix
1539, 30 mN/m	$\alpha$ -helix
1519, 30 mN/m	$\alpha$ -helix

**Table 3.4 Assignment of bands present in p-polarization IRRAS of human insulin Langmuir monolayer in Figure 3.11.**

Figure 3.10 shows p-polarization of HI Langmuir monolayer at 60 degrees at various surface pressures. The band at 1517 cm<sup>-1</sup> corresponds to  $\alpha$ -helix. At surface pressure 1 mN/m, there are two visible bands visible: 1652 and 1637 cm<sup>-1</sup>. With increasing surface pressure, the two bands overlap and become a broad band. At 30 mN/m, the band is visible as a single band with frequency at 1648 cm<sup>-1</sup>. This is the band corresponding to amide II region of  $\alpha$ -helix. Thenext band appears as a broad band at 1 mN/m at 1531 cm<sup>-1</sup>. With increasing surface pressure, it breaks into three bands: 1550, 1536 and 1522 cm<sup>-1</sup>. The bands at 1550 and 1522 cm<sup>-1</sup> correspond to amide II region in  $\alpha$ -helix and  $\beta$ -sheet, respectively. This splitting of bands suggests that the band present at 1531 cm<sup>-1</sup> at lower surface pressures is composed of both  $\alpha$ -helix an  $\beta$ -sheet. At higher surface pressure the band separates in to discrete individual peaks. The other peaks present in the

spectra are due to the presence of amino acids and alkane chains. The band at  $1448\text{ cm}^{-1}$  corresponds to C–H scissoring of  $\text{CH}_2$  and  $\text{CH}_3$ . All the three major bands indicative of  $\alpha$ -helix are present in the p-polarization IRRAS of HI Langmuir monolayer.

Figure 3.11 shows p-polarization of HI Langmuir monolayer at  $10\text{ mN/m}$  at six different angles of  $30, 35, 40, 60, 65$  and  $70$  degrees. Before Brewster angle, the angles at  $30, 35$  and  $40\text{ mN/m}$  show none of the bands characteristic of  $\beta$  sheet. All three angles show bands near  $1650\text{ cm}^{-1}$  and  $1545\text{ cm}^{-1}$  which corresponds to amide I and amide II absorption, respectively. The band at  $1517\text{ cm}^{-1}$ , which corresponds to  $\alpha$ -helix is present in  $35$  and  $40$  degrees. After the Brewster angle, all three angles of  $60, 65$  and  $70$  degrees show a band between  $1650$  and  $1655$ , which corresponds to amide I absorption in  $\alpha$ -helix. At an angle of  $60$  degrees, a peak is visible at  $1523\text{ cm}^{-1}$ , which corresponds to  $\beta$  sheet. None of the other bands present in the spectra are characteristic of  $\alpha$ -helix or  $\beta$ -sheet. The spectra suggests that HI is in the form of  $\alpha$ -helix at air-water interface. With increasing angle at constant pressure of  $10\text{ mN/m}$ , the  $\alpha$ -helix character is found to decrease in the spectra. The s-polarization IRRAS of HI Langmuir monolayer obtained at different surface pressures is presented in Figure 3.12. At surface pressure of  $1\text{ mN}\cdot\text{m}^{-1}$ , a band is present at  $1650\text{ cm}^{-1}$  which corresponds to  $\alpha$ -helix. With increasing surface pressure, this band disappears and merges into the band at  $1666\text{ cm}^{-1}$ . The band at  $1666\text{ cm}^{-1}$  includes  $\beta$ -turn and  $\alpha$ -helix. The band at  $1694\text{ cm}^{-1}$  corresponds to  $\beta$ -sheet. Band at  $1519\text{ cm}^{-1}$  also corresponds to  $\alpha$ -helix. The band observed at  $1670$  at an incident angle of  $60^\circ$  may be assigned to sterically constrained C=O moiety present in  $\beta$ -turn or split in the peak is noticed due to transition dipole coupling in  $\beta$ -sheet. While varying the surface pressure, the most intense bands appeared at  $1554$  and  $1539\text{ cm}^{-1}$ , both bands correspond to  $\alpha$ -

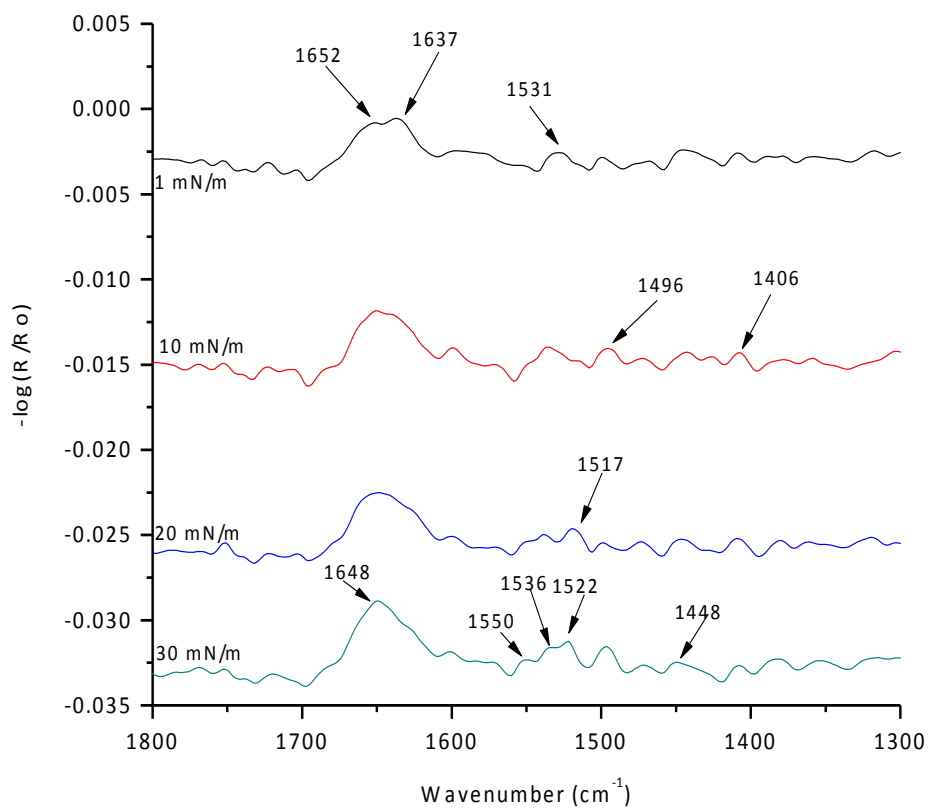


**Figure 3.10 p-Polarized IRRAS of human insulin Langmuir monolayer at subphase pH 5.6 using an incident angle of 60°, and varying the surface pressures.**

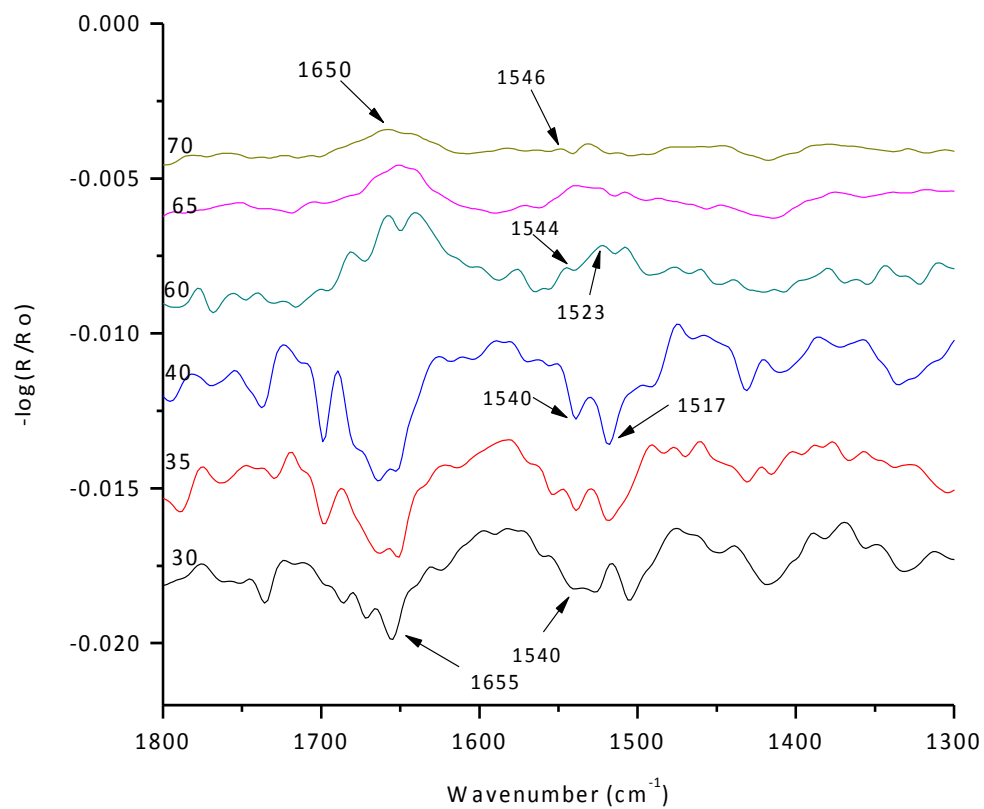


**Figure 3.11** p-Polarized IRRAS of human insulin Langmuir monolayer at subphase pH 5.6 and surface pressure 10 mN/m, and varying the incident angles.

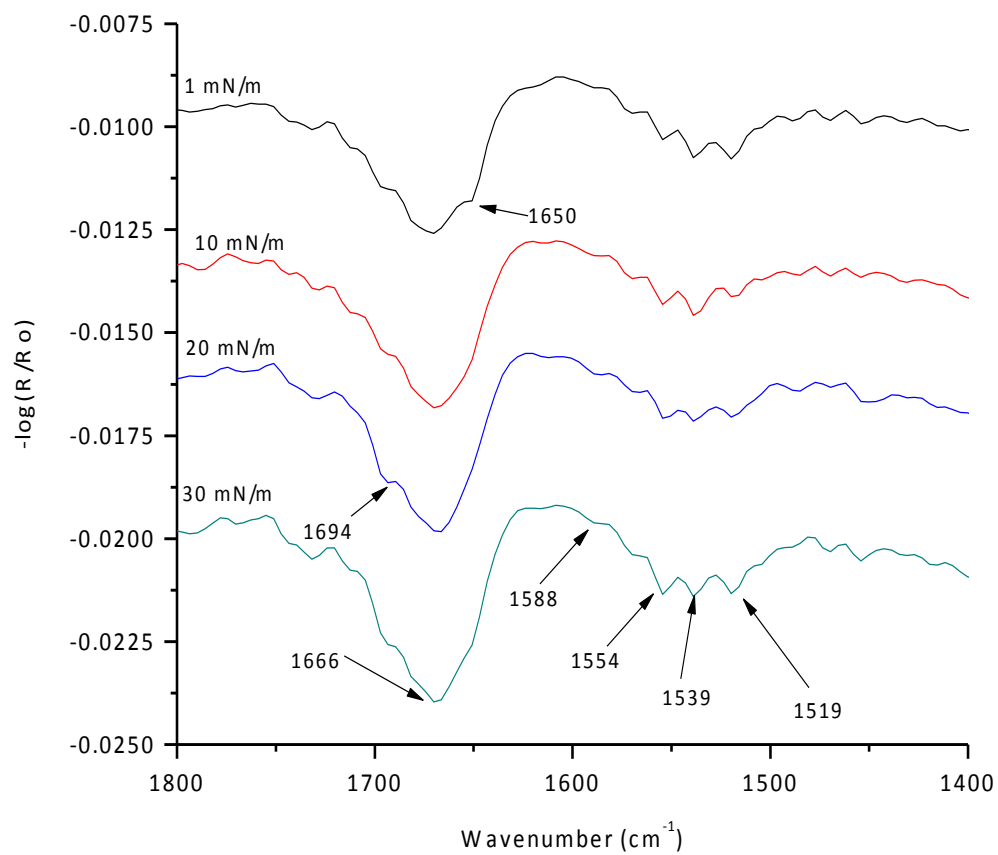


**Figure 3.12 s-Polarized IRRAS of human insulin Langmuir monolayer at subphase pH 5.6 and incident angle of 25°, and varying the surface pressures.**

helix in amide II region. COO<sup>-</sup> antisymmetric and symmetric stretching mode characteristic of aspartic acid is characterized by a peak at 1588 cm<sup>-1</sup>. All the three major bands are indicative of  $\alpha$ -helix in the s-polarization IRRAS of HI Langmuir monolayer.

From the above CD, FTIR and IRRAS data, it can be concluded that HI dissolved in pH 2 exists in a helical conformation in solution and at the air-water interface.

### **3. 3 Carbon dots: background**

Carbon dots (CD) are a new class of highly fluorescent nanoparticles less than 10 nm. They have been touted as a replacement for toxic quantum dots due to their benign nature which makes them an attractive tool for biological research. CD were first reported in 2004 as one of the three components of single walled carbon nanotubes.<sup>52</sup> Since then these nanoparticles called 'C-dots or carbon dots' have been synthesized by various routes, surface modified and characterized by various groups to better understand their properties.<sup>51</sup> Several studies with CD for bioimaging have been published in the past few years.<sup>83; 84,85</sup> However orientation of CD at a membrane level has not been studied yet. Langmuir monolayer methodology can be used to study the interaction and conformation for CD at air-water interface as Langmuir monolayers are used as in vitro model of biological membranes.<sup>78</sup> This technique allows us to study intermolecular interactions between molecules spread at the interface which form the monolayer.

### **3. 4 Carbon dots: synthesis**

The protocol for synthesis for CD was followed from literature and is mentioned in Chapter 2 of this thesis<sup>86</sup> The procedure for synthesis is given in greater detail in the

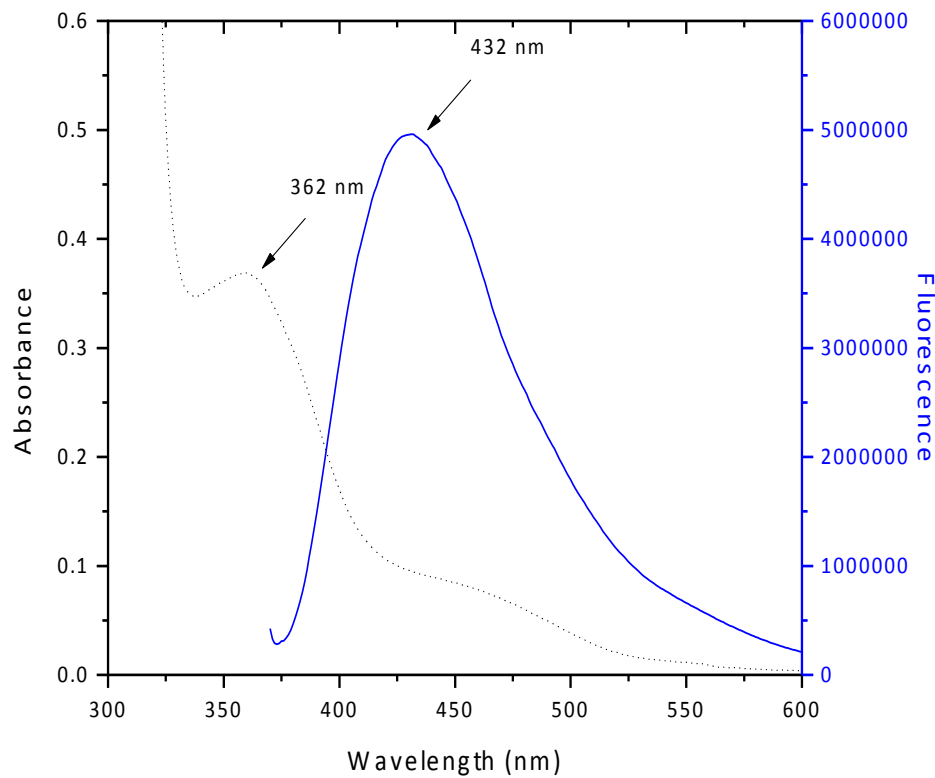


**Figure 3.13 Absorption (dash line) and photoemission (solid line,  $\lambda_{ex} = 340$  nm) for carbon dots in a aqueous solution of chloroform.**

supporting information. Briefly, 15 ml octadecane and 1.5 g hexadecylamine were heated in a three neck flask under argon flow. When temperature stabilized at 300 °C, 1 g citric acid was added to the mixture. The resulting solution was light yellow in color and was allowed to cool to room temperature. The synthesized CD was dried under high vacuum and dissolved in chloroform. The light yellow CD solution emitted blue light under UV light Figure 3.13 shows the spectra absorption at 342 nm, and fluorescence



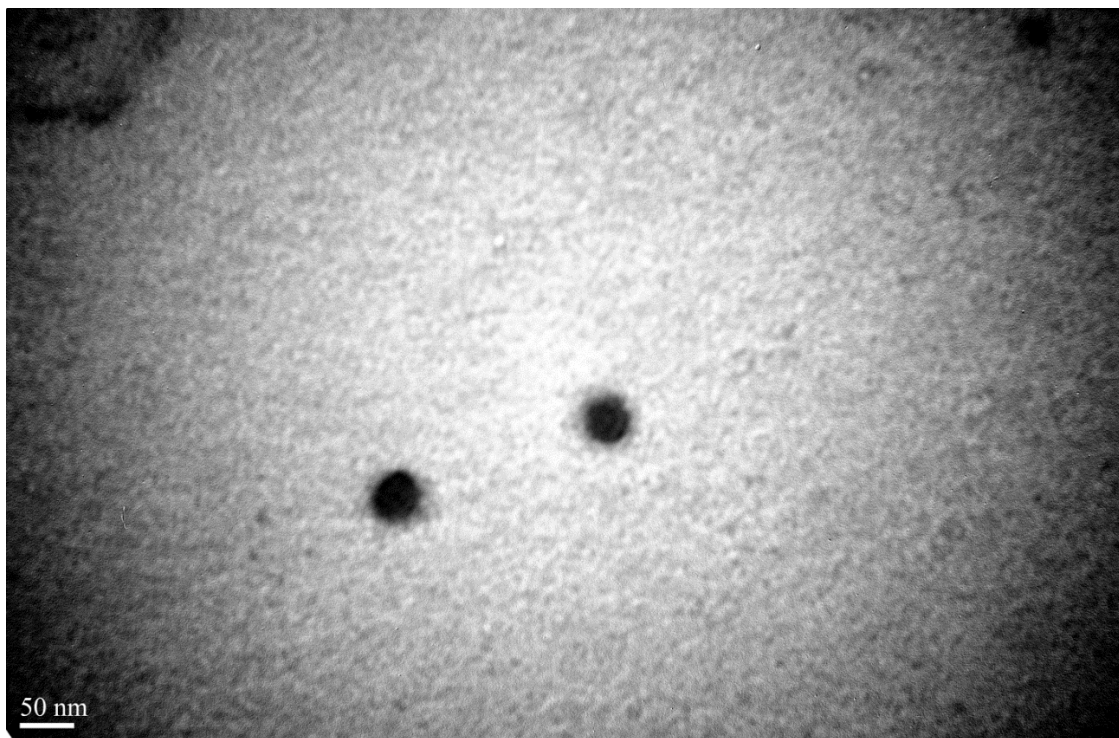


**Figure 3.14: TEM Image of carbon dots.**

at 432nm when excited at 340 nm for CD. The shift in emission wavelength with increase in excitation wavelength characteristic of CD was observed during fluorescence. Figure 3.14 shows the TEM images obtained for the synthesized CD. The CD were found to be between 4-9 nm in diameter.

### **3.5 Carbon dots Langmuir monolayer**

Examination as a Langmuir monolayer at air-water was performed using a concentration of 0.3 mg/ml of CD with water as the subphase. CD dissolved in chloroform was deposited on the water subphase with a syringe and allowed to evaporate for 15 minutes. Figure 3.15 shows the surface pressure isotherm for CD. The lift-off of the surface pressure corresponds to  $0.12 \text{ \AA}^2 \text{ molecule}^{-1}$ . With increase in surface pressure, the CD

undergo transition from gaseous to liquid expanded phase and finally to condensed phase. At surface pressure of 45 mN/m, the CD monolayer collapses. A successful deposition of Langmuir Blodgett film of the CD monolayer at the air-water interface requires the surface pressure of the monolayer to be maintained between 10 mN/m and the collapse surface over a period of time.<sup>59</sup> In order to gauge the stability of the monolayer, stability experiments were performed. Figure 3.16 shows the CD monolayer when held at at 30 mN/m for 30 min. A decrease in area of the monolayer was at this surface pressure was calculated to be less than 16%. The three compression-decompression cycles at 30 mN/m in Figure 3.17 show a minimal decrease in area

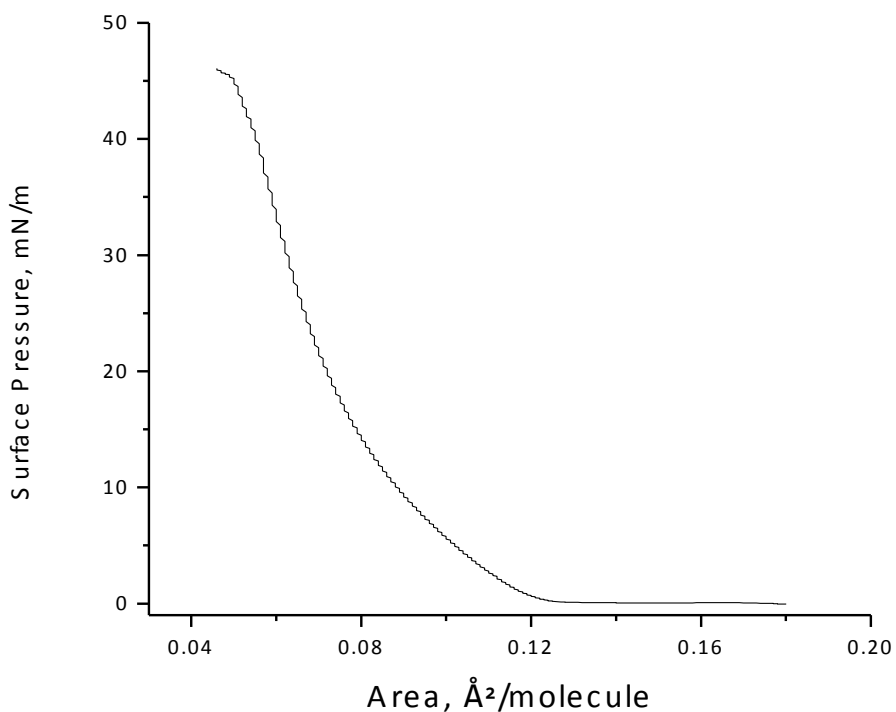


**Figure 3.15** Surface pressure–area isotherms of carbon dots Langmuir monolayer at subphase pH 5.6.

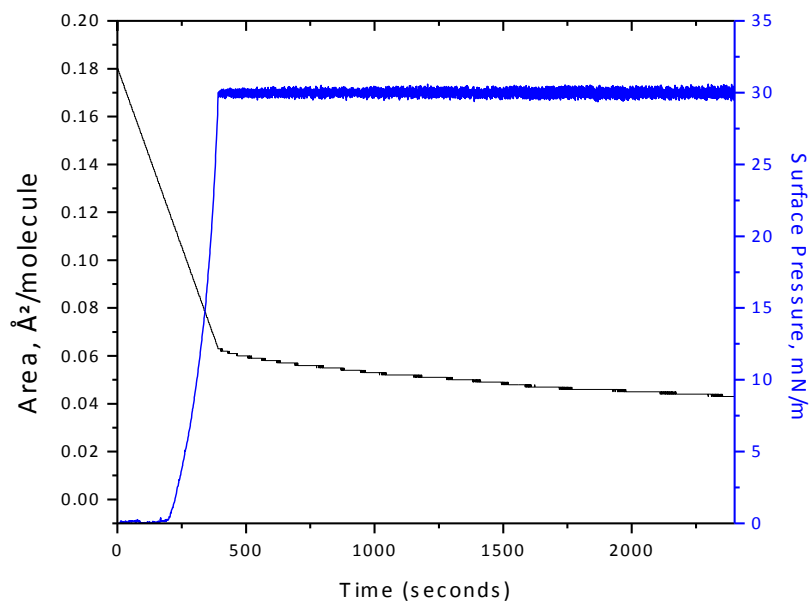


**Figure 3.16** Stability measurements at surface pressure 30 mN/m held for 30 minutes for carbon dots Langmuir monolayer at subphase pH 5.6.

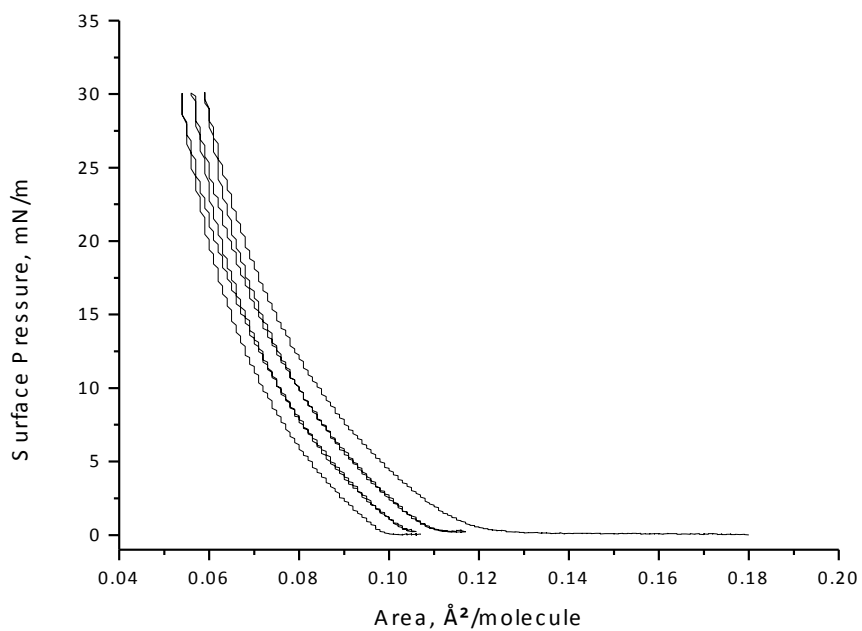


**Figure 3.17** Three compression-decompression cycles up to a surface pressure of 30 mN/m of carbon dots Langmuir monolayer at subphase pH 5.6.

between the three cycles. Both these experiments indicate that CD monolayer is stable and remains at air-water interface at high surface pressure without losing conformation. This property makes it viable for CD to be deposited as Langmuir Blodgett film.

### 3.6 Carbon dots Langmuir Blodgett film

Langmuir Blodgett (LB) is a technique whereby the monolayer at air-water interface can be vertically deposited onto a solid support such as a quartz slide.<sup>59</sup> The quartz slide is held mechanically by a clamp and dipped into the water subphase. Once the needed

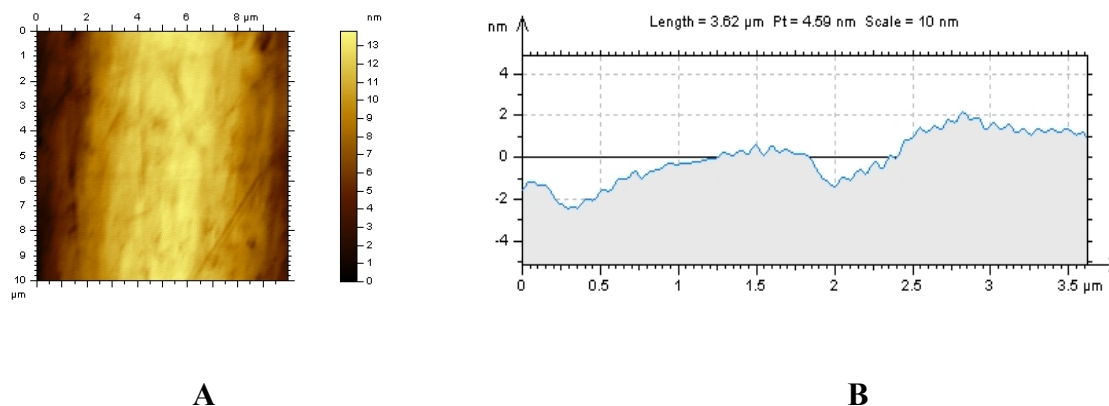
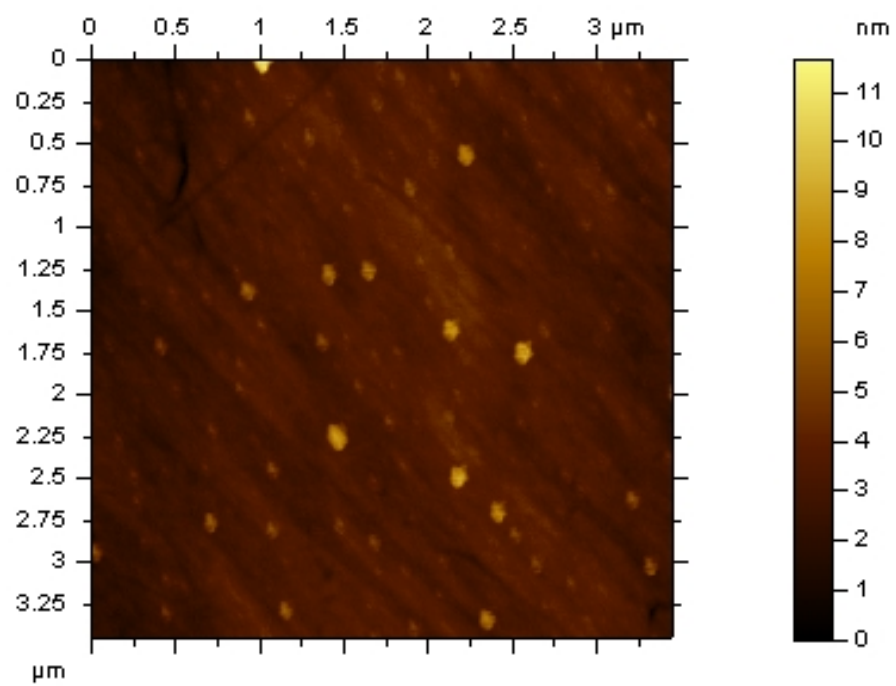
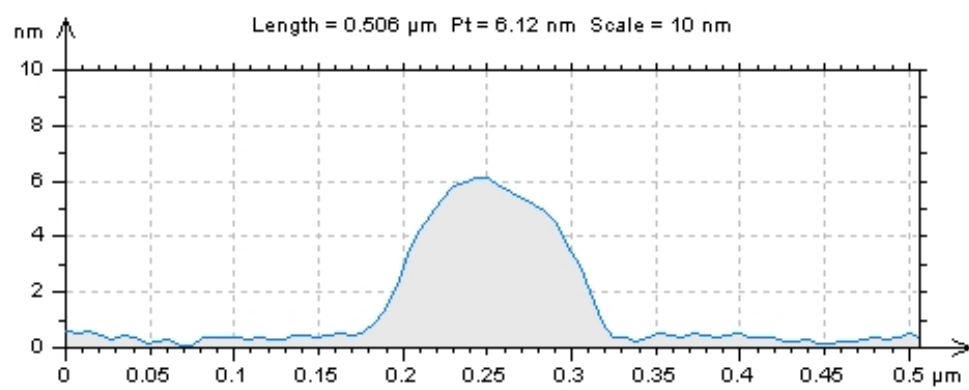


**Figure 3.18 AFM image (10 μmX 10 μm) of blank quartz slide and the B) topography of the imaged quartz slide.**

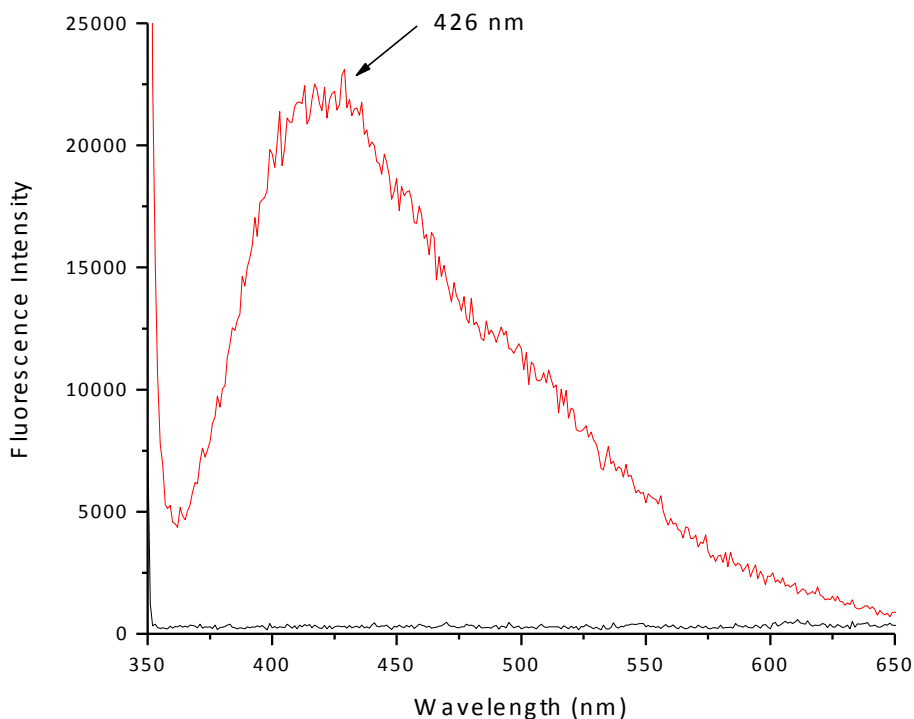
surface pressure of 30 mN/m was obtained, the slide was withdrawn from the subphase at a speed of 1 mm/min and left to air dry for 30 minutes. Once the slide was dried, it now had 1 layer film of CD. It was examined by fluorescence spectroscopy and atomic force microscopy. Figure 3.18 shows AFM image of a blank quartz slide. The fluorescence and AFM image of LB film of CD is presented in Figure 3.19. Figure 3.19 C shows the fluorescence spectrum of the blank quartz slide (black line) before surface



A



B



C

**Figure 3.19 AFM image (4  $\mu\text{m}$  X 4  $\mu\text{m}$ ) of A) blank quartz slide drop casted with carbon dots, B) topography of the imaged quartz slide and C) Fluorescence spectra of blank quartz slide (black line) and slide drop casted with carbon dots dissolved in chloroform (red line). ( $\lambda_{\text{excitation}} = 340 \text{ nm}$ , slit width at the excitation and emission, 5 and 5 nm, respectively)**

deposition of 1 layer of LB film. There is no fluorescence visible for quartz which verifies that the slide is clean. After 1 layer deposition of the CD monolayer, the fluorescence spectrum shows an emission peak at 426 nm (red line). This corresponds to the fluorescence spectra obtained for CD as solution at 432 nm in Figure 3.13. The intensity of the fluorescence for the CD monolayer is 1000 times lower than the intensity

of CD solution. CD solution and CD monolayer, both had a concentration of 0.3 mg/ml. For the monolayer preparation, 40  $\mu$ l of 0.3 mg/ml solution is spread over a trough of an area of  $5.9 \text{ cm} \times 21.1 \text{ cm}$  which already contains 30 ml water. This dilutes and reduces the concentration of CD monolayer present in the monolayer and this low concentration is deposited on the quartz slide when it picks up the CD monolayer. Due to this low concentration, the intensity of fluorescence spectra of the CD monolayer is much lower compared to the CD solution. However, as presence of emission peak in the same region as in the solution confirms that the presence of CD monolayer in the Langmuir Blodgett film.

### 3.7 Conclusion

The surface chemistry of a HI Langmuir monolayer was studied by surface pressure- and surface potential-area isotherms, and in situ spectroscopic measurements, namely by UV-vis and fluorescence. Presence of the amino acid tyrosine resulted in insulin's characteristic absorbance and fluorescence spectra. Surface chemistry of HI Langmuir monolayer indicates a stable HI monolayer until collapse at  $25.2 \text{ mN m}^{-1}$  as shown by UV-vis and stability studies at the air-water interface. Microdomain formation of HI monolayer was examined by epifluorescence of HI-FITC and BAM. In both cases, a homogeneous HI Langmuir monolayer was observed at all surface pressures without any indication of the formation of domains in the  $\mu\text{m}$  range in the topography of the film. Secondary structure of the HI in solution and at air-water interface was examined by IRRAS. The data were showed for both phases a high  $\alpha$ -helix content, which mainly indicates the presence of monomers in the HI Langmuir monolayer. The surface chemistry of CD Langmuir monolayer was studied by surface pressure, stability studies

and Langmuir Blodgett (LB) films. CD Langmuir monolayer was found to be stable at high surface pressure which made it viable for the molecule to be deposited as LB film. The behavior of HI and CD as a Langmuir monolayer at air-water interface lays a foundation for the next part of the study in Chapter 6 where interaction between HI and CD in solution will be examined to study fibrillation.



## Chapter 4

### Study of Aggregation of Human Insulin Langmuir Monolayer

#### 4.1 History and background

Human insulin (HI) exists as a monomer, dimer and a hexamers in the living body. It is effective as monomer and is stored in a hexamer form with  $Zn^{2+}$  ions at the center of the assembly.<sup>87</sup> The hexameric structure of insulin containing six insulin monomers and three  $Zn^{2+}$  ions, where they are united by three equivalent dimers each containing two insulin monomers and one  $Zn^{2+}$  ion.<sup>88</sup> Figure 4.1 shows the diagram of insulin in aggregated state when it is stored in the pancreas.<sup>22</sup> In the bloodstream, the three structure levels of insulin, mainly consisting of monomers, dimers and hexamers, are in equilibrium with each other.<sup>89; 90</sup> Such equilibrium can be affected by different environment conditions such as pH and temperature, as well as on the concentration of insulin or metal ions.<sup>91</sup> In modern medical treatments for diabetes (especially type 1 and 2), most drugs that are used for helping patients with glycemic control are based on zinc-containing insulin in the hexameric state.<sup>92</sup> Therefore, research on the aggregation properties of insulin is of great importance for the development of medical treatment.

Although the mechanism of insulin aggregation equilibrium is not completely understood, several studies have shown that specific conditions can have an effect on the structural equilibrium.<sup>93; 94</sup> These studies have been mainly performed in aqueous and crystalline phases of insulin, however, research has seldomly reported insulin evaluations at the air-water interface. Pérez-López et al. have recently shown that the presence of  $Zn^{2+}$  ions in the subphase has a profound effect on the surface chemistry of the insulin

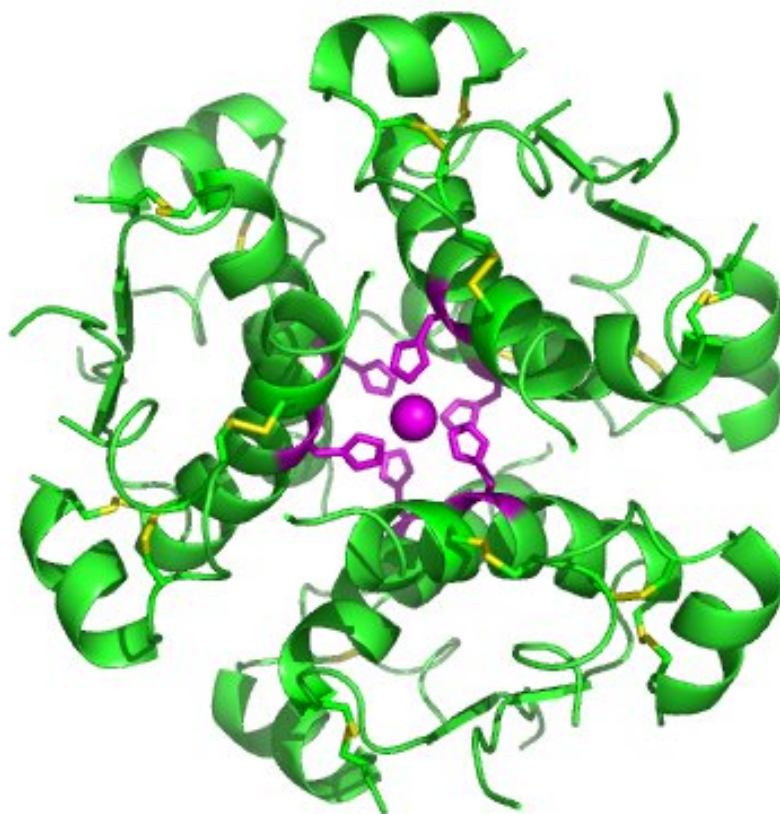


**Figure 4.1** Insulin is stored as a hexamers in the pancreas, held together by three zinc ions.<sup>22</sup>

Langmuir monolayer.<sup>33</sup> Due to this reason, we have extended the study of the insulin aggregation process by comparing surface chemistry and spectroscopy of the insulin Langmuir monolayer in the absence and presence of  $\text{Zn}^{2+}$  ions in the subphase.

#### **4.2 Sample preparation**

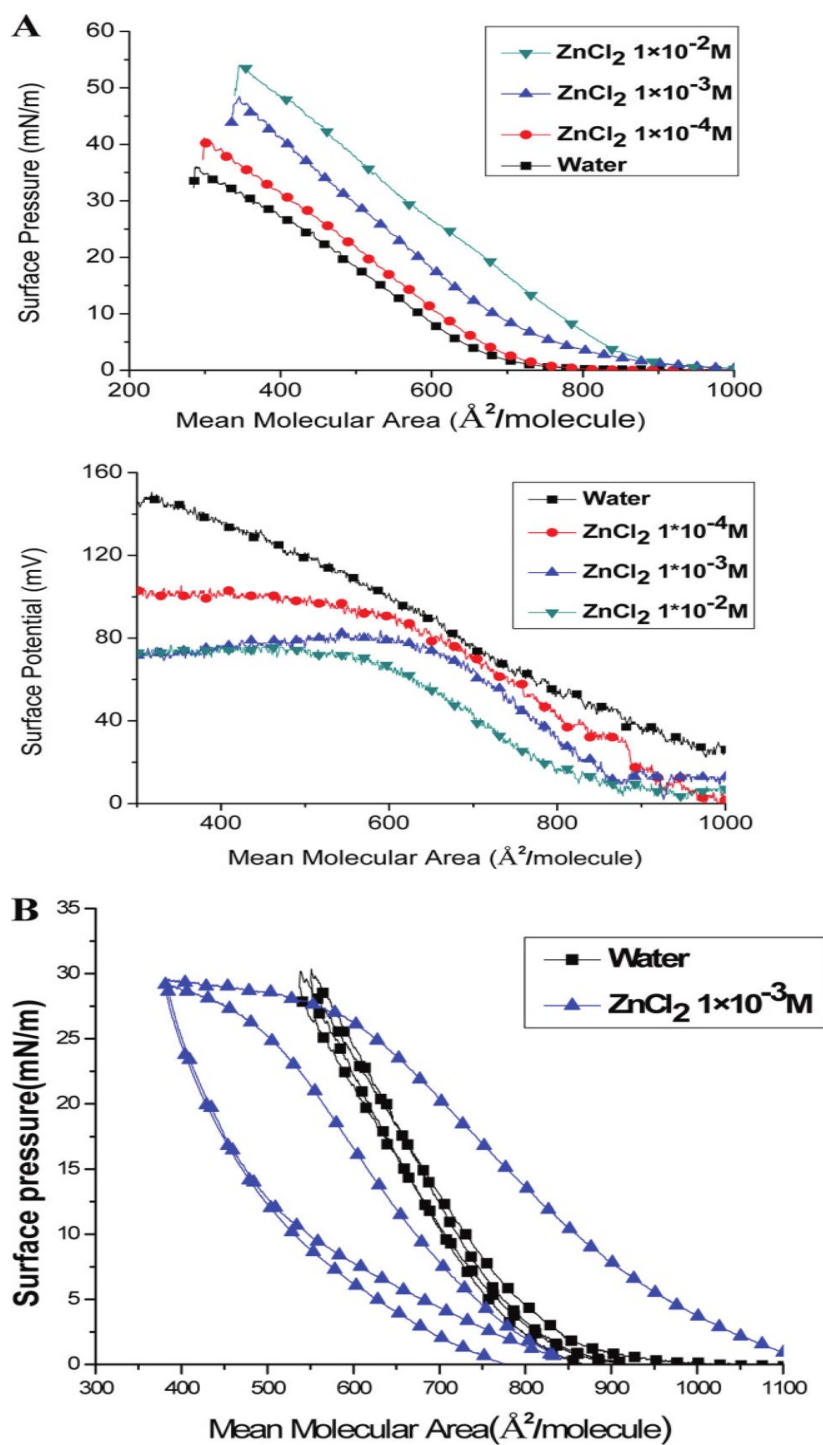
The experiments were conducted using two different spreading aqueous solutions, one at pH 2 and another at pH 9, where ground human insulin (HI) was dissolved. All the experiments were performed with these HI samples and the data were reproduced in the

absence and presence of Zn (II) ions in the aqueous subphase (pH 5.6). Aqueous solution at pH 2 with HCl is typical for maintaining a stable acidic conformation of insulin. Pure water subphase was used due to the fact that  $\text{ZnCl}_2$  precipitate at pH 9 and because of the adequacy of working at the same experimental conditions of the subphase. Pure water at pH 5.6 was thus used to prepare all the subphases differing in Zn (II) ion concentration. Figure 4.2 A and 4.3 A presents the surface pressure ( $\pi$ )- and surface potential ( $\Delta V$ )- area (A) isotherms of the human insulin aqueous solutions prepared at pH 2 and pH 9 respectively, in the absence and presence of Zn (II) ions in the subphase.

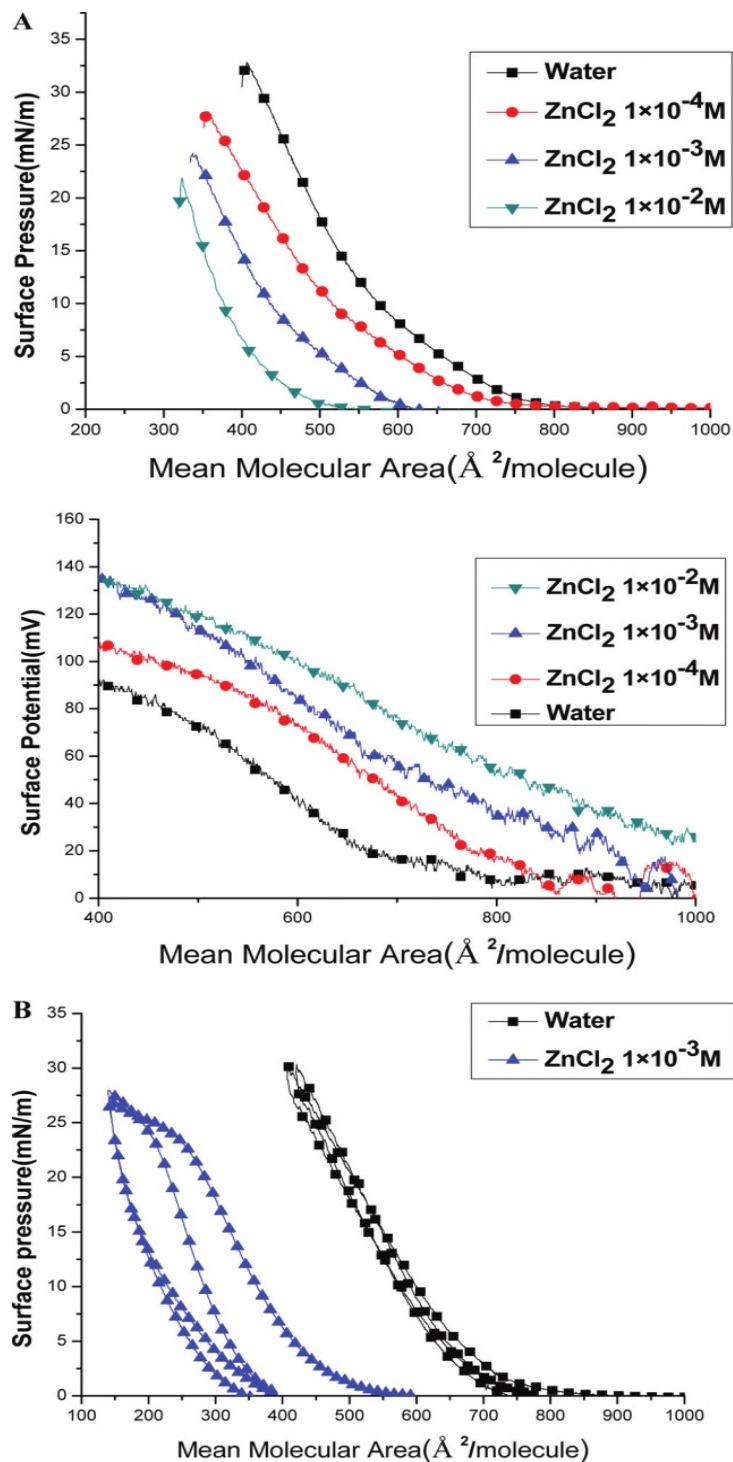
### **4.3 Surface pressure-and potential-area isotherms: effect of zinc concentration in subphase**

Figure 4.2A shows that: (i) the lift-off area per molecule increases with the increase in the concentration of Zn (II) ions; (ii) the slope of each isotherm in the region of 400 to 700  $\text{\AA}^2 \text{ molecule}^{-1}$  is approximately the same, but the limiting molecular area, which indicate the closest packing of the human insulin molecule, increases with the concentration of Zn (II) ions, i.e. from 660 (pure water) to 700, 780 and 850  $\text{\AA}^2 \text{ molecule}^{-1}$ ; (iii) the increase of Zn (II) concentration increases the surface collapse pressure, from 35 (pure water) to 40, 48 and 55 mN/m, respectively. From previous studies we can deduce that our data shows formation of aggregates at the air-water interface, i.e. dimers and hexamers.<sup>17; 23</sup>

Figure 4.3A showed a behavior opposite to the one seen on Fig. 4.2A: with the increase of the Zn (II) concentration, the lift-off (from 800 to 500  $\text{\AA}^2 \text{ molecule}^{-1}$ ), limiting



**Figure 4.2** Surface pressure- and surface potential-area isotherms of recombinant human insulin aqueous solution (pH 2) spread at the air-water interface in absence and presence of ZnCl<sub>2</sub> in the subphase (A); compression-decompression isotherm cycles in absence and presence of ZnCl<sub>2</sub> in the subphase (B).



**Figure 4.3** Surface pressure- and surface potential-area isotherms of recombinant human insulin aqueous solution (pH 9) spread at the air-water interface in absence and presence of ZnCl<sub>2</sub> in the subphase (A); compression-decompression isotherm cycles in absence and presence of ZnCl<sub>2</sub> in the subphase (B).

molecular area (from 630 to 450 Å<sup>2</sup> molecule<sup>-1</sup>) and surface pressure collapse area (from 425 to 250 Å<sup>2</sup> molecule<sup>-1</sup>) are reduced. From the data we can see that the basic (pH 9) human insulin spreading aqueous solution (BI) had an insulin conformation different to the one in the acidic (pH 2) medium (AI), as shown in Figure 4.6 and Tables 1 and 2. The presence of Zn (II) ions have a great influence on the different conformations since both the basic (BI) and acidic human insulin (AI) aqueous spreading solvent on pure water surface give a similar surface pressure-area isotherm. The surface potential-area isotherms of AI and BI are shown in Figure 4.2A and 4.3A. The trend observed in the  $\pi$ -A curves is followed by the  $\Delta V$ -A isotherms when one increases the concentration of Zn (II) ions.

Figures 4.2B and 4.3B show the compression-decompression isotherms of the AI and BI in the absence and presence of Zn (II) ions in the subphase, respectively. For both AI and BI the compression-decompression isotherms (2 cycles) in absence of Zn (II) ions were the same within experimental error (4.4%). However, a large difference in the hysteresis was observed in presence of Zn (II) ions, particularly for the AI cycles. For AI, there was certainly a high effect of Zn (II) ions on the conformation and orientation of the insulin in 2-D.

#### **4.4 UV-vis and fluorescence spectroscopy of human insulin in aqueous phase and as Langmuir monolayer**

Figures 4.4A-D show the photophysical properties of human insulin in two different phases: in aqueous solution (Fig. 4.4A,B) and in Langmuir monolayer (Fig. 4.4C, D). The controlled parameters were (i) pH, (ii) absence and presence of Zn (II) ions and (iii)

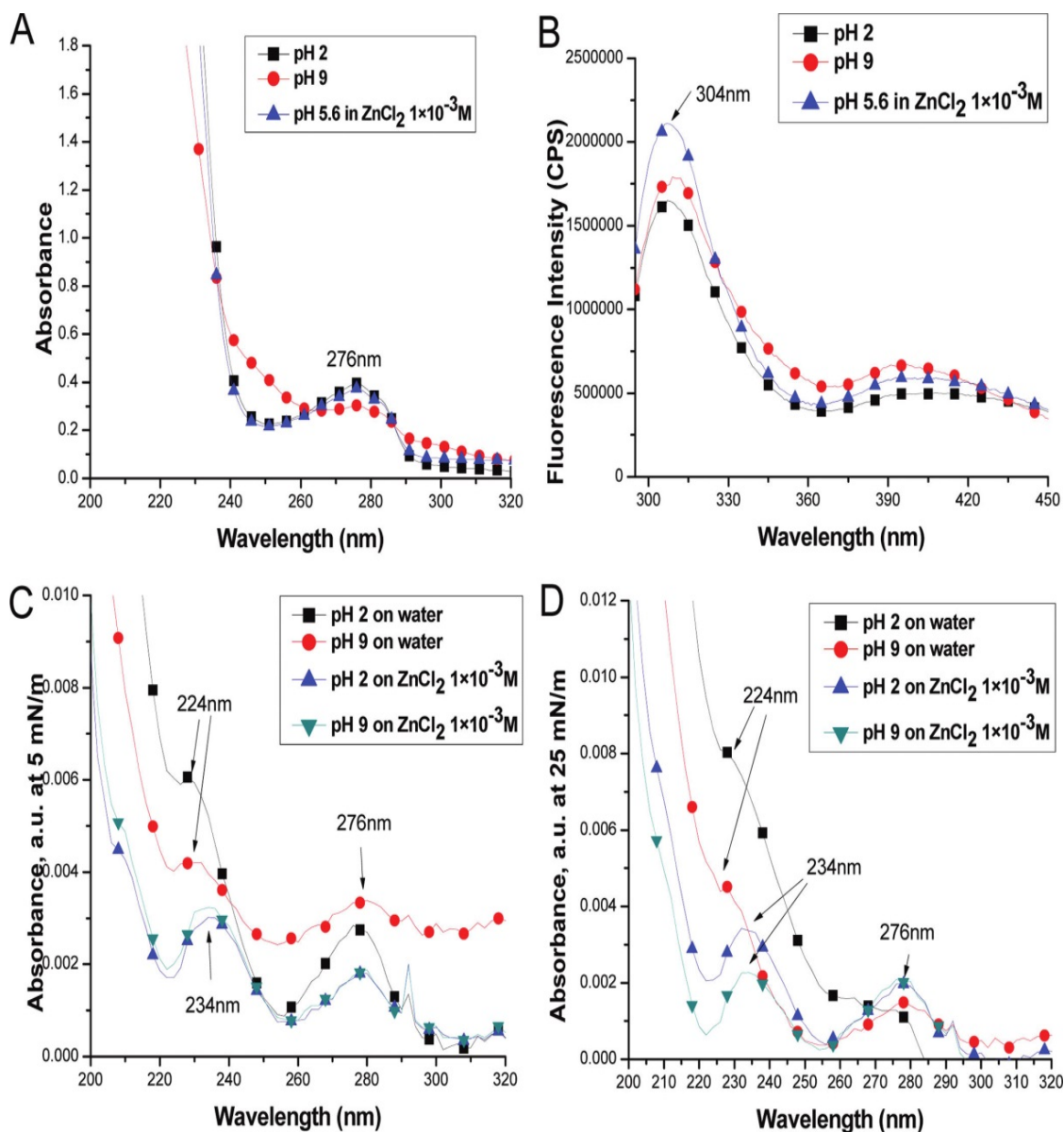


**Figure 4.4** UV-vis and fluorescence (excitation at 270 nm, Raman at 297 nm) spectra of  $10^{-4}$  M human insulin aqueous solutions (A, B) and UV-vis spectra of human insulin Langmuir monolayer at pH 2 and pH 9 in absence and presence of  $\text{ZnCl}_2$  ( $10^{-3}$  M) in the subphase at 5 mN/m (C) and at 25 mN/m (D).

surface pressure of the Langmuir monolayer. UV-vis and fluorescence spectra of aqueous solution at pH 2 and 9 in absence of Zn (II) ions showed tyrosine-corresponding peaks at 276 and 304 nm, respectively. (4.4 A,B), while the same peak maxima were seen in the presence of Zn (II) ions ( $10^{-3}$  M). A peak at 222 nm was also observed in all the solutions examined (data not shown). The latter peak maxima are particular to the tyrosine emission, as this deduction has been previously published (Ludwig and Asher, 1988)<sup>95</sup> for the tyrosine aqueous solution at pH 6.0. It is known that the band maxima corresponding to the tyrosine groups refer to the characteristic bands that are observed for phenol, which is a component of the tyrosine molecule. Regardless of the experimental conditions selected for the aqueous phase, a change in the band position was not observed. However, the shape of the spectra for the aqueous solution at pH 2 in the absence of Zn (II) ions and for the aqueous solution at pH 5.6 in the presence of Zn (II) ions differ from the one at pH 9 in the absence of Zn (II) ions. Such a difference in shape can be explained by a different conformation of the human insulin at these two pH values.

Figures 4.4C and 4.4D present the UV-vis properties of the human insulin Langmuir monolayer at two surface pressures, 5 and 25 mN/m, respectively. From these figures, similar peak positions are identified in the UV-vis spectra when the Langmuir monolayer was compressed to 5 mN/m (Fig. 4.3C) and 25 mN/m (Fig. 4.4D) in absence of Zn (II) ions. However, in presence of Zn (II) ions a shift is observed from 224 to 234 nm, while the peak at 276 nm remains the same at both surface pressures (Fig.4.4C, D). The fluorescence spectra for the Langmuir monolayer were also examined (not shown) but it is difficult to clearly observe insulin fluorescence peaks due to the small amount and low



quantum yield of tyrosine. From our results we have suggested a mechanism for the observed shift in the 224-234 nm range of the absorption spectra. In this mechanism, the Zn (II) ions would induce an aggregated state of the human insulin in 2-D, regardless of the pH and of the surface pressure imposed to the system. Hereon we have demonstrated the aggregation of human insulin induced by the Zn (II) ions in the subphase. To support the interpretation of our data, we have examined the effect that the Zn (II) ion presence may have to the human insulin in 2-D and aqueous phase by employing Fourier transform infrared (FTIR) and Circular dichroism (CD) spectroscopy, respectively.

#### **4.5 FTIR and IRRAS of human insulin in aqueous phase and Langmuir monolayer**

Information on the secondary structure of protein in IR spectroscopy was first elucidated by Elliot and Ambrose in 1950<sup>96</sup>, who observed a correlation between the frequency of the amide I and amide II IR absorptions and the secondary structure of the protein. Through the use of both IR and X-ray diffraction techniques, such study had shown that the position of amide I and amide II IR absorption might have been influenced by the hydrogen bonding in the protein, which is closely connected to the protein's secondary structure in space.<sup>97</sup> For most proteins in aqueous solution, an  $\alpha$ -helix-predominated structure will exhibit amide I and II absorptions in the spectral range from 1650 to 1660  $\text{cm}^{-1}$  and 1540 to 1550  $\text{cm}^{-1}$ , respectively, and a structure predominant on  $\beta$ -sheets exhibits similar absorptions at 1620 to 1635 and 1520 to 1535  $\text{cm}^{-1}$ .<sup>98</sup> Figure 4 shows the FTIR (Fig. 4.5 A) and IRRAS (Fig. 4.5 B-D) spectra of human insulin aqueous solutions differing in pH in the absence and presence of Zn (II) ions (Fig. 4.4A). Likewise, we have reported its Langmuir monolayer at a specific surface pressure,

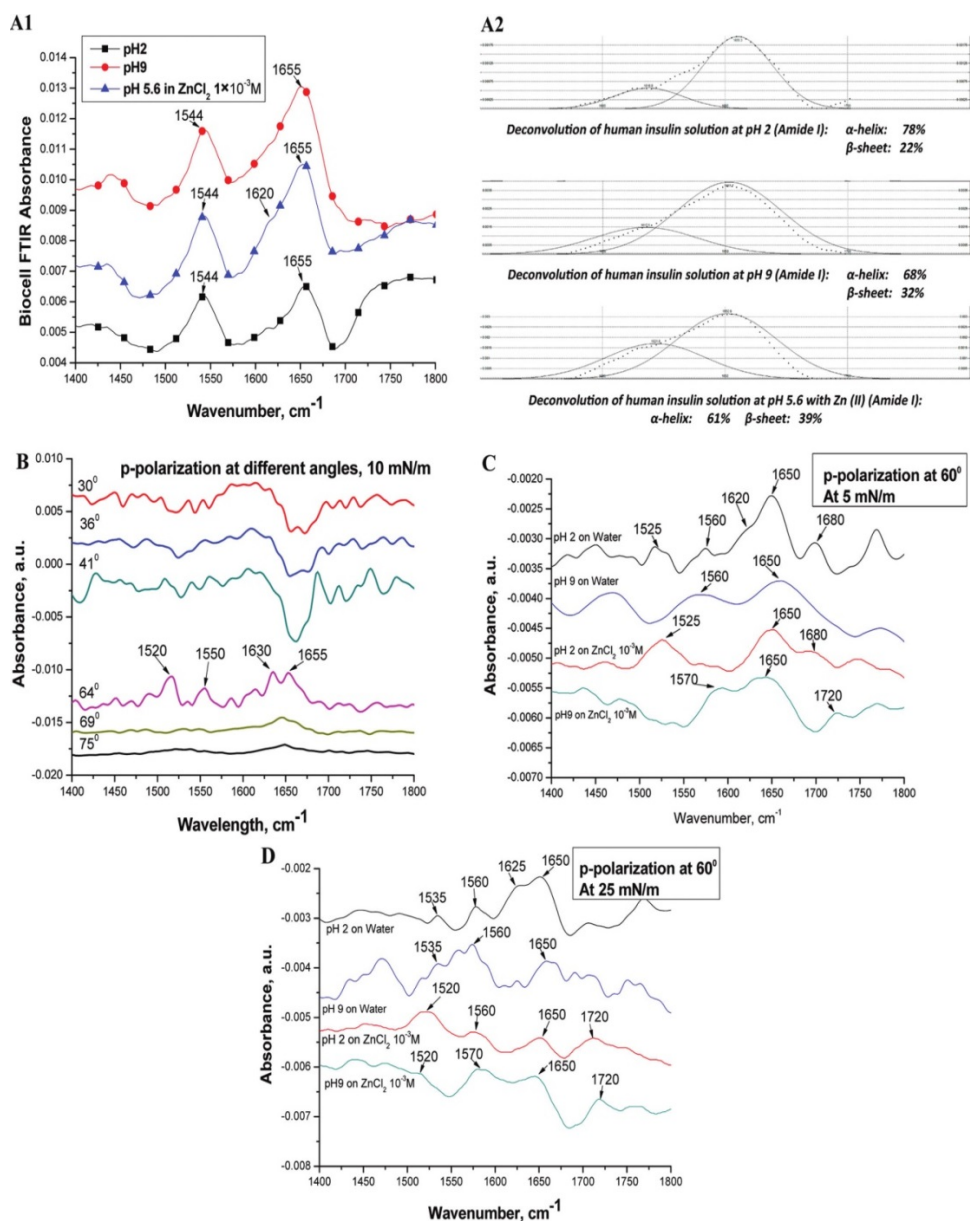


**Figure 4.5** FTIR spectra of human insulin aqueous solution and IRRAS spectra of insulin Langmuir monolayer: Bio-ATR cell spectra of insulin (1.5 mg/mL) in absence and presence of  $\text{ZnCl}_2$  at pH 2 and pH 9 (A); p-polarization IRRAS spectra of insulin Langmuir monolayer at a surface pressure of 10 mN/m and various angles of incidence at pH 2 (B); p-polarization at  $60^\circ$  IRRAS spectra of insulin Langmuir monolayer at pH 2 and pH 9 in absence and presence of  $\text{ZnCl}_2$  in the subphase at surface pressure 5 (C) and 25 mN/m (D).

varying in the angle of incidence (Fig. 4.5B) and at a specific angle, with p-polarization varying the surface helix of the protein. Table 4.1 lists the band assignments for the peaks. Figure 4.5A shows two peaks at around 1544 and 1655  $\text{cm}^{-1}$  which are attributed to the  $\alpha$ -helix of the protein. Through the comparison of the aforementioned spectra, it was observed that: (i) the absorption peak positions for amide I and II in the aqueous solution at pH 9.0 were slightly lower in magnitude than the ones present at pH 5.6 and pH 2.0. This difference in magnitude can be related to the difference in protein conformation between basic and acidic media; (ii) because the peak positions assigned to the  $\alpha$ -helix structure are identified in acidic and neutral aqueous phase, we can deduce that the  $\alpha$ -helix conformation is mostly maintained in the aggregates; (iii) the shoulder at 1620  $\text{cm}^{-1}$  that is seen from the plot corresponding to human insulin at pH 5.6 in the presence of Zn (II) ions (Fig. 4.4A) elucidates the formation of a hexamer, i.e. from the increase in the  $\beta$ -strand structure as aggregation occurs.

Infrared reflection-absorption spectroscopy (IRRAS) has been used to analyze the insulin protein at the air-water interface. Through the analysis we have determined the orientation and the secondary structure of the protein in 2-D. Figure 4.5B shows the spectra taken at 10 mN/m at different angles of incidence (pH at 2). This was done in order to select the appropriate angle of incidence of the light with highest signal-to-noise ratio. At angle of  $64^\circ$ , clear peaks of  $\alpha$ -helix at 1550 and 1655  $\text{cm}^{-1}$  and  $\beta$ -sheet at 1520 and 1655  $\text{cm}^{-1}$  were obtained with highest resolution. Due to our observation we selected an angle of  $60^\circ$  to measure the spectra at two surface pressures varying in pH and in the presence and absence of Zn (II) ions as shown in Fig. 4.5 C,D. Figure 4.5 C shows the spectra of human insulin Langmuir monolayer at 5 mN/m at various pH values in the

absence and presence of Zn (II) ions. A peak at  $1650\text{ cm}^{-1}$  that corresponds to  $\alpha$ -helix was observed in all spectra. Through further analysis of this spectra we have seen that: (i) the spectra of HI with basic spreading solvent (lines 2 and 4 from top) showed different peak maxima and shape from the spectra with acidic spreading solvent (lines 1 and 3 from top), indicating a conformational and orientational difference of the human insulin Langmuir monolayer that exists at different pH levels<sup>91</sup>; (ii) an increase on the quantity of  $\beta$ -strands on the solution in the presence of Zn (II) ions to the solution in absence of Zn

<b>Band position, <math>\text{cm}^{-1}</math> (Surface pressure, incident angle, pH)</b>	<b>Band assignment</b>
1630 (10 mN/m, $64^\circ$ , pH 2)	$\beta$ -sheet (amide I)
1655 (aqueous solution and 10 mN/m, $64^\circ$ , pH2) 1650 (5 mN/m and 25mN/m, $60^\circ$ , pH 2 and 9)	$\alpha$ -helix (amide I)
1620 (aqueous solution, pH 2)	$\beta$ -strands
1544 (aqueous solution, pH 2) 1550 (10 mN/m, $64^\circ$ , pH 2) 1525 (5 mN/m and 25mN/m, $60^\circ$ , pH 2) 1560 (5 mN/m and 25 mN/m, $60^\circ$ , pH 2)	$\alpha$ -helix (amide II)
1570 (5 mN/m and 25 mN/m, $60^\circ$ , pH 9)	$\beta$ -sheet (amide II)
1720 (5 mN/m and 25mN/m, $60^\circ$ , pH 9)	$\beta$ -turn

**Table 4.1 Band assignment of the FTIR and IRRAS spectra related to the secondary structure of human insulin in aqueous solution and as Langmuir monolayer.**

(II) ions has been observed as a wider peak at around  $1650\text{ cm}^{-1}$  is observed in the plot representative of the HI solution with Zn (II) ions. The new absorption peak at around  $1720\text{ cm}^{-1}$  in the presence of zinc ions was assigned to  $\beta$ -turn structures. From the data (Fig. 4.5C) we thus concluded that the hexameric state of insulin was formed at the air-water interface; (iii) the insulin Langmuir monolayer with acidic and basic spreading solvent had unique absorption peaks at around  $1525$  and  $1570\text{ cm}^{-1}$ , respectively. This observation shows a significant difference between samples under acidic and basic conditions, implying that the human insulin Langmuir monolayers under different pH levels have different orientations at the air-water interface.

The spectra of human insulin Langmuir monolayer at  $25\text{ mN/m}$  at various pH values in absence and presence of Zn (II) ions were shown in Fig. 4.5D. In contrast to the spectra obtained at  $5\text{ mN/m}$ , the spectra seen at  $25\text{ mN/m}$  (Fig. 4.5C) showed similar peaks; even though the intensity of each peak increased when the surface pressure increased, the position and shape remained close to each other. From such observation we can conclude that there were few, if any, conformational and orientational changes when the surface pressure increased. We can justify the small shift of the peaks in the spectra, e.g. from  $1560$  to  $1570\text{ cm}^{-1}$  and  $1525$  to  $1520\text{ cm}^{-1}$ , by the mechanism of intermolecular hydrogen bonding, which is induced by the increase of the surface pressure, making the peptide chains from different molecules close enough to interact with each other.<sup>91</sup>

Since the p-polarized IRRAS is more sensitive to the vibration perpendicular to the air-water interface,<sup>99; 100</sup> pertinent information can be obtained on the orientation of the human insulin Langmuir monolayer in 2-D. Therefore, the IRRAS data were used to

propose an orientation model of the human insulin Langmuir monolayer subject to different pH values of spreading solvent in the presence of Zn (II) ions in the subphase.

#### 4.6 CD spectroscopy of human insulin aqueous solution

CD spectroscopy is an appropriate technique to measure the secondary structure of the protein molecule in the far-UV region (190-260 nm).<sup>101</sup> The CD spectra of human insulin aqueous solution are shown in Figure 4.6 at various pH and in absence and presence of

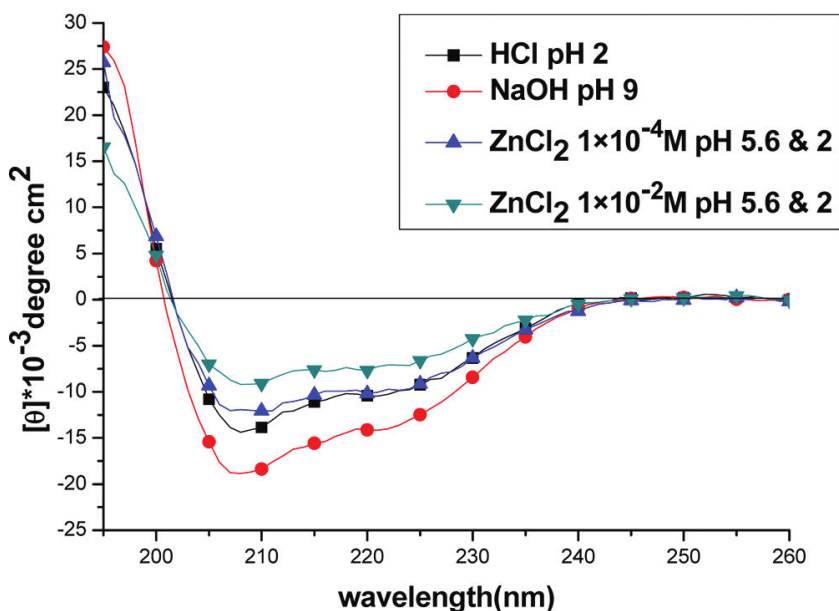


**Figure 4.6** CD spectra of human insulin aqueous solutions at pH 2 and pH 9 in absence of ZnCl<sub>2</sub> and at pH 5.6 in presence of ZnCl<sub>2</sub>. (Concentration of solution 10<sup>-4</sup> M; optical path length: 1 mm).

Conditions		Helix(%)	Beta-Sheet(%)	Others(%)	Scale Factor
HCl pH 2	Fraction	75	20	5	0.999
	Standard Error	1.8E-03	3.9E-03	3.2E-03	
NaOH pH 9	Fraction	61	33	6	1.000
	Standard Error	1.2E-03	2.9E-03	2.3E-03	
ZnCl <sub>2</sub> 1E-4M	Fraction	69	23	8	0.999
	Standard Error	1.9E-03	2.2E-03	3.2E-03	
ZnCl <sub>2</sub> 1E-2M	Fraction	59	22	19	0.999
	Standard Error	2.0E-03	3.3E-03	3.0E-03	

**Table 4.2 Secondary structure estimation of the aqueous human insulin CD spectra using Softsec software.**

Zn (II) ions. Table 4.2 shows Softsec software estimation of the secondary structure of the human insulin protein in the different aqueous environments previously chosen. The CD spectra showed maxima at about 208 and 220 nm with a crossing wavelength at 0 degree of ellipticity at about 203 nm. The positions of the maxima confirm the importance of the  $\alpha$ -helix of the protein in aqueous solution. The data showed that the  $\beta$ -sheet conformation is more important at pH 9 than at pH 2. At low concentration of Zn (II) ions ( $10^{-4}$  M), one does not observe a significant change in the  $\alpha$ -helix and  $\beta$ -sheet content, but at a higher concentration ( $10^{-2}$  M), the  $\alpha$ -helix content is reduced in favor of

other conformations, including  $\beta$ -strand and  $\beta$ -turn. This result can be justified by the fact that an induced aggregation on insulin reduces the  $\alpha$ -helix and increases  $\beta$ -strand as well as  $\beta$ -turn content. This deduction is congruent to the works already reported on the hexameric state of insulin, which showed more  $\beta$ -strands and  $\beta$ -turn conformations.<sup>102</sup>

#### **4.7 A proposed model for the human insulin Langmuir monolayer**

A proposed monolayer model of the human insulin Langmuir monolayer is presented in Figure 4.7 as an explanation to the emerging properties of insulin in different pH conformations and with the Zn (II) ion parameter. FTIR, IRRAS and CD spectroscopic analyses have shown that the insulin hexamer was able to be formed at the air-water interface when Zinc (II) ions were present in the subphase. When the insulin hexamers were compressed at the air-water interface, a monolayer film having two orientations was formed, as it is shown in Figures 5.6 A and B. In Figure 4.7 A, chain B of insulin is believed to be horizontally in contact with the water and in Figure 4.7 B, chain A of insulin is partially immersed into the subphase. A previous experiment has reported that insulin in basic condition has a relatively loose structure due to the titration of the A1 alpha-amino group.<sup>17</sup> Therefore, it is reasonable to assume that the insulin hexamer with basic conformation has an orientation as the one seen Figure 4.7 B at the air-water interface since a more loose structure of the insulin can increase the possibility of chain A to be immersed into the water instead of being folded inside the aggregation conformation. On the other hand, the orientation shown in Figure 4.7 A was assigned to the insulin hexamer present under acidic conditions. The proposed orientation of the insulin hexamer corresponds to the results of the IRRAS experiments we have done,



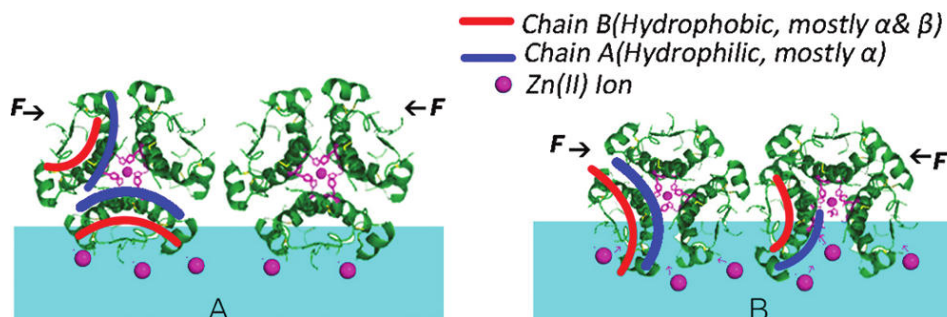


**Figure 4.7 The proposed insulin hexamer orientation at the air-water interface with acidic (A) and basic human insulin samples (B).**

where acidic conformations exhibit stronger signals of the  $\alpha$ -helix, while basic conformations exhibited greater  $\beta$ -sheet signals. At p-polarization, the IRRAS spectra were observed to be more sensitive than the ones having vertical orientation. It is clear that in the proposed orientation, human insulin under acidic conditions has chain A (mostly  $\alpha$ -helix) more likely to be in the vertical direction, while under basic conditions such is the case for chain B (mostly  $\beta$ -sheet and  $\beta$ -strands). As shown in Figure 4.7 B, when human insulin with basic spreading solvent forms a Langmuir monolayer, the submerged part of the chains in insulin are more prone to attack due to the abundance of zinc ions from the subphase. This can lead to a partial destruction of the insulin hexamer. This concept of the partial destruction of the insulin hexamer in basic condition can also be used to explain the experiment results of surface pressure and surface potential that we have obtained.

## 4.8 Conclusion

Several studies on insulin aggregation have been done in the aqueous and crystalline phases. However, such research done at the air-water interface has been seldom. We have reported the dynamics of insulin aggregation at the Langmuir monolayer including the effect that the aggregation has from Zn (II) in the subphase, while the secondary structural change in the aggregation process has been reported. The aggregation of human insulin was confirmed by measurements of surface pressure-area and surface potential-area isotherms and spectroscopic data. In general, the aggregation dynamics of insulin as a monolayer has been observed to be particularly similar in the aqueous and crystalline phases.

Nonetheless, through the peculiar environment of the air-water interface we have observed certain contrasting properties on the aggregation process as the environmental conditions were changed. The infrared absorption and CD spectroscopy approach from our study have confirmed that the secondary structure of the insulin protein possessed a higher content of  $\beta$ -sheet and  $\beta$ -strands as aggregation occurred under basic conditions. Based on the experimental data, we have proposed a human insulin (HI) monolayer model of the insulin conformation and dynamics under acidic and basic conditions. Overall we have shown the contrasting aggregation dynamics that human insulin has on pH at the air-water interface, shedding light for promising research on the effect that pH has on protein aggregation at cell membranes.

## Chapter 5

### Human Insulin-Fibril Assisted Synthesis of Fluorescent Gold Nanoclusters

#### 5.1 Background

Nanoparticles are increasingly being used in the field of medicine, for catalysis and as probes for imaging. Some of its biological applications have included tumor targeting, imaging, therapy and drug delivery.<sup>103-111</sup> Quantum dots have been in the forefront of nanoparticle research due to its high fluorescence which makes it an attractive candidate for application as a probe. Quantum dots are composed of semiconductor elements like CdSe, CdTe and PbS and have been shown to have adverse effect on biological systems. Even after elapse of a considerable time period, elements like cadmium and lead were are found accumulated in body organs like liver.<sup>112-114</sup> Synthesis procedures for quantum dots and many nanoparticles take place at high temperatures, require strong reducing agents and organic solvents.<sup>115</sup> A green chemistry synthesis procedure for nanoparticles involving aqueous solution, low temperature, no toxicity while maintaining a high fluorescence is a needed alternative for quantum dots.

#### 5.2 Gold nanoparticles: an overview

Transition metal nanoclusters composed of gold or silver are often sought for their stability and low levels of toxicity. Gold nanoparticles (Au NPs) and gold nanocrystals (Au NCs) have received significant attention in the research field because of their high biocompatibility and tunable imaging applications as fluorescent biomarkers. Au NPs have been shown to being benign in biological systems are used extensively as probes,

biosensors, drug carriers.<sup>116-121</sup> Au NPs are usually synthesized by the Turkevich method where hot chloroauric acid is added to sodium citrate. Sodium citrate acts as the reducing and the capping agent. Particle size between 10- 200 nm can be controlled by varying concentration of sodium citrate.<sup>122-124</sup> AuNPs in organic solvents are synthesized by Brust method where sodium borohydride acts as the reducing agent.<sup>125</sup> Au NCs also exhibit low toxicity and have been proven to be potentially compatible to viable organisms due to their unique properties, such as the negligible oxidation potential of gold and the Au NCs ultrafine size and arrangement. Au NCs are usually synthesized by reduction of chloroauric acid by sodium borohydride.<sup>126-129</sup>

### **5.3 Literature review and limitations of proposed mechanisms for synthesis of AuNCs by proteins**

A green chemistry method for synthesis of Au NCs was first reported by Xie and group in a study published in 2009. The reduction of gold salt was carried out by protein bovine serum albumin (BSA).<sup>130</sup> Chloroauric acid was added to BSA (50 mg/ml) in a basic aqueous solution and stirred for 12 hours at 37 °C to give Au NCs. The possible mechanism for synthesis was suggested due to reduction of the gold salt by the 21 tyrosines present in BSA protein. To verify this hypothesis, an experiment was performed in our lab where comparable concentration of tyrosine as in BSA was added under similar experimental conditions. However, fluorescent Au NCs were not synthesized. Other amino acids like histidine and cysteine were also used in place of BSA to synthesize Au NCs, however fluorescent Au NCs were not produced. This suggests that the reduction of the salt is not due to individual amino acids as suggested in the paper, but the structure of the protein as a whole plays a role in the reduction of the salt. Another study published in

2012, utilized bovine insulin (BI) as a template to synthesize Au NCs.<sup>131</sup> This study zeroed in on the S-S bond that holds the two chains of the protein together to play an important role in this synthesis and proposed that Au NCs formed could be used for biological imaging. However, this study was carried out at 4 °C and did not take into account that insulin fibrillates at body temperature.

Various proteins like BSA, insulin and lysozyme can produce Au NCs, however the mechanism might be different for different proteins. During the synthesis with insulin as a template in our lab at the physiological temperature of 37 °C , Au NCs were discovered to be formed within a matrix of insulin fibers. This is the first reported study that examines the role of insulin fibers on the synthesis of Au NCs. Our study examines the influence of insulin fibrillation on synthesis and fluorescence of Au NCs.

#### **5.4 Synthesis of gold nanoclusters**

In a typical synthesis, 5 mL of an aqueous, basic solution was made by the addition of NaOH to ultra-pure water so that the solution would reach pH 10.5. Human insulin (1.486 mg/mL, 256  $\mu$ M) was readily dissolved in this solution and left to incubate at 37°C for 6 h. The heated insulin solution was then added to 5 mL of an aqueous H<sub>2</sub>AuCl<sub>4</sub> solution (1.82 mM). Since addition of the H<sub>2</sub>AuCl<sub>4</sub> solution caused a significant pH drop in the total solution (pH 7), the mixture was brought back to moderate basic conditions (pH 10) through the addition of 1 mL of 2 mg/mL NaOH. After the base addition, the reaction was led to progress for an extended incubation at 37°C under constant stirring with a magnetic stir bar, finalizing after 36 h of incubation of the insulin-Au complex.

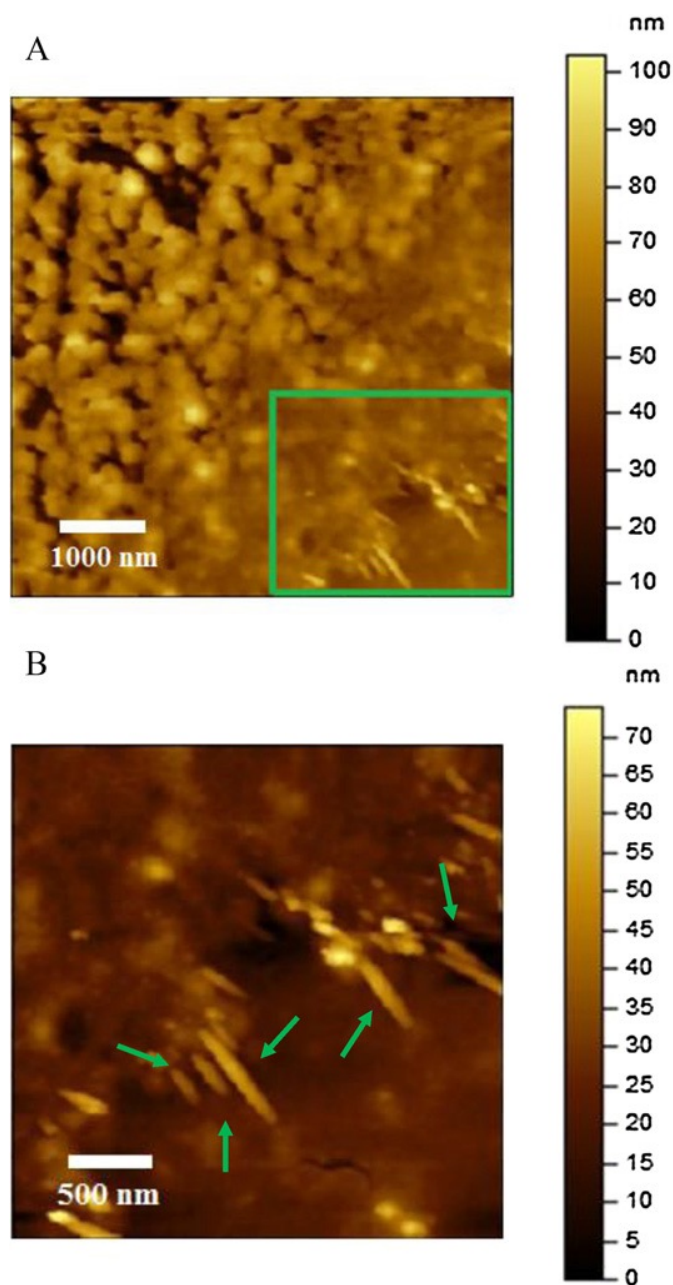


**Figure 5.1** AFM image ( $6\ \mu\text{m} \times 6\ \mu\text{m}$  scan) of (A) human insulin ( $256\ \mu\text{M}$ ) in aqueous solution pH 10.5 after 6 h of incubation at  $37\ ^\circ\text{C}$ . (B) The magnified section ( $3\ \mu\text{m} \times 3\ \mu\text{m}$  scan) of (A) (green box) shows rod-like insulin aggregates (green arrows). (For interpretation of the references to color in this figure legend, the reader is referred to the web version of the article.)

## 5.5 Characterization of gold nanoclusters by AFM and TEM Imaging

Initially, human insulin was heated at 37 °C in alkaline (pH 10.5) aqueous solution for 6 h. Fig. 5.1A shows the AFM image for the insulin solution after this step was taken. As we can see from the AFM image, there is a great variation in the structure of insulin. The structures approaching the top-left sector, for instance, are characteristic of aggregated insulin oligomers due to their varied globular structures. In contrast, the bottom-right sector of Fig. 5.1 A has a relatively homogeneous appearance, which has been deduced to pertain to insulin monomers, dissociated from their oligomeric forms due to the higher charge repulsion conditions of the basic pH environment. The latter sector, however, was not entirely homogeneous. Fig 5.1A, a magnified section (green box) within the homogeneous sector in Fig 5.1A, shows insulin ‘rod-like’ fibrils, which had most likely been generated after the insulin monomers facilitated nucleation and subsequent fibrillation by abnormal hydrophobic-site exposure and aggregation.

The TEM image in Fig 5.2A illustrates the morphology of insulin in the Au NCs solution, showing amyloid fibrils in a developed state and after the 36 h of incubation of the insulin–gold complex at 37 °C and constant stirring. In order to fully attribute the fibrillation process to the manipulation of the pH and temperature conditions, an insulin reference to the Au NCs synthesis was prepared and analyzed in the TEM image in Fig. 5.2B. The insulin reference emulated the insulin Au NCs synthesis by replacing addition of HAuCl<sub>4</sub> with addition of HCl, excluding HAuCl<sub>4</sub> as a factor that could influence insulin fibril formation. As amyloid fibril formation could be clearly observed on the insulin reference sample (Fig. 5.2B), the fibrillation process of insulin had been herein

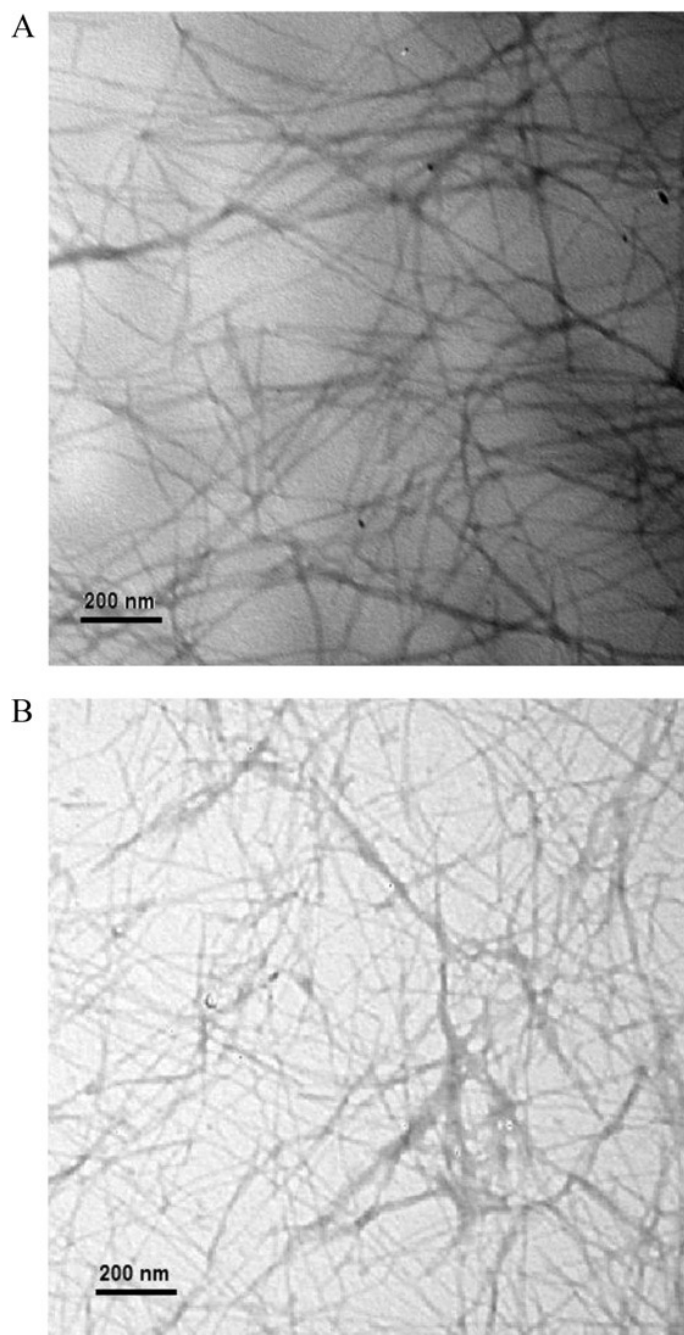


**Figure 5.2** TEM images of (A) the insulin fibrils Au NCs and its corresponding insulin reference (B) in aqueous solution, pH 10. The insulin reference emulates the current synthesis of insulin Au NCs shown in (B), replacing  $\text{HAuCl}_4$  for  $\text{HCl}$ , with an initial insulin incubation of 6 h and secondary incubation of 36 h at  $37^\circ\text{C}$ . Final insulin concentrations in insulin Au NCs and in the insulin reference were both approximated to be around  $128\ \mu\text{M}$  in solution.



shown to be caused by the heated, basic pH environment, dissociating oligomers into monomers by the charge-repulsion nature of the alkaline environment, and accelerating hydrophobic interactions into insulin fibrils from the stirring and the higher temperature conditions, which are known to increase molecular collisions.

### **5.6 Fluorescence spectroscopy analysis of gold nanoclusters**

Fig 5.3 shows normalized fluorescence bands of human insulin Au NCs made through:

- i) changes in the method (i.e. heating), and
- ii) changes in the solution environment (i.e. buffer solutions, pure aqueous solutions).

Fig. 5.3 shows relative fluorescence intensity values, which are fluorescence intensities normalized to the water Raman peak at 559 nm. Relative fluorescence intensity values can be very useful for imaging processes and biosensing applications, as these values measure the capacity to discriminate the fluorescence of the analyte from that of a secondary analyte. In the present case, the 550–800 nm range is an adequate domain for this type of comparison as the nanocluster fluorescence at 620 nm predominates in this spectrum.

The fluorescence bands shown in this figure all correspond to human insulin Au NCs syntheses made through the addition of  $\text{HAuCl}_4$  to an insulin solution, followed by addition of base (NaOH) and 12 h of constant stirring and incubation at 37 °C. As explained above, however, some of the insulin Au NCs made herein had undergone different synthesis conditions, and the changes had consequently affected their Au NCs fluorescence intensities.

Initially, we have made human insulin Au NCs in phosphate buffered saline (PBS) solution by dissolving unheated insulin in PBS, and following all the above mentioned procedures until its termination after 12 h of incubation (Fig 5.3A, pink). The synthesis that followed was that of human insulin Au NCs in borax buffer, made by dissolving unheated insulin in borax buffer, and also following the latter protocol until completion (Fig. 5.3A, blue). These syntheses were made through the use of buffer solutions, and their respective Au NCs fluorescence bands were poor in their intensity relative to the

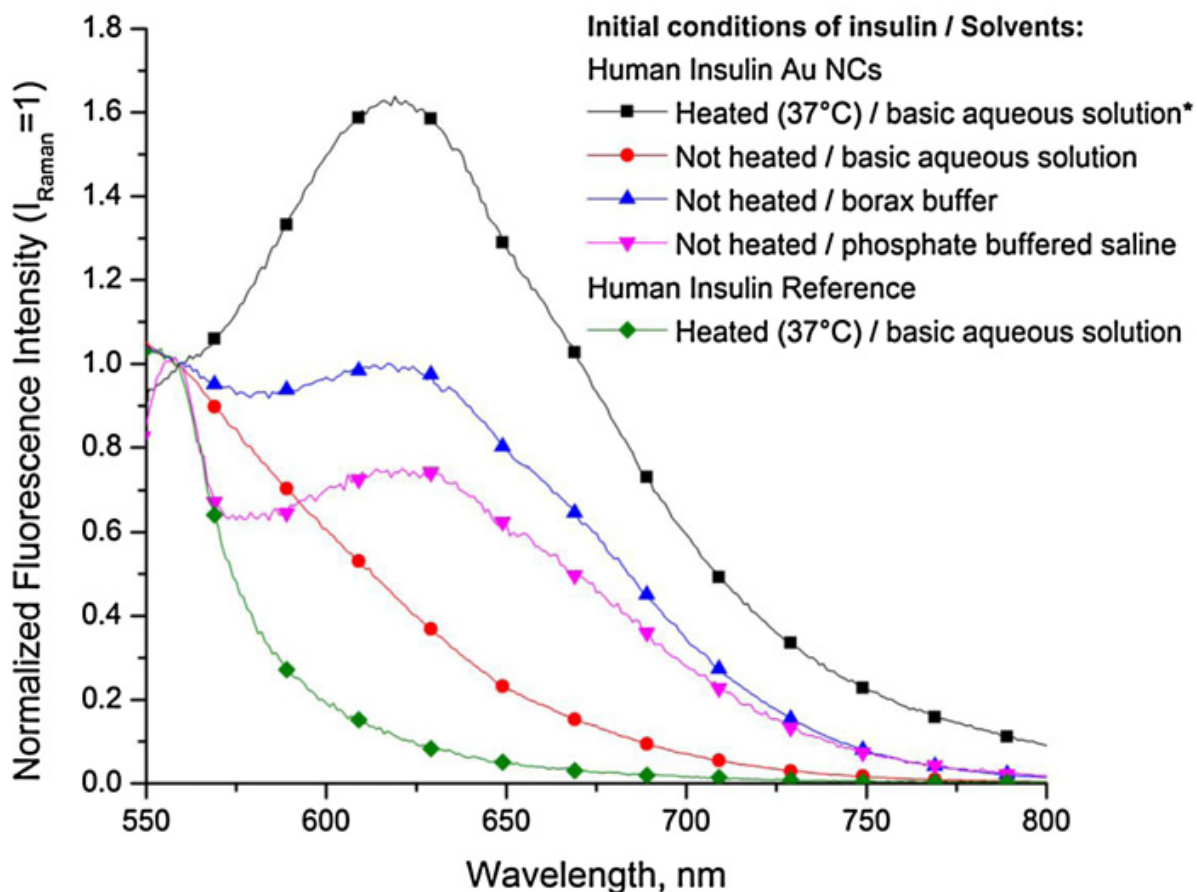


**Figure 5.3 Method comparison fluorescence spectrum ( $\lambda_{excitation} = 470 \text{ nm}$ ) of human insulin Au NCs, normalized at the water Raman peak at 559 nm (Au NCs emission at 620 nm). All samples had a 12 h Au NCs incubation time; the heated samples were heated at 37 °C for 6 h prior to the 12 h of Au NCs incubation.**

Raman peak, as the Raman peak was higher in height. Thus, a different approach had to be taken to generate Au NCs with higher fluorescence intensities. Throughout the previous sections we have defined a concise hypothesis of heat-assisted (37 °C) insulin fibrillation in a basic medium based on a series of deductions taken from the literature, while providing proof of the process through AFM and TEM technologies earlier in the report. In this section, we demonstrate how the parameters that were used to generate insulin fibrils in the alkaline medium can influence the nanocluster fluorescence intensity of human insulin Au NCs.

As the fibrillation hypothesis addressed insulin in an alkaline environment, a pure aqueous (buffer-free) alkaline solution was used. Fig. 5.3A(red) shows the fluorescence band of human insulin Au NCs in alkaline solution, made by dissolving unheated insulin in a NaOH-based aqueous solution, followed by the synthesis protocol until 12 h of incubation. It can be seen that the latter synthesis is comparable to the buffer-based syntheses as insulin was not heated prior to H<sub>Au</sub>Cl<sub>4</sub> addition. The normalized fluorescence intensity for this Au NCs synthesis is, however, lower than those syntheses prepared in buffers.

The fluorescence band (Fig 5.3A, black line) pertains to the fluorescence of insulin fibrils Au NCs in basic solution is defined in the paper as the main synthesis as it had been investigated in the AFM and TEM images (Fig 5.1 and Fig. 5.2, respectively). The insulin fibrils Au NCs synthesis differs from the others in its initial conditions. In this synthesis, the insulin solution was heated at 37 °C for 6 h prior to the H<sub>Au</sub>Cl<sub>4</sub> addition, whereas in the previous cases H<sub>Au</sub>Cl<sub>4</sub> was readily added after insulin was dissolved in its

solvent. The insulin fibrils Au NCs synthesis is the optimized synthesis as it exhibits the highest normalized intensity. Heating insulin at 37 °C prior to H<sub>Au</sub>Cl<sub>4</sub> addition proved to influence the fluorescence yield of the human insulin Au NCs, as insulin Au NCs made without the initial heating condition and incubated for a prolonged period of time, >12 h after H<sub>Au</sub>Cl<sub>4</sub> addition did not exhibit a higher Au NCs fluorescence intensity than the intensity of insulin fibrils Au NCs shown herein after 12 h of incubation. In addition, a reference (Fig. 5.3, green curve) made from an insulin solution exposed to the same conditions as the optimized synthesis shows that the fluorescence at 620 nm pertains to the Au NCs fluorescence band. Further proof of the optoelectronic properties of insulin fibrils Au NCs are discussed in the following section.

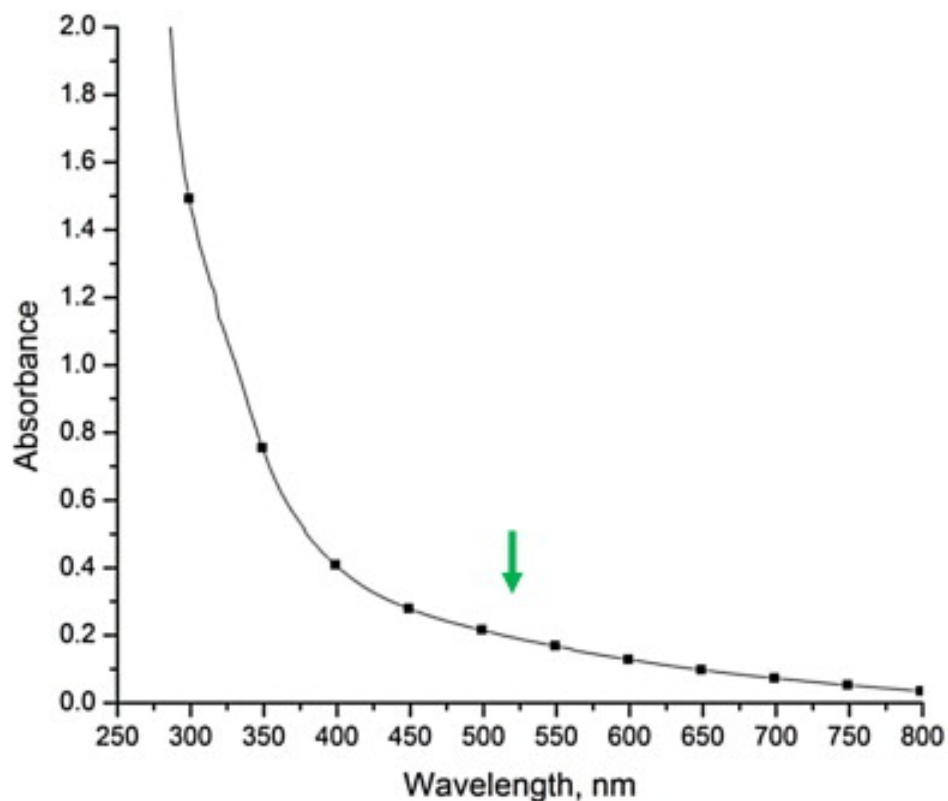


**Figure 5.4 UV-visible absorption spectrum of insulin fibrils (128 μM) Au NCs synthesized under optimized conditions. Initial insulin concentration: 256 μM in 5 mL alkaline solution.**

Fig. 5.4 shows the UV–Vis absorption spectrum of the optimized synthesis of insulin fibrils Au NCs. The surface plasmon band (SPB), typically located at around 520 nm, was absent from the absorption spectrum, indicating that there was no formation of Au nanoparticles with core diameters of more than 2 nm. Thus, for nanostructures particular to the observed case, fluorescence effects not attributed to light scattering nor inherent of the protein itself would have their origin in nanocluster systems classified as molecular ligand–metal clusters, with a metal core cluster size ranging from 1 to 3 nm. Because the as-prepared sample fluoresces at 620 nm, the absorption spectrum data confirms the presence of noble metal nanoclusters in the current synthesis approach and determines the system to be particular to molecular-ligand NCs.

The as-prepared insulin fibrils Au NCs exhibited a subtle yellow color under visible light and a fluorescence band at 620 nm characteristic of an  $\text{Au}_{25}$  cluster system . Fig 5.5 shows the fluorescence spectra (in counts per second) of the insulin fibrils Au NCs after ‘insulin–Au complex’ incubation times of 12 and 36 h. The Au NCs fluorescence band in Fig 5.5 shows no apparent growth between the 12 and 36 h interval, while showing little growth once the data had been normalized with respect to the water Raman peak

In Fig 5.6, the fluorescence band of the insulin Au NCs was taken at different excitation wavelengths to generate a three-dimensional, excitation–emission spectrum, showing the optimal  $\lambda_{\text{excitation}}$  at 470 nm. From the same plot we can confirm that the fluorescence at 620 nm had been exclusive to Au NCs and not a scattering light occurrence, as the contour lines show no wavelength shift from the 620 nm for different excitation wavelengths.

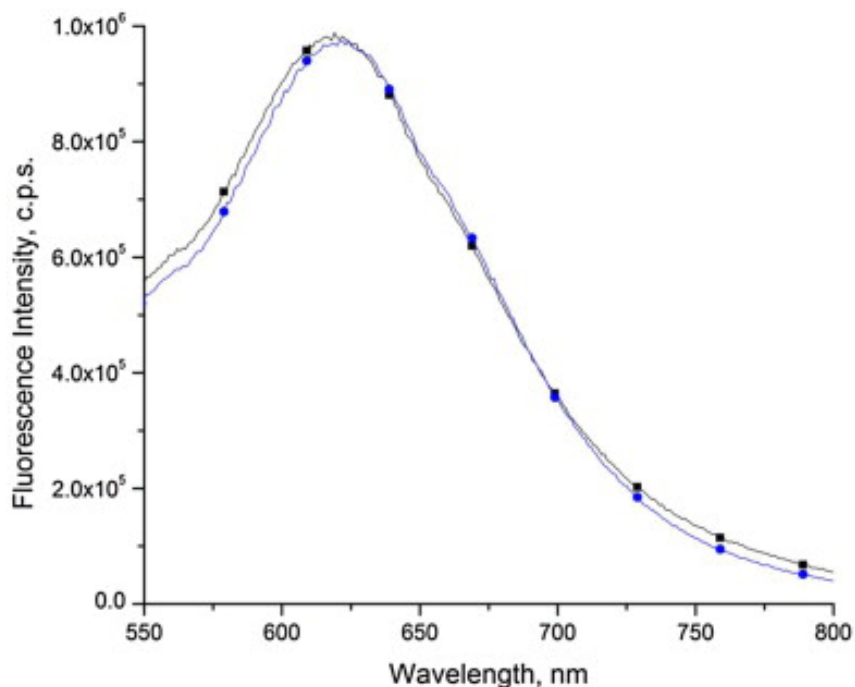


Figure 5.5 Time evolution of the fluorescence spectrum ( $\lambda_{\text{excitation}} = 470 \text{ nm}$ ) of insulin fibrils Au NCs synthesized under optimized conditions: pre-incubated (6 h at  $37^\circ\text{C}$ ) human insulin addition to  $\text{HAuCl}_4$  solution and subsequent incubation at  $37^\circ\text{C}$  for the listed times: 12 h (black) and 36 h (blue). NCs emitted at 620 nm.

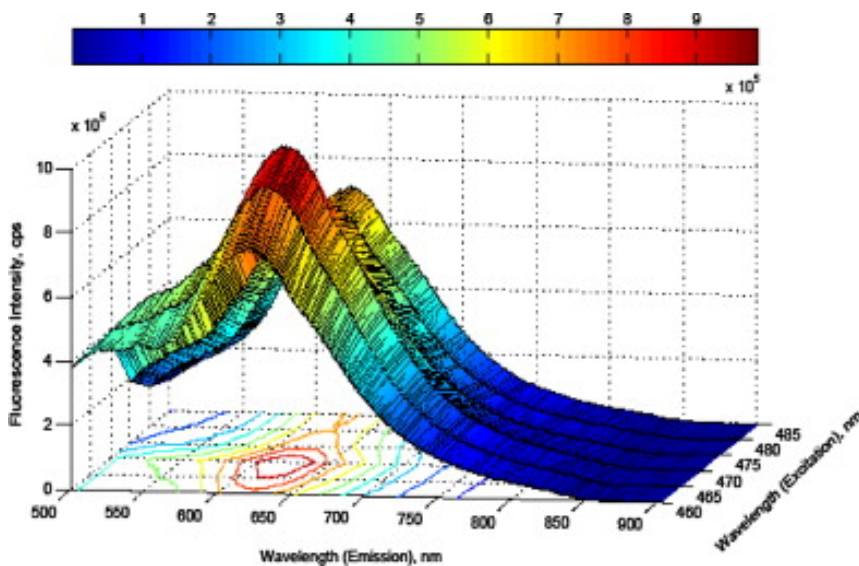


Figure 5.6 Combined fluorescence spectra of insulin fibrils ( $128 \mu\text{M}$ ) Au NCs at successive excitation wavelengths in 5 nm intervals: 460 nm (front) to 485 nm (back).

Experiments that had been performed in this investigation with BSA Au NCs following the protein-directed synthesis protocol produced Au NCs with a fluorescence band at 640 nm which exhibited a higher intensity relative to the fluorescence intensity of insulin fibrils Au NCs. It is assumed that this observed decrease in the NCs intensity of insulin Au NCs can be attributed to the lower amount of protein used for the current synthesis.

Since the NCs fluorescence band of the BSA Au NCs resonates at very close frequencies relative to the NCs band of insulin fibrils Au NCs, the emission wavelength of the latter (620 nm) would likely approach the emission wavelength of BSA Au NCs (640 nm) if insulin fibrils Au NCs fluorescence was increased. Experiments conducted throughout the investigation have shown that the increase in the insulin Au NCs fluorescence band occurs through the abscissa (increasing in intensity) and ordinate (“red-shifting”) axes conjunctively.

Human insulin from recombinant DNA, though endogenous and readily available in healthy humans, had a limited availability for research purposes as it had been relatively expensive. The

previously reported BSA Au NCs synthesis had a BSA reactant concentration of 752  $\mu\text{M}$  in 5 mL of solution, whereas the insulin concentration used in the current synthesis of insulin fibrils Au NCs has a reactant concentration of 256  $\mu\text{M}$  in 5 mL, an almost three-fold protein concentration reduction, with a remarkable difference in protein weight of about 242 mg less than the BSA weight from the previous protein-directed synthesis.

### 5.7 Synthesis of CdS quantum dots

HI (1mg/ml) solution is prepared by dissolving HI in an aqueous pH 2 solution. CdCl<sub>2</sub> and Na<sub>2</sub>S solutions of 1M are prepared in water. 10 ml insulin solution is placed in a round bottom flask. 50 ul of CdCl<sub>2</sub> and Na<sub>2</sub>S solution is added with stirring and at 37C. Aliquots were taken at different time periods during the experiment. CdS quantum dots were found within 30 minutes of the reaction. Similar procedure can followed with protein Bovine Serum albumin (BSA) except that it was dissolved in water instead of pH 2 solution.

### 5.8 Characterization of CdS qds

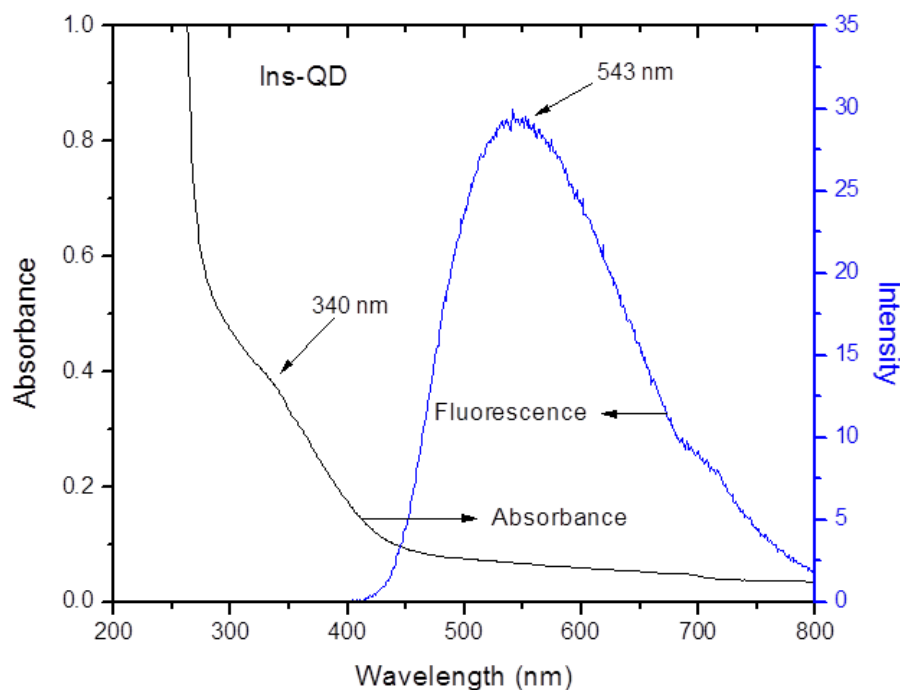


**Figure 5.7 UV-visible and fluorescence absorption spectrum of insulin CdS quantum dots.**



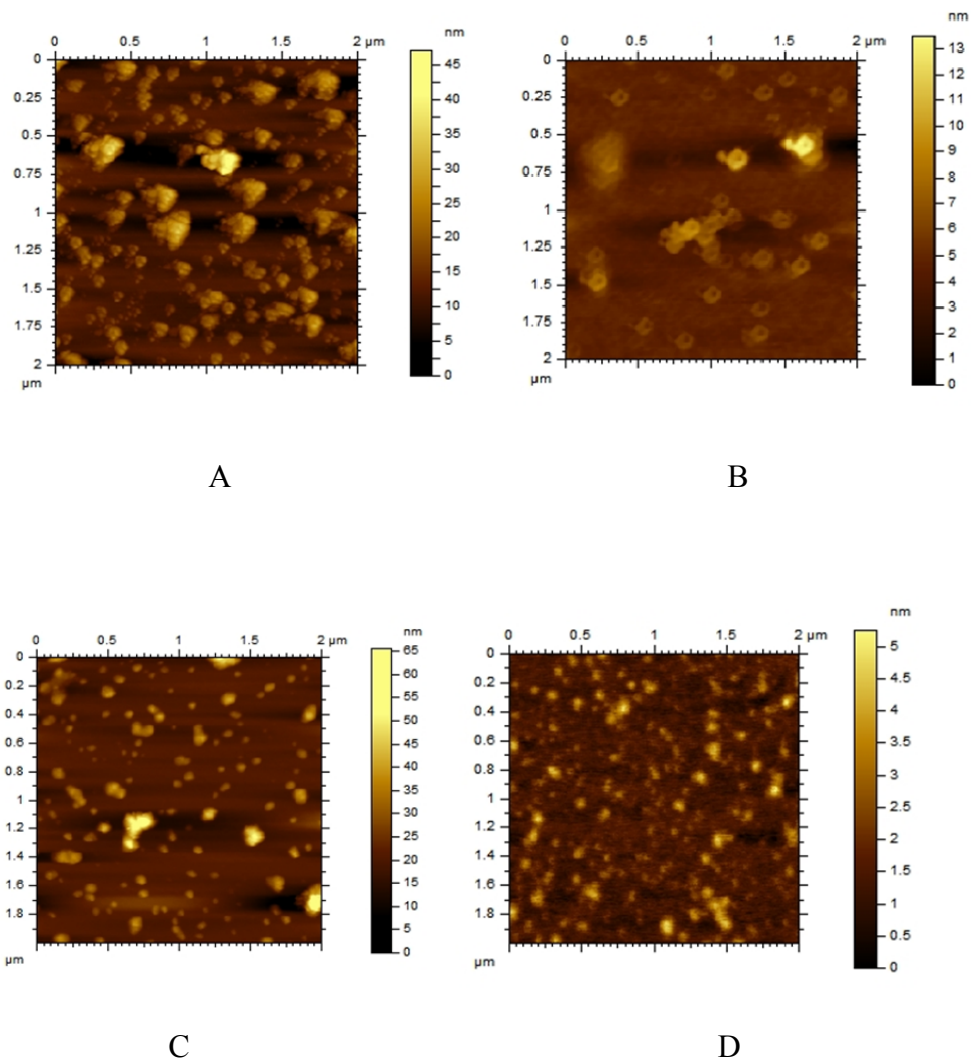


**Figure 5.8 AFM images ( $2\ \mu\text{m} \times 2\ \mu\text{m}$  scan) at 30 minutes for (A) insulin quantum dots B) insulin and at 12 hours for C) insulin quantum dots and D) insulin reference.**

An aliquot was taken from the reaction after 30 minutes. The presence of surface plasmon resonance band at 340 nm in the UV-vis spectrum in Fig 7.7 confirms the presence of quantum dots within 30 minutes the reaction. The fluorescence band was found constant at 543 nm. With increase in time for the reaction to 12 hours and 24 hours, there is a slight increase in fluorescence intensity.

AFM images in Fig. 5.8 show QDs and insulin reference at 30 minutes and 12 hours. AFM, fluorescence and UV-vis spectroscopies confirm presence of QDs within 30 minutes of reaction. The synthesized QD have high fluorescence intensity, are time-efficient manner and are prepared at room temperature.

## 5.9 Conclusion

The synthesis of insulin fibrils Au NCs has been reported as the addition of  $\text{HAuCl}_4$  solution to an alkaline aqueous solution where human insulin had been incubated for 6 h at  $37^\circ\text{C}$ , following by extended incubation at  $37^\circ\text{C}$  after the Au NCs precursor ( $\text{HAuCl}_4$ ) had been added. The “green” synthetic model employed for the synthesis of bovine serum albumin (BSA) Au NCs has been derived herein into a new theory for the synthesis of Au NCs in a fibril-dominant environment.

A deduction for the fibrillation of insulin in a basic environment has been provided in the study, while AFM and TEM measurements have confirmed the presence of amyloid fibrils in the human insulin solutions made through the methodology that had been hypothesized to favor fibril formation.

Human insulin Au NCs made through conditions favoring insulin fibrillation have been shown to have the highest fluorescence intensity values compared to those that do not, and while the Au NCs emission has not been found to be completely dependent of the fibrillation process, we can say that the two are highly correlated. The synthesized insulin fibrils Au NCs had high fluorescence intensity relative to the protein concentration that were used, as a comparison with the significantly higher protein amount of the previous protein-directed synthesis of BSA Au NCs was brought into light. The investigation gives

seeding insight to the fibrillation of insulin in alkaline environments and provides a new direction for research in the synthesis of protein Au NCs.

## Chapter 6

### Water Soluble Carbon Dots are Catalyst for Human Insulin Fibrillation

#### 6.1 History and background

Protein misfolding resulting in formation of amyloid plaques has been indicated to play a role in several diseases like Alzheimer's disease, diabetes type 2 and Parkinson's disease.<sup>1,2</sup> In the human body, there are 18 known proteins which have been observed to misfold and play a causative role in diseases. One of the main compound used to prevent protein fibrillation are nanoparticles like CdSe or CdTe quantum dots (QD). QD are highly fluorescent making them easy to track in a biological system, and are less than 10 nm in size enabling them to cross the blood brain barrier and interact with proteins. Experiments have shown that QDs can act either as a catalyst or an inhibitor for protein fibrillation based on several factors like the composition, concentration and size of the QD.<sup>3-6</sup> However, recent studies of QD have shown that cadmium based QD are toxic for biological systems due to leaching from the element cadmium.<sup>7</sup> This has resulted in search for benign nanoparticles which could be a viable replacement for QD.

A new class of highly fluorescent nanoparticles which have been touted as a replacement for QD are carbon dots (CD) due to their benign nature which makes them an attractive tool for biological research. Carbon dots were first reported in 2004 as one of the three components of single walled carbon nanotubes.<sup>8</sup> Due to their small size (6-8nm), CD can enter easily transverse in the human body, including the blood brain barrier. These properties make CD increasingly attractive for applications in biological systems. Several studies using carbon dots in biological systems, including various embryos of various

organisms have shown carbon dots to be non-toxic and a viable source for use in as a probe and for imaging.<sup>9-13</sup> However, effect of CD on protein fibrillation and aggregation in terms of their toxicity is an area which has not been investigated yet.

Although in the human body, only 18 proteins have been observed to misfold resulting diseases, all proteins can form fibrillate under appropriate conditions. A typical protein fibrillation involves a number of intermediate states, including nucleation, oligomerization, and fibril formation.<sup>132; 133</sup> The protein fibrillation investigated in this paper is for the protein Human Insulin. Human insulin is made up of two polypeptide chains called the A chain and the B chain which are joined to each other by disulfide bridges. As a monomer, the majority of the structure of insulin is composed of  $\alpha$ -helical structure and it dimerizes through the formation of  $\beta$ -sheet. Insulin is often found having a dimer structure which is due to hydrogen bonding between the C terminus of B chains.<sup>22</sup> Human insulin dimers come together to form hexamers in the presence of zinc ions. Monomers and dimers readily diffuse into blood, whereas hexamers diffuse poorly. Hence, absorption of insulin preparations containing a high proportion of hexamers is delayed and somewhat slow.<sup>23</sup> Increase in glucose levels in the blood is one of the major triggers for release of stored insulin from the pancreas. Human insulin hexamers molecules releases six monomeric insulin molecules in the bloodstream. Firstly, one insulin hexamer forms three insulin dimers. This is followed by formation of two monomers from one insulin dimer.

Human insulin in human body have not been observed to form fibers or plaques. However, in vitro, human insulin is readily converted to an inactive fibrillar form by incubation at high concentrations, low pH, and high temperatures. In the present study,

we have investigate the effect of dihydrolopoic acid (DHLA) capped carbon dots (CDs) on the fibrillation of human insulin protein. These carbons dots are hydrophilic and therefore are called Water soluble Carbon Dots (WCD). Two different ratios of WCD were added to human insulin and the fibrillation process of HI was observed. This is the first study which is observing effects of CD on a protein. The fibrillation of the protein was monitored by UV-vis and fluorescence spectroscopies. The conformational changes in the secondary structure were tracked through circular dichroism and monitored visually through Transmission Electron Microscopy (TEM) and Atomic Force Microscopy (AFM). One has observed that WCD as a catalyst for human insulin fibrillation as in the presence of WCD, human insulin fibrillation is initiated 7 times faster when compared to absence of WCD.

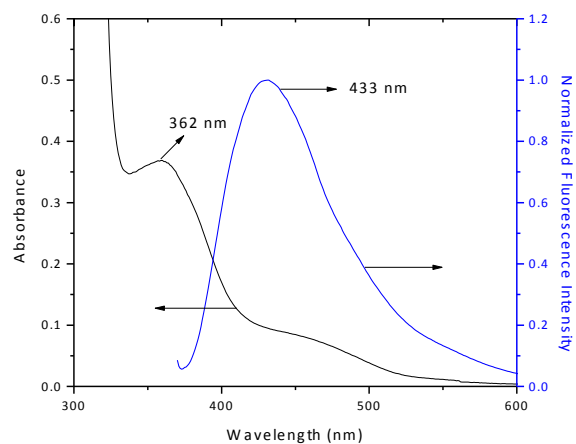
## **6.2 Synthesis and methods**

Aliquots of human insulin solutions were diluted 10-fold into a 5  $\mu$ M Congo red buffer solution. UV-vis sample measurements used a quartz cuvette with a 10 mm optical path length. Wavelength measurements were taken from 400 to 700 nm. Absorption spectra of the protein solutions in the presence of the Congo Red (CR) dye were compared with that of the Congo red buffer alone and the protein solutions in the absence of the Congo red dye.

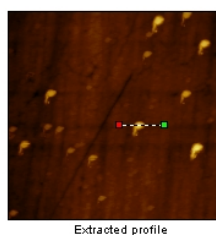
Thioflavin T binding assays were conducted by first preparing a 1 mM Thioflavin T stock solution in 1  $\times$  PBS buffer and stored at 4  $^{\circ}$ C and protected from light until usage. Aliquots of protein solutions were diluted 10-fold into the Thioflavin T stock solution. Fluorescence sample measurements used a quartz cuvette with a 10 mm optical path

length. Wavelength measurements were taken from 460 to 700 nm, using an excitation wavelength of 450 nm. All fluorescence intensity measurements were background-corrected with a 20  $\mu$ M Thioflavin T solution that did not contain human insulin and human insulin-WCD. The intrinsic fluorescence emission of tyrosine was used to monitor structural changes in the conformation of the protein. Wavelength measurements were taken from 300 to 500 nm, using an excitation wavelength of 275nm. Emission and excitation slit widths were typically 5 nm.

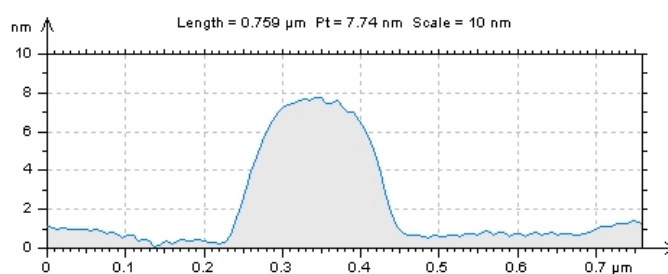
Carbon dots were synthesized by the procedure developed by Wang and co.<sup>86</sup> A mixture of 15 ml octadecene and 1.5 gram hexadecylamine were heated in a three-neck flask under Argon flow to 300 °C, and then 1 gram of citric acid was injected into the mixture. The solution was allowed to remain at 300 °C for 5 minutes and slowly allowed to cool to room temperature. The solution was purified by precipitating with acetone and dissolved in chloroform. Figure 6.1 characterizes the ODC carbon dots synthesized. ODC are light yellow in color and show absorbance at 360 nm. When excited at 360 nm, the emission spectra was observed at 433 nm as shown in Figure 6.1A. Imaging through AFM (Figure 6.1B and 6.1C) and TEM (Figure 6.1D) confirms that the OCD are between 6-8 nm similar to the literature.



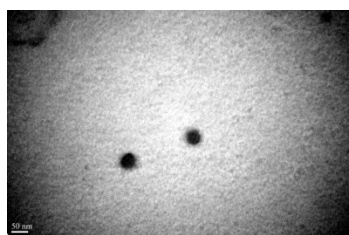
A



B



C



D

**Figure 6.1** Characterization of oil soluble carbon dots (OCD) dissolved in chloroform. A) fluorescence spectra when excited at 360 nm, slit width of 5 nm, 5 nm and cell length 1 cm. Visual confirmation presence of OCD by B) AFM image (11  $\mu\text{m}$  X 11  $\mu\text{m}$ ) of OCD; C) Extracted profile of one WCD; D) TEM image of WCD.



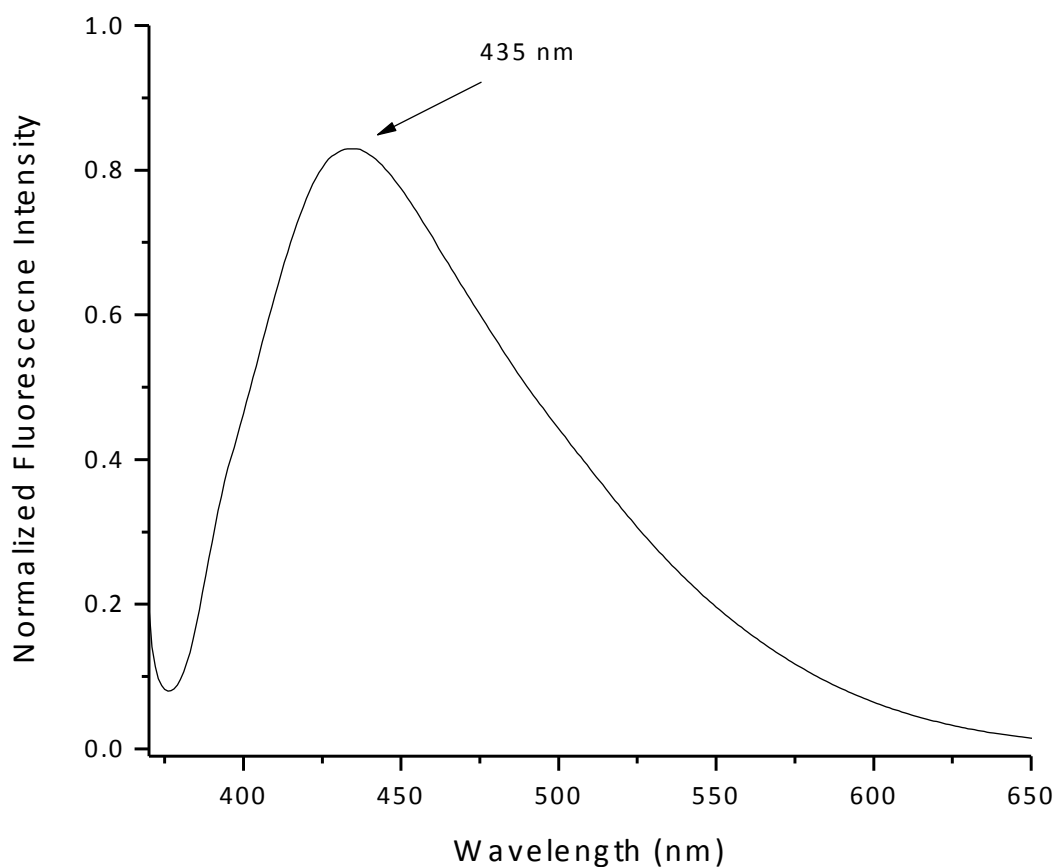
Dihydrolipoic acid (DHLA) was synthesized by reducing lipoic acid with sodium borohydride and the product formed was isolated in chloroform. 3 ml of OCD was added to 0.5 g of DHLA in methanol as solvent and heated to 60 °C for 4 hours. Potassium tert-butoxide was added to basify the solution and it was centrifuged to obtain precipitates, which were dissolved in water to get the Water Soluble Carbon Dots (WCD).

1 mg/ml human insulin was dissolved in pH 2 solution with 25 mM NaCl and incubated at 37°C with stirring.<sup>134</sup> Samples were withdrawn at various time periods and characterized for fiber formation. WCD of two different ratios (protein-to-WCD mass concentrations of 5000:1 and 500:1) were added to human insulin sample under similar incubation conditions. WCD was added to samples were withdrawn at time intervals of 30 minutes and characterized for fibril formation.

### **6.3 Characterization of the WCD**

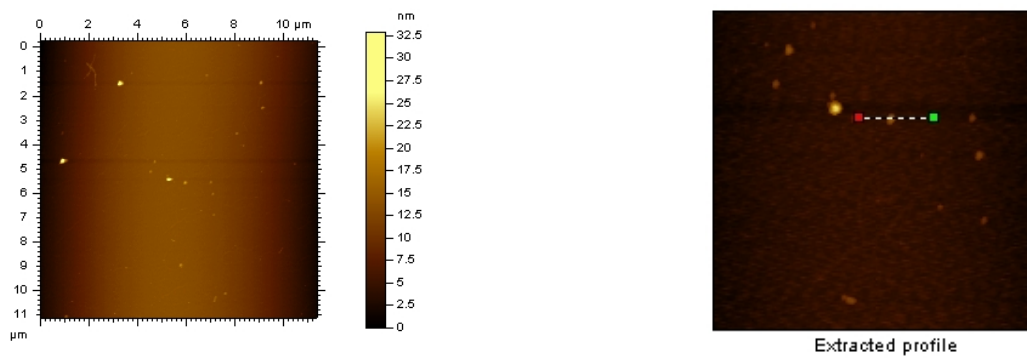
Characterization of the WCD was carried out using fluorescence spectroscopy and microscopy. The characteristic fluorescence spectra for OCD where a shift in wavelength in excitation results in a shift in the emission wavelength was also observed for WCD.<sup>86</sup> Figure 2A shows the fluorescence spectra of WCD when excited at 360 nm showing an emission peak at 435 nm. Encapsulation of OCD with DHLA resulted in hydrophilic WCD and this procedure does not affect the shape or result in any shift in the fluorescence peak. Figure 2B shows a drop cast of WCD on a mica slide. The figure shows several spherical structures. Figure 2C is an enlarged scan of the mica slide to characterize a single WCD. Figure 2C shows the topography for the WCD and it was observed to be between 6-8 nm in diameter. TEM image in Figure 2D correlates with AFM and

confirms diameter of WCD to be between 6-8 nm. Several WCD spherical in shape was observed in the TEM image. TEM image of WCD confirms WCD dissolved in water was evaporated to calculate their mass. The protein to WCD ratios used were 1: 5000 and 1: 500.



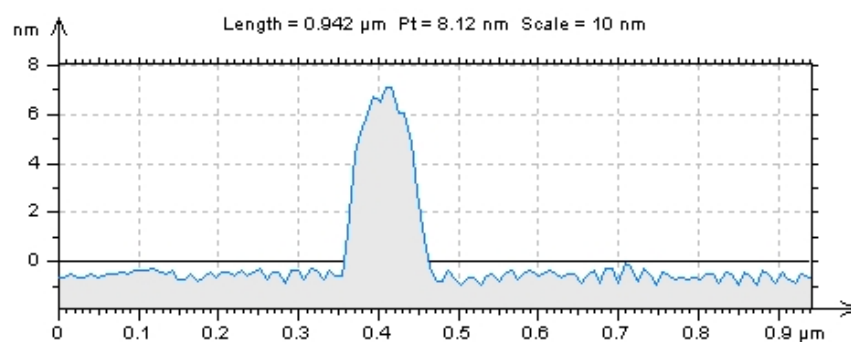
A

**Figure 6.2A: DHLA capped WCD's A) fluorescence spectra when excited at 360 nm, slit width of 5 nm, 5 nm and cell length 1 cm.**

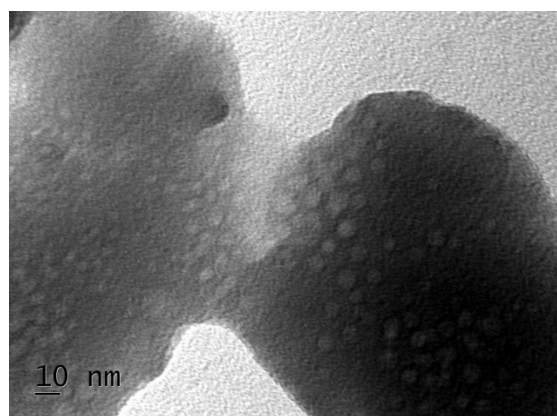


B

C



D



E

**Figure 6.2 Visual confirmation presence of WCD by B) AFM image (11 μm X 11 μm) of WCD; C) Extracted profile of one WCD; D) AFM topography image of WCD and E) TEM image of WCD.**

#### 6.4 Spectroscopic characterization of fibrillation of human insulin with WCD

Human insulin solutions were incubated with constant protein concentration of 1 mg/ml in 100 mM NaCl solution at pH 2 in the absence or presence of varying WCD concentrations (protein-to-WCD mass concentrations of 5000:1 and 500:1) at 37 °C. High protein to WCD ratios were chosen to ensure high loading capacity of Human Insulin on the surface of WCD. Different ratios were chosen for the purpose of distinguishing any rates of aggregation. The choice of WCD was due to the fact that WCD are increasingly replacing QDs due to their benign nature in biological applications.

It has been previously reported that the protein insulin has the ability to form fibrils in vitro under various (i.e., temperature-induced protein denaturation)solution conditions.<sup>134</sup> Hence, human insulin was subjected to thermal conditions that have been previously shown to be effective in inducing protein aggregation. Thermal conditions at 37 °C were chosen because it is proposed that human insulin undergoes a temperature-induced denaturation process through a three-state transition: (1) an initial lag phase, (2) an initiation stage where fiber formation starts taking place and increases rapidly with time and, (3) the final saturation phase where there is plateau in fiber formation.

Figure 6.3 shows Thioflavin T (ThT) fluorescence of human insulin and of human insulin with WCD of ratios 5000:1 and 500:1. With increase in time of incubation, the intensity of fluorescence emission at 485 nm increases.<sup>135; 136</sup> Figure 2 plots ThT human insulin fibrillation intensity at 485 nm with increasing incubation time. All the samples show increase in fluorescence intensity with increase in time. For the insulin sample, a well-

defined lag time is observed where there is no significant increase in fluorescence intensity at 485 nm for the first 4 hours of incubation. After the first 4 hours, a gradual increase in intensity is observed, which then reaches a plateau. On comparing with the human insulin samples incubated with WCDs, there is an increase in intensity from the very beginning. No lag time is observed for these samples. These samples directly enter the initiation stage and then go on to the plateau stage. The spectra also shows an increase in intensity of fibrillation with increase in concentration of WCD. The intensity of fluorescence was highest when the concentration of insulin to WCD was 500:1 ( $\blacktriangle$ , blue triangle), followed by 1 WCD for every 5000 insulin ( $\bullet$ , red circle) and lastly human

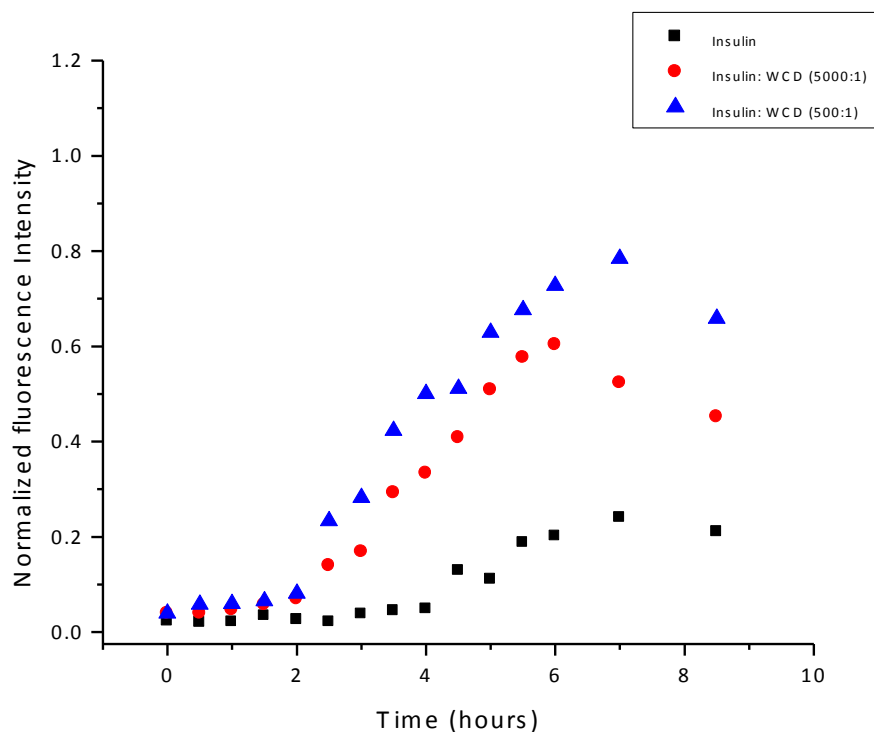
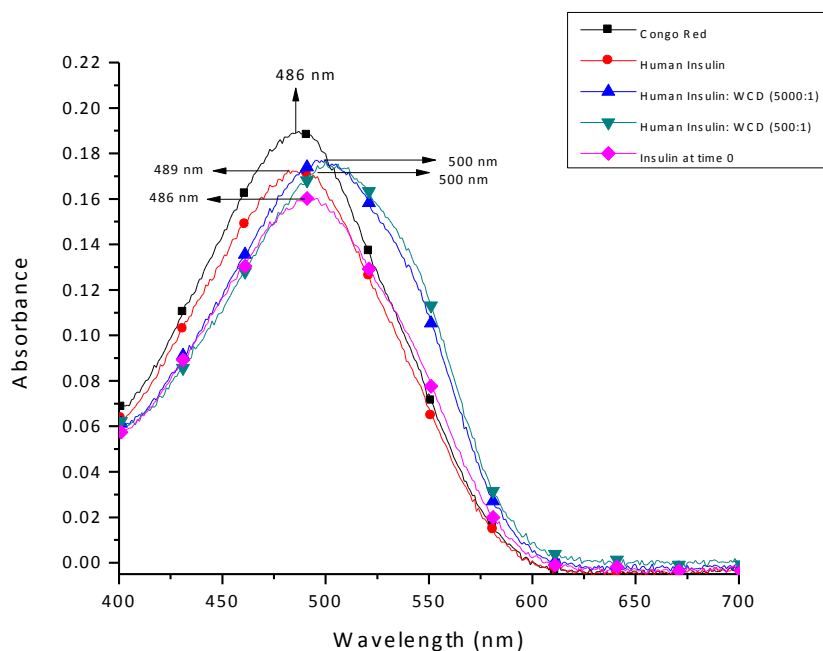


**Figure 6.3** Time evolution of Thioflavin T fluorescence of Human Insulin and Human Insulin-WCD at 37 C and pH 2, where ( $\blacksquare$ , black) Human Insulin, ( $\bullet$ , red circle) Human Insulin: WCD (5000:1) and, ( $\blacktriangle$ , blue triangle) Human Insulin: WCD (500:1). Slit width at the excitation and emission, 5 and 5 nm, respectively.

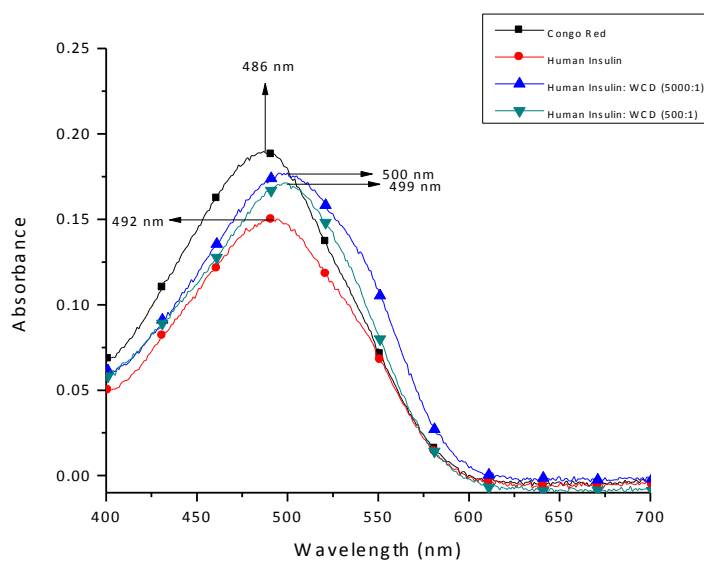
insulin (■, black) alone, suggesting that higher concentrations of WCD results in a higher rate of fibrillation.

The time periods 0.5, 3.5 and 6 hours are chosen for further characterization based on 1) AFM and TEM microscopy which will be discussed later in the paper and 2) based on the Tht T-human insulin curve as each time period represents one of the three phases of human insulin fibrillation which are lag phase, initiation of fibrillation and saturation of fibrillation, respectively. Congo Red absorbance spectroscopy for the three time periods

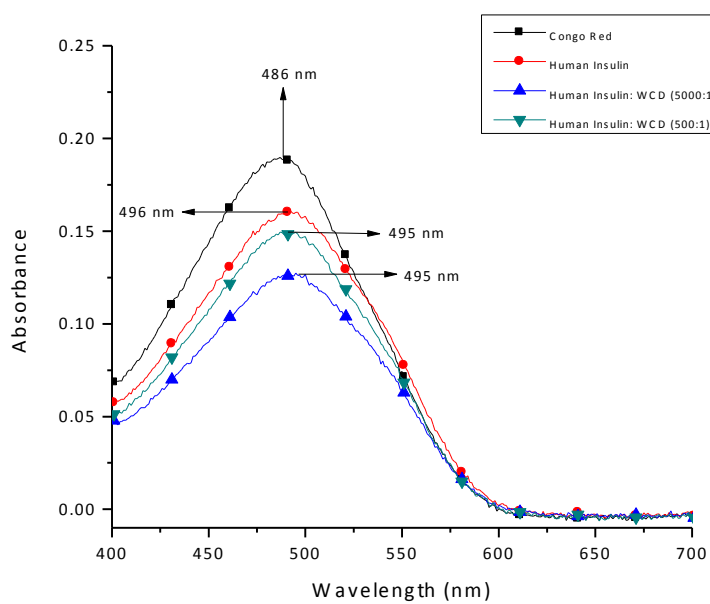


A

**Figure 6.4A Absorption spectra of Congo Red in Human Insulin and Human Insulin-WCD solution at incubation time of A) 0.5 hours. Congo Red alone (black), Human Insulin (red), Human Insulin: WCD (5000:1) (blue) and Human Insulin: WCD (500:1) (green)**



B



C

**Figure 6.4 Absorption spectra of Congo Red in Human Insulin and Human Insulin-WCD solution at incubation time of B) 3.5 hours and C) 6 hours.**

are compared in Figure 4. Congo Red (CR) has absorbance at 486 nm and Insulin/CR at 22 C has absorbance peak at 486 nm.<sup>137; 138</sup> Both these samples act as controls to compare the different human insulin samples at the three stages of incubation. CR on interaction with protein does not have a change in absorbance spectrum. However, CR on interaction with protein fibers results in a red shift in absorbance spectrum.

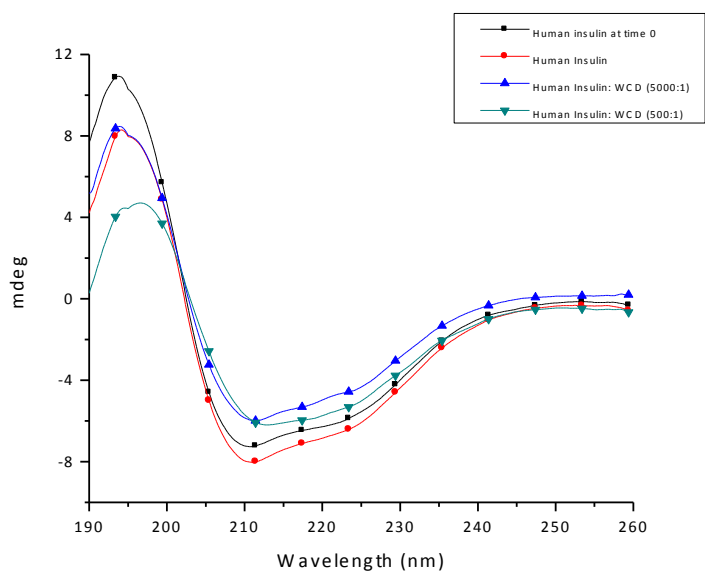
Figure 6.4A shows the time period 0.5 hours since the incubation of the protein. Human insulin has absorbance peak at 489 nm while both samples of Insulin incubated with WCD with ratios 500:1 and 5000:1 have an absorbance peak at 500 nm. Figure 6.4A, 6.4B and 6.4C show CR spectra for aliquots from the three incubations at 0.5, 3.5 and 6 hours, respectively. Human insulin samples incubated with WCDs have a significant red shift in their absorbance spectra which indicates interaction of protein fibers with CR when compared to insulin incubating in the absence of WCDs. Figure 6.4B presents absorbance spectra at 3.5 hours incubation. The insulin absorbance is now at 492 nm while the insulin incubated with WCD with ratios 5000:1 and 500:1 have absorbance at 499 and 500 nm, respectively. At 3.5 hours of incubation, all the human insulin samples show a red shift in absorbance indicating a presence of protein fiber. However, it is noticeable that human insulin incubated in presence of WCD shows a smaller red shift in absorbance when compared to human insulin incubated in presence of WCD. Figure 6.4C presents the absorbance spectra during the plateau phase of insulin fibrillation where all three insulin samples show 9-10 nm red shift indicating presence of insulin fibers. CR absorbance shows that with increasing time of incubation, all three insulin samples show a red shift in absorbance. However in presence of WCD, the red shift in absorbance is pronounced in the first 0.5 hours whereas in the absence of WCD, human insulin



gradually moves towards the red shift in absorbance. This complements the ThT study that human insulin undergoes fibrillation at a higher rate in presence of WCD.

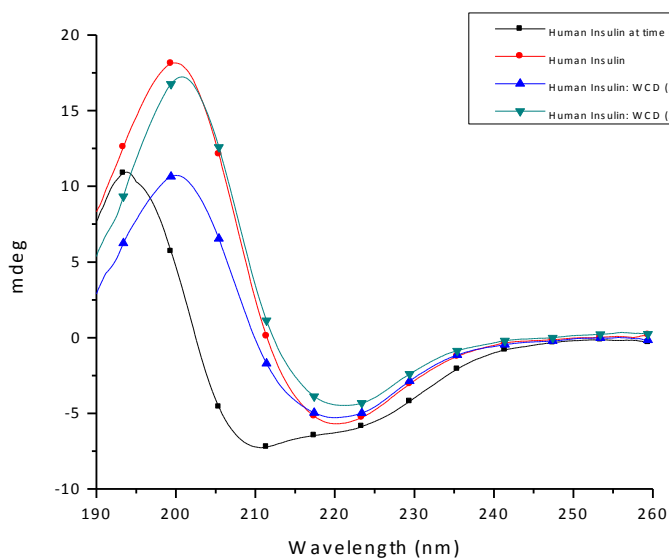
### 6.5 Secondary structure changes in fibrillation of insulin

The structural changes of the human insulin in presence and absence of WCD was monitored by circular dichroism and tyrosine fluorescence. The spectra give information about the protein conformational change in the presence and absence of WCD. Figure 6.5 shows the circular dichroism for the aliquots from the three phases. Figure 6.5A, 6.5B and 6.5C show circular dichroism spectra for aliquots from the three incubations at 0.5, 3.5 and 6 hours, respectively. All figures show human insulin before incubation (black

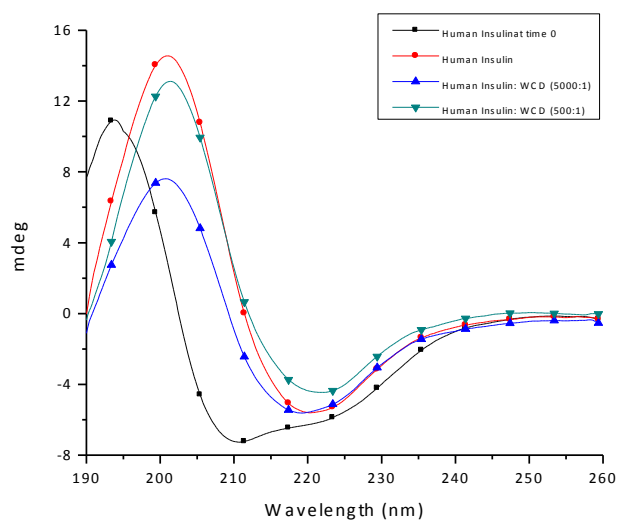


A

**Figure 6.5A** Circular dichroism spectra of human insulin before incubation at time 0 hours (black), human insulin (red), human insulin: WCD with ration 5000:1 (blue) and human insulin: WCD with ratio of 500:1 (green) at incubation times of A) 0.5 hours.



B



C

**Figure 6.5 Circular dichroism spectra of human insulin before incubation at time 0 hours (black), human insulin (red), human insulin:WCD with ration 5000:1 (blue) and human insulin:WCD with ratio of 500:1 (green) at incubation times of B) 3.5 hours and C) 6 hours.**

line with square) as a control. Human insulin before the beginning of incubation shows characteristic  $\alpha$ -helix conformation characteristic of the protein. The far-UV circular dichroism spectra shows the two negative bands at 208 and 222 nm and the positive band at 193 nm. When analyzed by Dichroweb, the  $\alpha$ -helical content was found to be 63%. Table 6.1 gives the change in content of  $\alpha$ -helix and  $\beta$ -sheet for the various aliquots. Figure 6.5A shows the aliquots from all the three samples at 0.5 hours. Thirty minute after incubation all the three samples show a decrease in  $\alpha$ -helical content and increase in  $\beta$ -sheet content. However, human insulin's spectra is most similar to the spectra of the control human insulin which was not incubated. The spectra of human insulin with WCD show a flattening of the spectra between 210 and 240 nm which results in the disappearance of the double negative bands which are characteristic of  $\alpha$ -helical conformation. The  $\alpha$ -helical content decreases to 54%, 45% and 45% and  $\beta$ -sheet increases to 7%, 12% and 11% for human insulin, human insulin-WCD (5000:1) and human insulin-WCD (500:1), respectively. Compared to the control, the human insulin at 0.5 hours incubation has the least decrease in  $\alpha$ -helix and increase in  $\beta$ -sheet. This indicates that insulin conformation at 0.5 hours is most similar to the conformation of the insulin control when compared to the human insulin incubated with WCD. Both the insulin samples with the two different concentrations of WCD show a higher amount of  $\beta$ -sheet structure which suggests that WCD play role in move towards  $\beta$ -sheet structure of human insulin.

Figure 6.5B shows aliquots from all three samples at 3.5 hours. Compared to the control human insulin which was not incubated, a dramatic change is observed in all the three circular dichroism spectra. The double negative bands at 210 and 240 nm and the positive

Time (hours)	$\alpha$ -helix	$\beta$ -sheet
<b>Human Insulin</b>		
0	63%	2%
0.5	54%	7%
3.5	49%	38%
6	37%	21%
<b>Human Insulin: WCD (1:5000)</b>		
0.5	45%	11%
3.5	40%	17%
6	31%	22%
<b>Human Insulin: WCD (1:500)</b>		
0.5	45%	11%
3.5	32%	48%
6	34%	21%

**Table 6. 1 Secondary structure estimation of Human Insulin fibrillation in the presence and absence of WCD using Dichroweb software.**

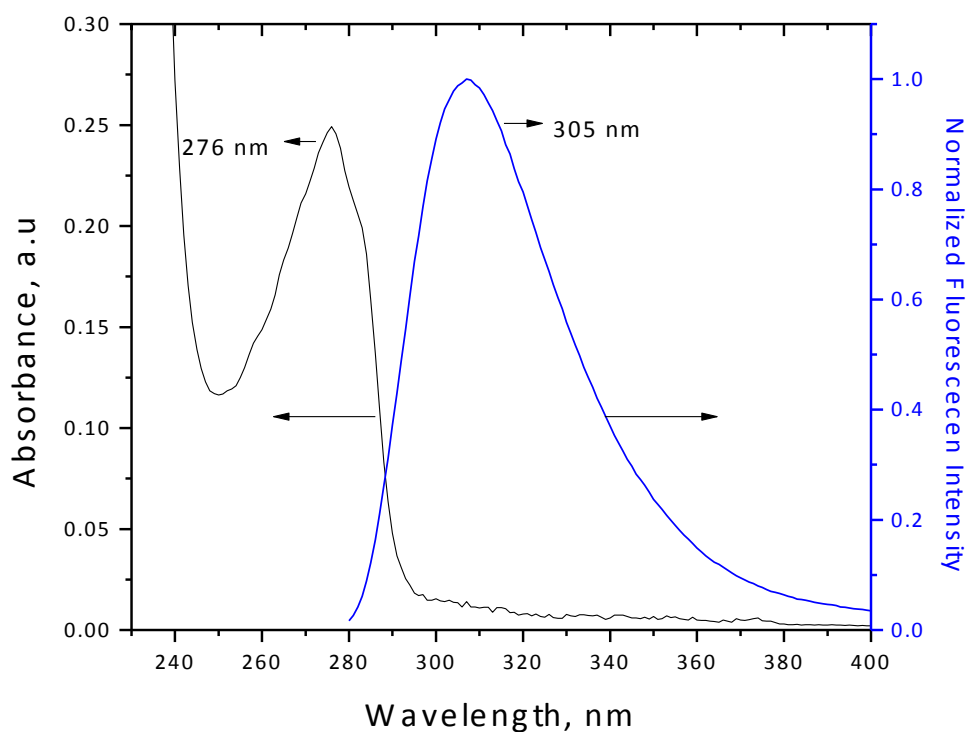
band at 193 nm characteristic of  $\alpha$ -helical conformation have completely vanished and are replaced by one broad negative band at 220 nm and a positive band at 200 nm. This trend in increase of  $\beta$ -sheet and decrease in  $\alpha$ -helix is also confirmed when the spectra is characterized by Dichroweb program. The  $\alpha$ -helix decreases to 49%, 40% and 32% and the  $\beta$ -sheet content increases to 38%, 17% and 48% for human insulin, human insulin: WCD (5000:1) and human insulin: WCD (500:1), respectively. Figure 4C shows aliquots from all three samples at 6 hours. The human insulin samples continue their departure from  $\alpha$ -helix. The  $\alpha$ -helix decreases to 37%, 31% and 34% and the  $\beta$ -sheet content increases to 21%, 22% and 21% for human insulin, human insulin: WCD (5000:1) and human insulin: WCD (500:1), respectively. At 6 hours which is the saturation phase of

incubation, all the human insulin samples have a similar the  $\beta$ -sheet content between 21-22%, which indicates that once certain amount of time has passed, all the human insulin samples irrespective of presence or absence of WCD have similar  $\beta$ -sheet content.

Circular dichroism spectroscopy indicates that all human insulin samples were transformed to  $\beta$ -sheet in conformation with increase in time of incubation. However, the rate of this transformation of the protein increases if incubated with WCD. Also, it has to be said that with a higher the concentration of WCD during incubation, a trend is visible that the rate of  $\beta$ -sheet transformation of the protein takes place in a shorter amount of time.

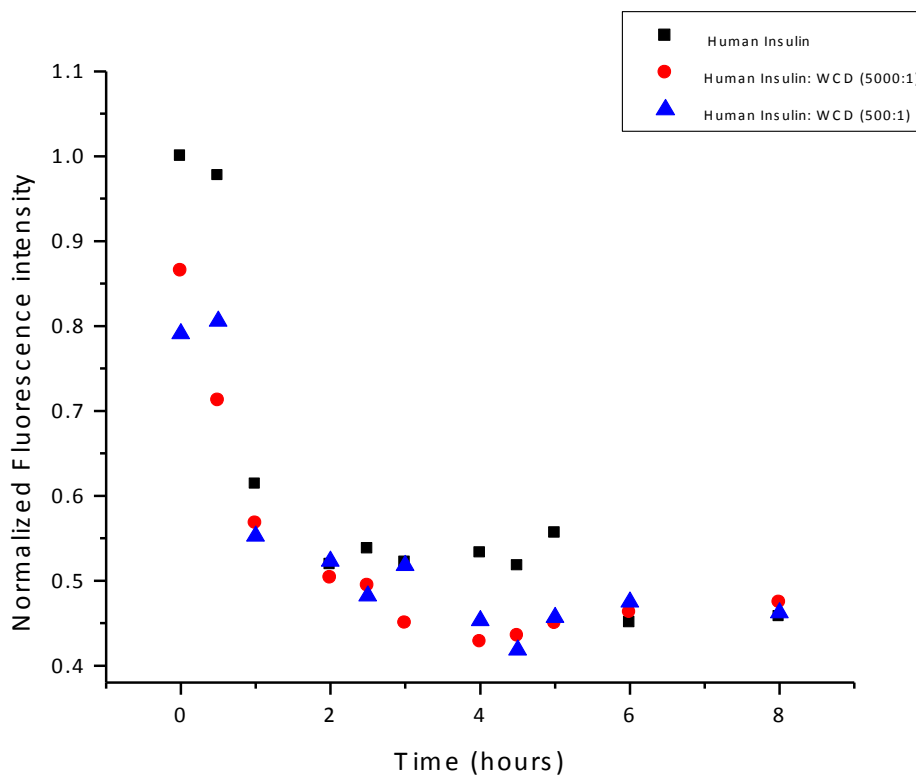
The change in secondary structure of a protein can also be observed by monitoring the change in intrinsic fluorescence of one of the three aromatic amino acids (phenylalanine, tyrosine, and tryptophan) present in the protein.<sup>139-141</sup> Human insulin contains three phenylalanine, four tyrosine and it has no tryptophan residues. Figure 6.6A shows the absorbance and fluorescence spectra of human insulin. Human insulin is expected to show two absorbance peaks, one near 220 nm due to peptide bond and the other at 276 nm due to the presence of aromatic tyrosine amino acid. In aqueous solution, the absorbance peak due to tyrosine is visible at 276 nm but the peak near 220 nm is not visible. However, studies have shown that the peak near 220 nm is visible when insulin is at air-water interface as a Langmuir monolayer.<sup>65; 142</sup> When excited at 276 nm, human insulin shows emission spectra at 305 nm which is due to the presence of the four tyrosines in human insulin. Monitoring tyrosine fluorescence can be used as complementary study with CD measurements to study the structural changes in insulin with incubation with WCD.

Figure 6.6B shows the intensity of human insulin and human insulin-WCD samples when excited at 276 nm and emission was measured at 305 nm. The spectra shows a decrease in the intensity at 305 nm with increasing time of incubation at 37 °C for all three samples. On examining of the spectra, it is observed that the human insulin samples without the WCDs has the highest fluorescence at 305 nm and a gradual decrease in



A

**Figure 6.6 A) UV-vis ( $5 \times 10^{-5}$  M) and fluorescence ( $5 \times 10^{-7}$  M;  $\lambda_{\text{excitation}} = 270$  nm) spectra of aqueous solution of human insulin.**



B

**Figure 6.6B Insulin fibrillation detected by tyrosine fluorescence when excited at 276 nm and emission measured at 305 nm : (■, black) Human Insulin, (●, red circle) Human Insulin: WCD (5000:1) , (▲, blue triangle) Human Insulin: WCD (500:1). Slit width at the excitation and emission, 5 and 5 nm, respectively.**

fluorescence intensity of human insulin with WCD is close to each other and cannot be distinguished based on the different WCD concentrations used. Both the human insulin samples containing WCD show a lower intensity of fluorescence when compared to human insulin. The distinguished based on the different WCD concentrations used.

Human insulin consists of four tyrosines, out of which three are located in hydrophobic pockets not exposed to the aqueous environment. Decrease in fluorescence of tyrosine with increasing time of incubation suggests quenching of the fluorescence of all the four tyrosines. This indicates a change in conformation of human insulin which exposes the tyrosines in the hydrophobic areas to the solvent. By the end of 1 hour, there is a substantial quenching of tyrosine fluorescence for all three human insulin samples which suggests that human insulin undergoes a structural conformation exposing the tyrosines to aqueous environment. The unravelling of human insulin molecule seems to be an step in the process of fibrillation of human insulin. A further decrease in tyrosine fluorescence in the presence of WCD suggests that either the WCD are responsible for quicker unravelling of the protein or that WCD are able to catalyze the process of fibrillation of human insulin once the protein is unravelled. Both CD and tyrosine fluorescence indicate that fibrillation of insulin involves a change in structural conformation of the protein and that WCD plays a role increasing the rate of fibrillation of the protein.

## **6.6 Imaging and analysis**

AFM imaging (3 $\mu$ m X 3  $\mu$ m) of insulin and insulin-WCDs were analyzed at 30 minutes time intervals throughout the incubation process to monitor progress of fiber formation. Figure 6.7 shows the incubation time intervals of 0.5, 3.5 and 6 hours for all the three human insulin samples. At time 0 hour (before the beginning of incubation) at room temperature, all three samples show no fiber or aggregate formation. The next sample was taken at 0.5 hours after incubation. The topography of the human insulin sample in the absence of WCD looks the similar to the one at time 0 hour. However, both the insulin samples with WCD show presence of fibers. Human insulin does not show



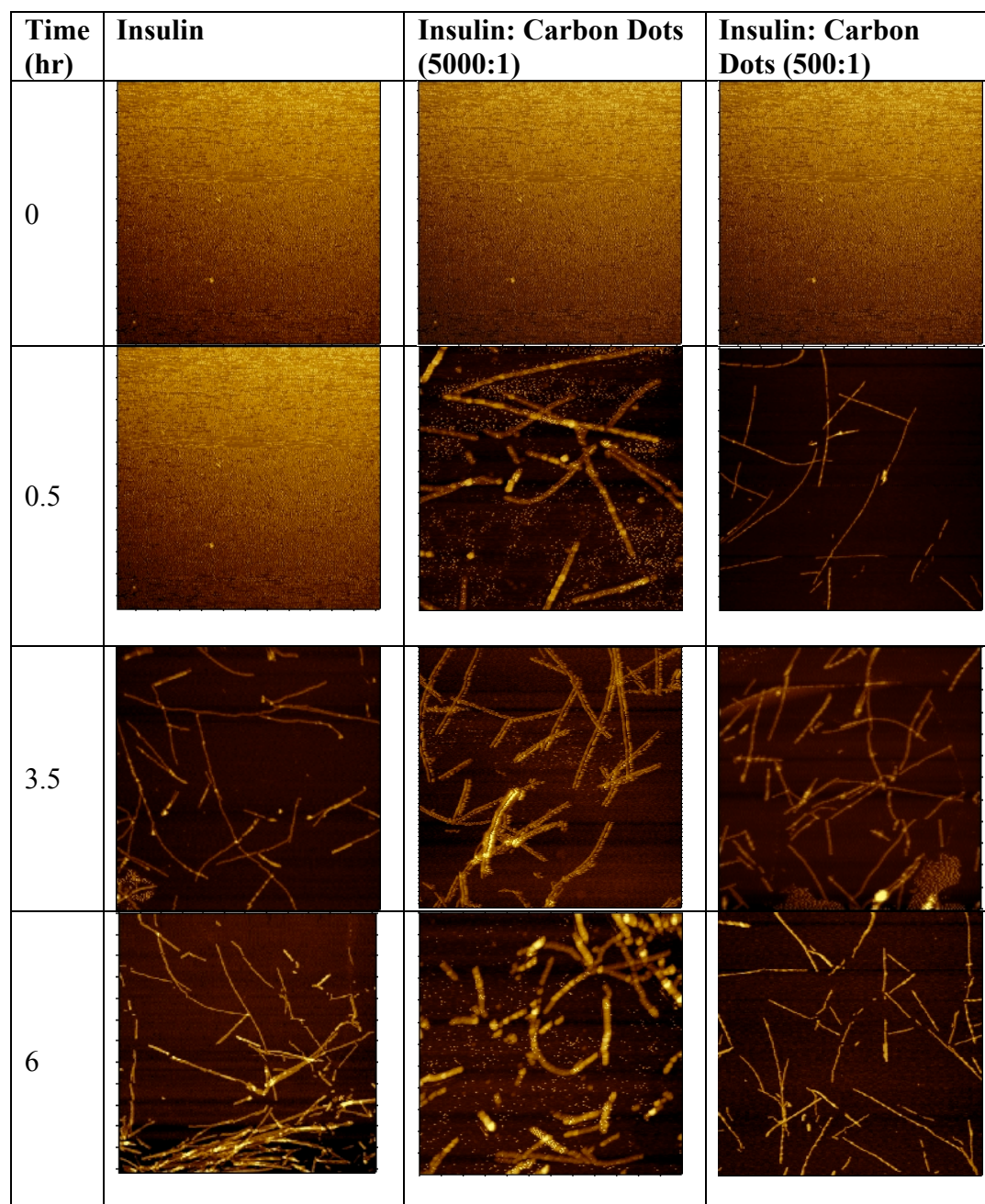


**Figure 6.7:** AFM images (3  $\mu\text{m}$  X 3  $\mu\text{m}$ ) of Insulin and Human Insulin: WCD at two different ratios.

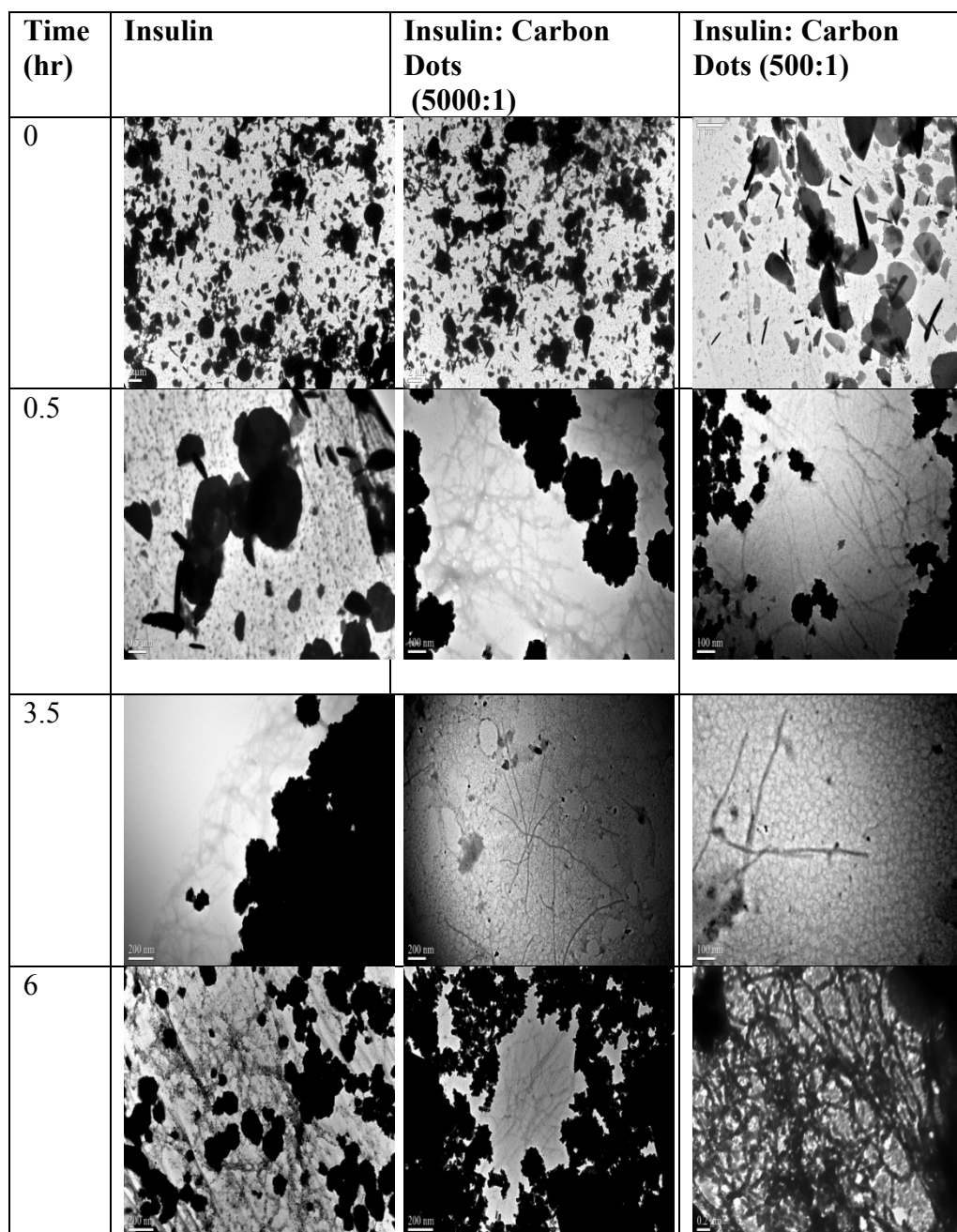


**Figure 6.8: TEM images of Insulin and Human Insulin: WCD at two different ratios.**

presence of fibers until 3.5 hours. However, the insulin samples with WCD show presence of fibers 30 minutes after incubation. All three samples were next measured at 6 hours and all three samples showed presence of fibers.

AFM analysis confirms that presence of WCD acts as a catalyst and increases the rate of fibrillation in the protein, thereby eliminating the lag phase which is characteristic of insulin fibrillation. Fully formed fibers are observed within 30 minutes of incubation with WCD whereas it takes 3.5 hours for human insulin fibers to appear when incubating in the absence of WCD. WCD increases fibrillation in human insulin by a factor of seven. Analysis of TEM images in Figure 6.8 complement the AFM analysis.

## **6.7 Conclusion**

It is widely accepted that the typical protein fibrillation involves a number of intermediate states, including nucleation, oligomerization, and fibril formation.<sup>132; 133</sup> The formation of nucleation species is the key rate-determining step, as it is a thermodynamically unfavored process during protein fibrillation. It has been well recognized that the presence of nanoparticles can significantly affect the conformations of proteins due to the interactions between nanoparticles and proteins.<sup>143-145</sup> Therefore, it is not unexpected that the presence of nanoparticles may accelerate or inhibit the protein fibrillation. Although extensive studies are now being carried out on the effects of nanoparticles on protein fibrillation, our knowledge is still relying on a case-by-case approach.<sup>146</sup> In general, the effects are due to the interaction between proteins and the surface of nanoparticles. To be more specific, the interaction depends on the protein surface properties (charge, stability, hydrophobicity), and on the nanoparticle

characteristics (charge, size, coating, components).<sup>143-146</sup> Due to the complexity, a “dual” effect (i.e. both promoting and inhibiting) of nanoparticles on protein fibrillation was also observed in some cases, depending on the concentrations of proteins and the surface area of nanoparticles.<sup>147</sup>

In the present study, a promoting effect on the insulin fibrillation by shortening the lag time of nucleation was observed in the presence of water soluble carbon dots. Although the detailed molecular mechanism of nucleation on the surface of carbon dots remains elusive, the fibrillation process is believed to be based on the locally increased concentration of insulin in the vicinity of the carbon dots surface due to the adsorption.<sup>143;</sup>  
<sup>148-150</sup> Followed by adsorption on the surface, the insulin monomers unfold the conformations, which facilitate the subsequent assemblies of disordered oligomeric structures. After that, these assemblies undergo a process of re-ordering into  $\beta$ -sheet structures, which is driven by the hydrogen bonding formation.<sup>150</sup>

Interestingly, the enhanced fibrillation effect was more obvious at the ratio of 1:500 (carbon dots: insulin, w/w) than that at 1:5000 under the same concentration of human insulin. Parameters of nanoparticles under this condition, such as surface charge, coating, and surface curvature, were all the same. Due to the fact that the size of monomeric insulin was much smaller than carbon dots and that the amount of monomeric insulin was much excess, the adsorption of insulin should not affect much the concentration of insulin in the solution phase. However, the ratio of 1:500 provided 10 more times carbon dots surface area than that of 1:5000. Therefore, the main difference should be from the total surface area available on carbon dots for insulin adsorption. Upon adsorption, the insulin monomers unfold the conformations, which facilitate the formation of insulin oligomers.

More surface areas generate more oligomers. Due to exchange equilibrium of insulin molecules between the surface and solution phase, more oligomers will be desorbed from the surface to solution in the case of 1:500 than that in 1:5000. The continuing assembly of oligomers will produce more nuclei. Once the critical concentration of nucleation was reached, elongation of insulin fibril will rapidly occur.

Protein aggregation, protofilaments, fibrillation and plaque formation have been indicated to play role in several diseases. This study analyses the human insulin protein fibrillization in vitro in the presence of water soluble carbon dots (WCD) and their effect on self-assembly process of fiber formation. These experiments were conducted under thermal conditions of 37 °C with low nanoparticle concentrations. This study indicates that WCD may play a role in the secondary structure conformational change of human insulin from  $\alpha$ -helix toward  $\beta$ -sheet structure. On the basis of the results, it is hypothesized that presence of WCD results in a higher rate of fiber formation for human insulin, and that WCD may act as a catalyst for fiber formation in human insulin. Due to absence of metals toxic to living organism like cadmium, carbon dots are increasing used in biological systems for imaging, as probes and for targeting cancer cells.<sup>151</sup> Therefore, a thorough investigation of carbon dots and its interaction with biological molecules is essential.

## REFERENCES

1. Vannoy, C.H., and Leblanc, R.M. (2010). Effects of DHLA-capped CdSe/ZnS quantum dots on the fibrillation of human serum albumin. *J Phys Chem B* 114, 10881-10888.
2. Thakur, G., Micic, M., Yang, Y., Li, W., Movia, D., Giordani, S., Zhang, H., and Leblanc, R.M. (2011). Conjugated quantum dots inhibit the amyloid  $\beta$  (1–42) fibrillation process. *Int J Alzheimers Dis* 2011.
3. Banting, F.G. (1929). The history of insulin. *Edinburgh Med J* 36, 1-18.
4. Polonsky, K.S. (2012). The past 200 years in diabetes. *New Engl J Med* 367.
5. Vajo, Z., Fawcett, J., and Duckworth, W.C. (2001). Recombinant DNA technology in the treatment of diabetes: insulin analogs. *Endor Rev* 22, 706-717.
6. Berson, S.A., and Yalow, R.S. (1961). Immunochemical distinction between insulins with identical amino-acid sequences. *Nature* 191, 1392-1393.
7. Dobson, M. (1776). Nature of urine in diabetes. *Medical Observations and Enquiries* 5, 218-230.
8. Brogard, J.M., Vetter, T., and Bickle, J.F. (1992). Discovery of pancreatic diabetes in Strasbourg. *Diabetes Metab* 18, 104-114.
9. Kleiner, I.S. (1919). The action of intravenous injections of pancreas emulsions in experimental diabetes. *J Biol Chem* 40, 153-170.
10. Laguesse, E. (1983). Sur la formation des ilots de Langerhans dans le pancréas. . *Comptes rendus hebdomadaires des séances et memoires de la société de biologie* 5, 819-820.
11. Murlin, J.R., and Kramer, B. (1913). The influence of pancreatic and duodenal extracts on the glycosuria and the respiratory metabolism of depancreatized dogs. *J Biol Chem* 15, 365-383.
12. Opie, E.L. (1900). The relation of diabetes mellitus to lesions of the pancreas. Hyaline degeneration of the islands of Langerhans. *J Exp Med* 5, 527-540.
13. Paulesco, N.C. (1921). Action de l'extrait pancréatique injecté dans le sang, chez un animal diabétique. *Comptes rendus des séances de la Société de biologie* 85.

14. Rosenfeld, L. (2002). Insulin: Discovery and Controversy. *Clin Chem* 48, 2270-2288.
15. Scott, E.L. (1912). On the influence of intravenous injections of an extract of the pancreas on experimental pancreatic diabetes. *Am J Physiol* 29, 306-310.
16. Steiner, D.F., and James, D.E. (1992). Cellular and molecular biology of the beta cell. *Diabetologia* 35, S41-S48.
17. Adams, M.J., Blundell, T.L., E.J., D., Dodson, G.G., Vijayan, M., Baker, E.N., and Harding, M.M. (1969). Structure of rhombohedral 2 zinc insulin crystals. *Nature* 224, 491-495.
18. Sanger, F., and Thompson, E.O.P. (1953). The amino-acid sequence in the glycyl chain of insulin. 1. The identification of lower peptides from partial hydrolysates. *Biochem J* 53, 353-366.
19. Sanger, F., and Thompson, E.O.P. (1953). The amino-acid sequence in the glycyl chain of insulin. 2. The investigation of peptides from enzymic hydrolysates. *Biochem J* 53, 366-374.
20. Sanger, F., and Tuppy, H. (1951). The amino-acid sequence in the phenylalanyl chain of insulin. 1. The identification of lower peptides from partial hydrolysates. *Biochem J* 49, 463-481.
21. Sanger, F., and Tuppy, H. (1951). The amino-acid sequence in the phenylalanyl chain of insulin. 2. The investigation of peptides from enzymic hydrolysates. *Biochem J* 49, 4.
22. Chang, X., Jorgenson, A.M., Bardrum, P., and Led, J.J. (1977). Solution structures of the R6 human insulin hexamer. *Biochemistry* 36, 9409-9422.
23. Nieto-Suarz, M., Vila-Romeu, N., and Prieto, I. (2008). Behaviour of insulin Langmuir monolayers at the air-water interface under various conditions. *Thin Solid Films* 516, 8873-8879.
24. Langmuir, I., and Waugh, D.F. (1940). Pressure-soluble and pressure-displaceable components of monolayers of native and denatured proteins. *J Am Chem Soc* 62, 2771-2793.
25. Harrap, B.S. (1954). The properties of insulin films, spread at air water interface. *J Coll Sci Imp U Tok* 9, 522-534.
26. Tanford, C., and Epstein, J. (1954). The physical chemistry of insulin. I Hydrogen ion titration curve of zinc-free insulin. *J Am Chem Soc* 76, 2163-2169.

27. Fredericq, E. (1953). Reversible dissociation of insulin. *Nature* 171, 570-571.
28. Fredericq, E. (1952). L'état d'agrégation de l'insuline en couches monomoléculaires superficielles. *BBA* 9, 601-608.
29. Harrap, B.S. (1955). The molecular weight of insulin, determined by the surface balance technique. *J Coll Sci Imp U Tok* 10, 351-361.
30. Llopis, J., and Rebollo, D.V. (1960). Influence of temperature on insulin monolayers. *Arch Biochem Biophys* 88, 142-149.
31. Birdi, K.S. (1976). Interaction of insulin with lipid monolayers. *J Colloid Interf Sci* 57, 228-232.
32. Nieto-Suarz, M., Vila-Romeu, N., and Dynarowicz-Latka, P. (2008). Behaviour of inusulin-spingomyelin mixed Langmuir monolayers spread at the air-water interface. *Colloid Surface A* 321, 189-195.
33. Perez-Lopez, S., Blanco-Vila, N.M., and Vila-Romeu, N. (2011). Bovine insulin-phosphatidycholine mixed langmuir monolayers: behaviour at the air-water interface. *J Phys Chem B* 115, 9387-9394.
34. Schwinke, D.L., Ganesan, M.G., and Weiner, N.D. (1983). Monolayer studies if insulin-lipid interactions. *J Pharm Sci-US* 72, 244-248.
35. Shigenobu, H., and McNamee, C. (2012). The interaction of insulin, glucoes, and insulin-glucose mixtures with a phospholipid monolayer. *J Colloid Interf Sci* 388, 274-281.
36. Rahmati, K., Koifman, J., and Tsoukanova, V. (2008). Two-step pattern in kinetics of protein adsorption onto poly(ethylene glycol)-grafted phospholipid monolayers. *Colloid Surface A* 321, 181-188.
37. Balashev, K., Ivanova, T., Mircheva, K., and Panaiotov, I. (2011). Savinase proteolysis of insulin Langmuir monolayers studies by surface pressure and surface potential accompanied by atomic force microscopy (AFM) imaging. *J Colloid Interf Sci* 360, 654-661.
38. Johnson, S., Liu, W., Thakur, G., Dadlani, A., Patel, R., Orbulescu, J., Whyte, J., Micic, M., and Leblanc, R.M. (2012). Surface chemistry and spectroscopy of human insulin Langmuir monolayer. *J Phys Chem C* 116, 10205-10212.
39. Liu, W., Johnson, S., Micic, M., Orbulescu, J., Whyte, J., Garcia, A., and Leblanc, R.M. (2011). Study of aggregation of human insulin Langmuir monolayer. *Langmuir* 28, 3369-3377.



40. Grasso, E.J., Oliveria, R.G., Oksdath, M., and Maggio, B. (2013). Controlled lateral packing of insulin monolayers influences neuron polarization in solid supported cultures. *Colloid Surface B* 107, 59-67.
41. Resch-Genger, U., Grabolle, M., Cavaliere-Jaricot, S., Nitschke, R., and Nann, T. (2008). Quantum dots versus organic dyes as fluorescent labels. *Nature methods* 5, 763-775.
42. Clifford, J.P., Konstantatos, G., Johnston, K.W., Hoogland, S., Levina, L., and Sargent, E.H. (2008). Fast, sensitive and spectrally tuneable colloidal-quantum-dot photodetectors. *Nature Nanotechnology* 4, 40-44.
43. Barth, S., Hernandez-Ramirez, F., Holmes, J.D., and Romano-Rodriguez, A. (2010). Synthesis and applications of one-dimensional semiconductors. *Progress in Materials Science* 55, 563-627.
44. McKimmie, L.J., Lincoln, C.N., Jasieniak, J., and Smith, T.A. (2009). Three-pulse photon echo peak shift measurements of capped CdSe quantum dots. *The Journal of Physical Chemistry C* 114, 82-88.
45. Prasad, P. (2004). Emerging opportunities at the interface of photonics, nanotechnology and biotechnology. *Molecular Crystals and Liquid Crystals* 415, 1-7.
46. Resch-Genger, U., Grabolle, M., Cavaliere-Jaricot, S., Nitschke, R., and Nann, T. (2008). Quantum dots versus organic dyes as fluorescent labels. *Nat Methods* 5, 763-775.
47. Derfus, A.M., Chan, W.C., and Bhatia, S.N. (2004). Probing the cytotoxicity of semiconductor quantum dots. *Nano Lett* 4, 11-18.
48. Kirchner, C., Liedl, T., Kudera, S., Pellegrino, T., Muñoz Javier, A., Gaub, H.E., Stölzle, S., Fertig, N., and Parak, W.J. (2005). Cytotoxicity of colloidal CdSe and CdSe/ZnS nanoparticles. *Nano Lett* 5, 331-338.
49. Lovrić, J., Cho, S.J., Winnik, F.M., and Maysinger, D. (2005). Unmodified cadmium telluride quantum dots induce reactive oxygen species formation leading to multiple organelle damage and cell death. *Chem Biol* 12, 1227-1234.
50. Rzigalinski, B.A., and Strobl, J.S. (2009). Cadmium-containing nanoparticles: perspectives on pharmacology and toxicology of quantum dots. *Toxicol Appl Pharmacol* 238, 280-288.
51. Baker, S.N., and Baker, G.A. (2010). Luminescent carbon nanodots: emergent nanolights. *Angew Chem Int Ed* 49, 6726-6744.

52. Xu, X., Ray, R., Gu, Y., Ploehn, H.J., Gearheart, L., and Scrivens, W.A. (2004). Electrophoretic analysis and purification of fluorescent single-walled carbon nanotube fragments. *J Am Chem Soc* 126, 12736-12737.
53. Orbulescu, J. (2011). Contrasting view on asphaltene and human cardiac troponin I: a surface chemistry and spectroscopy perspective. Ph.D in Chemistry, University of Miami, Coral Gables, Florida.
54. Langmuir, I. (1917). The constitution of fundamental properties of solids and liquids. II Liquids. *J Am Chem Soc* 39, 1848-1906.
55. Gaines, G.L. (1966). Insoluble monolayers at the liquid-gas interfaces.(New York: Interscience).
56. BiolinScientific. (2013). Surface Tension by KSV NIMA. In. (Finland.
57. (2001). KSV Instruction Manual. KSV Nima Inc Helisnki, Finland.
58. Xu, J. (2008). Self-organization of semiconductor quantum dots at the air-water interface and the application for amyloid imaging. Doctrate in Chemistry, University of Miami, Coral Gables, FL.
59. Langmuir, I., and Schaefer, V. (1939). Properties and structure of protein monolayers. *J Am Rev* 24, 181-202.
60. Ulman, A. (2001). Ultrathin Organic Films.(Academic Press).
61. (2001). I-Elli 200 User Manual.(Gottingen, Germany).
62. Kelly, S., and Price, N. (2000). The use of circular dichroism in the investigation of protein structure and function. *Curr Protein Pept Sc* 1, 349-384.
63. Greenfield, N.J. (2007). Using circular dichroism spectra to estimate the protein secondary structure. *Nat Protoc* 1, 2876-2890.
64. Elmore, D.L., Shanmukh, S., and Dluhy, R.A. (2002). A study of binary phospholipid mixtures at the air water interface using infrared reflection absorption spectroscopy and 2D IR correlation analysis. *J Phys Chem A* 106, 3420-3428.
65. Johnson, S., Li, W., Thakur, G., Dadlani, A., Patel, R., Orbulescu, J., Whyte, J., Micic, M., and Leblanc, R.M. (2012). Surface chemistry and spectroscopy of human insulin langmuir monolayer. *J Phys Chem B* 116, 10205-10212.

66. Du, X., Miao, W., and Liang, Y. (2005). IRRAS studies on chain orientation in the monolayers of amino acid amphiphiles at the air-water interface depending on metal complex and hydrogen bond formation with the headgroups. *J Phys Chem B* 109, 7428-7434.
67. Mendelsohn, R., Brauner, J., and Gericke, A. (1998). External infrared reflection-absorption spectrometry of monolayer films at the air/water interface. *Ann Rev Phys Chem* 46, 305-334.
68. Dluhy, R.A. (2000). Infrared spectroscopy of biophysical monomolecular films at interfaces: theory and applications. *Spectrosc Rev* 35, 315-351.
69. (2009). Agilent Technologies Atomic Force Microscopy User Manual.
70. Qu, L., Adam. Peng, Z., and Peng, X. (2001). Alternative routes toward high quality CdSe Nanocrystals. *Nano Lett* 1, 333-337.
71. Wang, F., Pang, S., Wang, L., Li, Q., Kreiter, M., and Liu, C. (2010). One-step synthesis of highly luminescent carbon dots in noncoordinating solvents. *Chem Mater* 22, 4528-4530.
72. Owens, D.R., Zinman, B., and Bolli, G. (2003). Alternative routes of insulin delivery. *Diabetic Med* 20, 886-898.
73. Baker, E., Blundell, L., Cutfield, J., Cutfield, S., Dodson, E., Dodson, G., Crowfoot Hodgkin, D., Hubbard, R., Isaacs, N., Reynolds, C., et al. (1988). The structure of 2-zinc pig insulin crystals at 15 Å resolution. *Philos Trans R Soc London, Ser B* 319, 369-4956.
74. Nieto-Suarez, M., Villa-Romeu, N., and Prieto, I. (2007). Behavior of insulin monolayers at the air-water interface under various conditions. *Thin Solid Films* 516, 8873-8879.
75. Bowen, R., Austgen, L., and Rouge, M. (2006). The structure of insulin. In *Hypertexts for Biomedical Sciences* (Fort Collins, Colorado.), p Online textbook.
76. Jiménez, J., Nettleton, E., Bouchard, M., Robinson, C., Dobson, C., and Saibil, H. (2002). The protofilament structure of insulin amyloid fibrils. *Proc Natl Acad Sci USA* 99, 9196-9201.
77. Sunde, M., Serpell, L., Bartlam, M., Fraser, P., Pepys, M., and Blake, C. (1997). Common core structure of amyloid fibrils by synchrotron X-ray diffraction. *J Mol Biol* 273, 729-739.
78. Gaines, G.L.Jr. (1966). *Insoluble Monolayers at the Liquid-Gas Interfaces*. (New York: Interscience).

79. Harrap, B.S. (1954). The properties of insulin films, spread at the air-water interface. *J Coll Sci Imp U Tok* 9, 522-534.
80. Lakowicz, J.R. (1999). *Principles of Fluorescence Spectroscopy*. Second Edition.(New York: Kluwer Academic/Plenum Publishers).
81. Fainerman, V.B., Vollhart, D., and Johann, R. (2000). Arachidic acid monolayers at high pH of the aqueous subphase: studies of counterion bonding. *Langmuir* 16, 7731-7736.
82. Greenfield, N.J. (2006). Using circular dichroism spectra to estimate protein secondary structure. *Nat Protoc* 1, 2876-2890.
83. Cao, L., Wang, X., Mezziani, M.J., Lu, F., Wang, H., Luo, P.G., Lin, Y., Harruff, B.A., Veca, L.M., Murray, D., et al. (2007). Carbon dots for multiphoton bioimaging. *J Am Chem Soc* 129, 37.
84. Gao, Z., Shen, G., Zhao, X., Dong, N., Jia, P., Wu, J., Cui, D., Zhang, Y., and Wang, Y. (2013). Carbon dots: a safe nanoscale substance for the immunologic system of mice. *Nanoscale Res Lett* 8, 276.
85. Yang, S., Wang, X., Wang, H., Lu, F., Luo, P.G., Cao, L., Mezziani, M.J., Liu, J., Liu, Y., Chen, M., et al. (2009). Carbon dots as nontoxic and high-performance fluorescence imaging agents. *J Phys Chem C* 113, 18110-18114.
86. Wang, F., Pang, S., Wang, L., Li, Q., Kreiter, M., and Liu, C. (2010). One-step synthesis of highly luminescent carbon dots in noncoordinating solvents. *Chem Mater* 22, 4258-4530.
87. Chang, X., A.Jorgenson, A.M., Bardrum, P., and Jens, J. (1997). Solution structures of the R6 human insulin hexamer. *Biochem* 36, 9409-9422.
88. Brange, J., and Langkjaer, L. (1997). *Protein Delivery: Physical Systems*.(Plenum Press: New York).
89. Chothia, C., Lesk, A.M., Dodson, G.G., and Hodgkin, D.C. (1983). Transission of conformational change in insulin. *Nature* 302, 5908.
90. Derewenda, U., Derewenda, Z., Dodson, G.G., Reynolds, C.D., Smith, G.D., and Sparks, C. (1989). Phenol stabilizes more helix in a new symmetrical zinc insulin hexamer. *Nature* 338, 594-596.
91. Graham, B., Dodson, E., Dodson, G.G., Hodgkin, D.C., and Mercola, D. (1976). Structure of insulin in 4-zinc insulin. *Nature* 261, 166-168.

92. Dodson, G.G., and Steiner, D. (1998). The role of assembly in insulin's biosynthesis. *Curr Opin Struc Biol* 8, 189-194.
93. Grudzielanek, S., Smimovas, V., and Winter, R. (2006). Solvation-assisted pressure tuning of insulin fibrillation: from novel aggregation pathways to biotechnological applications. *J Mol Biol* 356, 497-509.
94. Vytutas, S., Winter, R., Funck, R., and Dzwolak, W. (2006). Protein amyloidogenesis in the context of volume fluctuations: a case study on insulin. *ChemoPhysChem* 7, 1046-1049.
95. Ludwing, M., and Sanford, A. (1988). Ultraviolet resonance Raman excitatin profiles of tyrosines:dependence of Raman cross sections on excited-state intermediates. *JACS* 110, 1005-1011.
96. Elliot, A., and Ambrose, E. (1950). Structure of synthetic polypeptides. *Nature* 165, 921-922.
97. Elliot, A. (1954). Infra-red spectra of polypeptides with small side chains. *Proc R Soc London, Ser A* 226, 408-421.
98. Dong, A., Ping, H., and Caughey, W. (1990). Protein secondary structure in water from second-derivative amide I infrared spectra. *Biochem* 29, 3303-3308.
99. Du, X., Mio, W., and Liang, Y. (2005). IRRAS studies on chain orientation in the monolayers of amino acid amphiphiles at the air-water interface depending on metal complex and hydrogen bond formation with the feadgroups. *J Phys Chem B* 109, 7428-7434.
100. Wang, Y., Du, X., Guo, L., and Liu, H. (2006). Chain orientation and headgroup structure in Langmuir monolayers of stearic acid and metal stearate (Ag, Co, Zn, and Pb) studied by infrared reflection-absorption spectroscopy. *J Chem Phys* 124, 1-9.
101. Sreerama, N., Venyaminov, S., Sergei, Y., and Woody, R. (2000). Estimation of protein secondary structure from circular dichroism spectra: Inclusion of denatured proteins with native proteins in the analysis. *Anal Biochem* 287, 243-251.
102. Dzwolak, W., Ravindera, R., Lenderman, J., and Winter, R. (2003). Aggregation of bovine insulin probed by DSC/PPC calorimetry and FTIR spectroscopy. *Biochem* 42, 11347-11355.
103. Pacardo, D.B., Sethi, M., Jones, S.E., Naik, R.R., and Knecht, M.R. (2009). Biomimetic synthesis of Pd nanocatalysts for the Stille coupling reaction. *ACS nano* 3, 1288-1296.

104. Davis, M.E., Chen, Z.G., and Shin, D.M. (2008). Nanoparticles therapeutics: an emerging treatment modality for cancer. *Nat Rev Drug Discov* 7, 771-782.
105. Peer, D., Karp, J.M., Hong, S., Farokhzad, O.C., Margalit, R., and Langer, R. (2007). Nanocarriers as an emerging platform for cancer therapy. *Nat Nanotechnol* 2, 751-760.
106. Cho, K., Wang, X., Nie, S., Chen, Z.G., and Shin, D.M. (2008). Therapeutic nanoparticles for drug delivery in cancer. *Clin Cancer Res* 14, 1310-1316.
107. Lammers, T., Hennink, W.E., and Storm, G. (2008). Tumor-targeted nanomedicines: principles and practice. *Br J Cancer* 99, 392-397.
108. Bharali, D.J., Khalil, M., Gurbuz, M., Simone, T.M., and Mousa, S.A. (2009). Nanoparticles and cancer therapy: a concise review with emphasis on dendrimers. *Int J Nanomed* 4, 1-7.
109. Tanaka, T., Decuzzi, P., Cristofanilli, M., Sakamoto, J.H., Tasciotti, E., Robertson, F.M., and Ferrari, M. (2009). Nanotechnology for breast cancer therapy. *Biomed Microdevices* 11, 49-63.
110. Farokhzad, O.C., and Langer, R. (2009). Impact of nanotechnology on drug delivery. *ACS Nano* 3, 16-20.
111. Youan, B.B. (2008). Impact of nanoscience and nanotechnology on controlled drug delivery. *Nanomedicine* 3, 401-406.
112. Bruneau, A., Fortier, M., Gagne, F., Gagnon, C., Turcotte, P., Tayabali, A., Davis, T.A., Auffret, M., and Fournier, M. (2013). In vitro immunotoxicology of quantum dots and comparison with dissolved cadmium and tellurium. *Environ Toxicol.*
113. Wiecinski, P., Metz, K.M., King Heiden, T.C., Louis, K., Mangham, A., Hamers, R.J., Heideman, W., Peterson, R.E., and Pedersen, J.A. (2013). Toxicity of oxidatively degraded quantum dots. *Environmental Science & Technology*.
114. Liu, J., Erogbogbo, F., Yong, K.T., Ye, L., Liu, J., Hu, R., Chen, H., Hu, Y., Yang, Y., Yang, J., et al. (2013). Assessing clinical prospects of silicon quantum dots: studies in mice and monkeys. *ACS Nano*.
115. Peng, Z.A., and Peng, X. (2001). Formation of high-quality CdTe, CdSe, and CdS nanocrystals using CdO as precursor. *Journal of the American Chemical Society* 123, 183-184.

116. Wang, H.H., Lin, C.A., Lee, C.H., Lin, Y.C., Tseng, Y.M., Hsieh, C.L., Chen, C.H., Tsai, C.H., Hsieh, C.T., Shen, J.L., et al. (2011). Fluorescent gold nanoclusters as a biocompatible marker for in vitro and in vivo tracking of endothelial cells. *ACS Nano* 5, 4337-4344.
117. Jans, H., and Huo, Q. (2012). Gold nanoparticle-enabled biological and chemical detection and analysis. *Chem Soc Rev* 41, 2849-2866.
118. Lin, Y.W., Huang, C.C., and Chang, H.T. (2011). Gold nanoparticle probes for the detection of mercury, lead and copper ions. *The Analyst* 136, 863-871.
119. Peng, G., Tisch, U., Adams, O., Hakim, M., Shehada, N., Broza, Y.Y., Billan, S., Abdah-Bortnyak, R., Kuten, A., and Haick, H. (2009). Diagnosing lung cancer in exhaled breath using gold nanoparticles. *Nature Nanotechnology* 4, 669-673.
120. Huo, Q., Colon, J., Cordero, A., Bogdanovic, J., Baker, C.H., Goodison, S., and Pensky, M.Y. (2011). A facile nanoparticle immunoassay for cancer biomarker discovery. *J Nanobiotechnology* 9, 20.
121. Huo, Q. (2010). Protein complexes/aggregates as potential cancer biomarkers revealed by a nanoparticle aggregation immunoassay. *Colloid Surface B* 78, 259-265.
122. Kimling, J., Maier, M., Okenve, B., Kotaidis, V., Ballot, H., and Plech, A. (2006). Turkevich method for gold nanoparticle synthesis revisited. *The Journal of Physical Chemistry B* 110, 15700-15707.
123. Shankar, S.S., Bhargava, S., and Sastry, M. (2005). Synthesis of gold nanospheres and nanotriangles by the Turkevich approach. *Journal of Nanoscience and Nanotechnology* 5, 1721-1727.
124. Turkevich, J., Stevenson, P.C., and Hillier, J. (1951). A study of the nucleation and growth processes in the synthesis of colloidal gold. *Discuss Faraday Soc* 11, 55-75.
125. Brust, M., Walker, M., Bethell, D., Schiffrin, D.J., and Whyman, R. (1994). Synthesis of thiol-derivatised gold nanoparticles in a two-phase liquid-liquid system. *J Chem Soc*, 801-802.
126. Wang, G., Huang, T., Murray, R.W., Menard, L., and Nuzzo, R.G. (2005). Near-IR luminescence of monolayer-protected metal clusters. *Journal of the American Chemical Society* 127, 812-813.

127. Shichibu, Y., Negishi, Y., Tsunoyama, H., Kanehara, M., Teranishi, T., and Tsukuda, T. (2007). Extremely high stability of glutathionate-protected Au<sub>25</sub> clusters against core etching. *Small* 3, 835-839.
128. Negishi, Y., Nobusada, K., and Tsukuda, T. (2005). Glutathione-protected gold clusters revisited: bridging the gap between gold (I)-thiolate complexes and thiolate-protected gold nanocrystals. *Journal of the American Chemical Society* 127, 5261-5270.
129. Negishi, Y., Chaki, N.K., Shichibu, Y., Whetten, R.L., and Tsukuda, T. (2007). Origin of magic stability of thiolated gold clusters: a case study on Au<sub>25</sub> (SC<sub>6</sub>H<sub>13</sub>)<sub>18</sub>. *Journal of the American Chemical Society* 129, 11322-11323.
130. Xie, J., Zheng, Y., and Ying, J.Y. (2009). Protein-directed synthesis of highly fluorescent gold nanoclusters. *Journal of the American Chemical Society* 131, 888-889.
131. Liu, C.L., Wu, H.T., Hsiao, Y.H., Lai, C.W., Shih, C.W., Peng, Y.K., Tang, K.C., Chang, H.W., Chien, Y.C., and Hsiao, J.K. (2011). Insulin-directed synthesis of fluorescent gold nanoclusters: Preservation of insulin bioactivity and versatility in cell imaging. *Angewandte Chemie International Edition* 50, 7056-7060.
132. Kelly, J.W. (1998). The alternative conformations of amyloidogenic proteins and their multi-step assembly pathways. *Current Opinion in Structural Biology* 8, 101-106.
133. Li, S., and Leblanc, R.M. (2014). Aggregation of insulin at the interface. *The Journal of Physical Chemistry B* 118, 1181-1188.
134. Groenning, M., Frokjaer, S., and Vestergaard, B. (2009). Formation mechanism of insulin fibrils and structural aspects of the insulin fibrillation process. *Curr Protein Pept Sci* 10, 509-528.
135. Ban, T., Hamada, D., Hasegawa, K., Naiki, H., and Goto, Y. (2003). Direct observation of amyloid fibril growth monitored by thioflavin T fluorescence. *J Biol Chem* 278, 16462-16465.
136. Krebs, M., Bromley, E., and Donald, A. (2005). The binding of thioflavin-T to amyloid fibrils: localisation and implications. *J Struct Biol* 149, 30-37.
137. Puchtler, H., Sweat, F., and Levine, M. (1962). On the binding of Congo red by amyloid. *J Histochem Cytochem* 10, 355-364.



138. Klunk, W.E., Pettegrew, J., and Abraham, D.J. (1989). Quantitative evaluation of congo red binding to amyloid-like proteins with a beta-pleated sheet conformation. *J Histochem Cytochem* 37, 1273-1281.
139. Bekard, I.B., and Dunstan, D.E. (2009). Tyrosine autofluorescence as a measure of bovine insulin fibrillation. *Biophys J* 97, 2521-2531.
140. Permyakov, E.A., Yarmolenko, V.V., Burstein, E.A., and Gerday, C. (1982). Intrinsic fluorescence spectra of a tryptophan-containing parvalbumin as a function of thermal, pH and urea denaturation. *Biophys Chem* 15, 19-26.
141. Arutyunyan, A., L'vov, K., Mnatsakanyan, A., Oganesyanyan, V., and Shakhnazaryan, N. (1985). Light quenching of fluorescence of aromatic amino acids. *J Appl Spectrosc* 43, 992-994.
142. Liu, W., Johnson, S., Micic, M., Orbulescu, J., Whyte, J., Garcia, A.R., and Leblanc, R.M. (2012). Study of the aggregation of human insulin langmuir monolayer. *Langmuir* 28, 3369-3377.
143. Linse, S., Cabaleiro-Lago, C., Xue, W.-F., Lynch, I., Lindman, S., Thulin, E., Radford, S.E., and Dawson, K.A. (2007). Nucleation of protein fibrillation by nanoparticles. *Proceedings of the National Academy of Sciences* 104, 8691-8696.
144. Mahmoudi, M., Kalhor, H.R., Laurent, S., and Lynch, I. (2013). Protein fibrillation and nanoparticle interactions: opportunities and challenges. *Nanoscale* 5, 2570-2588.
145. Yoo, S.I., Yang, M., Brender, J.R., Subramanian, V., Sun, K., Joo, N.E., Jeong, S.-H., Ramamoorthy, A., and Kotov, N.A. (2011). Inhibition of amyloid peptide fibrillation by inorganic nanoparticles: functional similarities with proteins. *Angewandte Chemie International Edition* 50, 5110-5115.
146. Colvin, V.L., and Kulinowski, K.M. (2007). Nanoparticles as catalysts for protein fibrillation. *Proceedings of the National Academy of Sciences* 104, 8679-8680.
147. Cabaleiro-Lago, C., Quinlan-Pluck, F., Lynch, I., Dawson, K.A., and Linse, S. (2010). Dual effect of amino modified polystyrene nanoparticles on amyloid  $\beta$  protein fibrillation. *ACS chemical neuroscience* 1, 279-287.
148. Lynch, I., and Dawson, K.A. (2008). Protein-nanoparticle interactions. *Nano Today* 3, 40-47.
149. Wu, W.-h., Sun, X., Yu, Y.-p., Hu, J., Zhao, L., Liu, Q., Zhao, Y.-f., and Li, Y.-m. (2008). TiO<sub>2</sub> nanoparticles promote  $\beta$ -amyloid fibrillation in vitro. *Biochemical and Biophysical Research Communications* 373, 315-318.

150. Auer, S., Trovato, A., and Vendruscolo, M. (2009). A condensation-Ordering mechanism in nanoparticle-catalyzed peptide aggregation. *PLoS Comput Biol* 5, e1000458.

151. Li, Q., Ohulchanskyy, T.Y., Liu, R., Koynov, K., Wu, D., Best, A., Kumar, R., Bonoiu, A., and Prasad, P.N. (2010). Photoluminescent carbon dots as biocompatible nanoprobe for targeting cancer cells in vitro. *J Phys Chem C* 114, 12062-12068.